Silicon Phthalocyanines in Large Area, Flexible Organic Photovoltaics processed by Blade Coating

BY

Chithiravel Sundaresan

A thesis submitted in partial fulfillment of the requirements for the
Doctorate in Philosophy degree in Chemical Engineering

Department of Chemical and Biological Engineering
Faculty of Engineering
University of Ottawa

Ph.D. in Chemical Engineering University of Ottawa

Department of Chemical Engineering Ottawa, ON, Canada

Title: Silicon Phthalocyanines in Large area, Flexible Organic Photovoltaics processed by Blade Coating

Author: Chithiravel Sundaresan MSc, B.Ed.,

Supervisor: Professor. Benoît H. Lessard
Department of Chemical and Biological Engineering
University of Ottawa

Co-Supervisor: Dr. Salima Alem
Advanced Electronics and Photonics Research centre
National Research Council Canada

Number of Pages: 137

Abstract

Organic photovoltaics (OPVs) is an emerging energy technology that can offer lightweight and conformable power sources suitable for many niche applications. Currently, the most promising OPV devices are based on materials with high synthetic complexity, and they are fabricated on a lab scale via spin coating on glass substrates, with small active areas (< 0.1 cm^2). While spin coating is a powerful method for uniform and controlled film deposition, it is not suited for large-scale manufacturing. In order to facilitate the transfer from laboratory to industrial production, we must use scalable deposition techniques and investigate the impact of the scalability on the properties of the active layers and the devices' performance.

Silicon Phthalocyanines (SiPcs) are a class of semiconductor molecules with low synthetic complexity that are widely used in organic electronics such as organic thin film transistors and organic light-emitting diodes. In OPVs, SiPcs were demonstrated as an effective ternary additive in spin-coated devices. However, its potential use in scalable large-area devices has not been explored yet. In this thesis, a series of SiPcs were investigated as active materials in flexible inverted OPVs, using a scalable deposition technique: the blade coating. We first used SiPcs as a ternary additive in PCDTBT: $PC_{71}BM$-based bulk heterojunction (BHJ) OPVs. We demonstrated that SiPcs can effectively enhance the device's performance by increasing the charge generation in the NIR region and maintaining an optimal nanomorphology of active layers. We achieved a maximum power conversion efficiency (PCE) of 5.5% by adding 10wt.% of SiPc. We also used SiPc as a non-fullerene acceptor, paired with P3HT polymer in an active layer processed from green solvents. The use of green processes in OPV device fabrication is crucial for the commercial deployment of the technology. We explored different active layer configurations: BHJ, sequential, and alternate-sequential (Alt-Sq). The Alt-Sq configuration, where the acceptor is deposited sequentially on top of the polymer, led to the best device performance, balanced charge carrier mobilities, and favorable morphology. The results presented in this thesis demonstrate significant steps toward large-scale implementation of SiPcs in low-cost, large-area, flexible OPVs.

Résumé

Le photovoltaïque organique (OPV) est une technologie émergente pour la production d'énergie électrique. Elle permet le développement des sources d'alimentation légères et conformables adaptées à de nombreuses applications de niche. Actuellement, les dispositifs OPV les plus prometteurs sont basés sur des matériaux à fort indice de complexité de synthèse et sont fabriqués à l'échelle laboratoire via la tournette sur des substrats de verre, avec de petites surfaces actives (< 0,1 cm^2). Bien que le dépôt à la tournette permette une formation de films contrôlée et uniforme, cette technique n'est pas viable en production industrielle. Pour faciliter le transfert industriel, il est important d'utiliser des techniques de dépôt à grande échelle pour la fabrication des OPV et d'étudier l'impact de la mise à l'échelle sur les propriétés de la couche active et la performance des dispositifs.

Les phtalocyanines de silicium (SiPc) sont une classe de molécules semi-conductrices à faible indice de complexité de synthèse. Ils sont largement utilisés dans l'électronique organique telle que : les transistors organiques à couche mince et les diodes électroluminescentes organiques. Dans le photovoltaïque organique, les SiPc sont principalement utilisés comme additifs ternaires mais leur potentiel n'a pas encore été explorée dans des cellules imprimées à grande surface.

Cette thèse présente l'investigation d'une série de SiPcs en tant que matériau actif dans la fabrication d'OPV flexibles. Les couches actives sont déposées par une technique de dépôt à grande échelle : *Blade cotinga*. Le SiPc a été utilisé dans un premier temps comme additif ternaire dans des cellules hétérojonction composées d'un mélange de PCDTBT et $PC_{71}BM$. Nous avons démontré que l'ajout du troisième composé améliore la performance des dispositifs en augmentant la génération de charges dans la région du proche infrarouge tout en maintenant une morphologie optimale de la couche active. Un rendement de conversion maximale de 5,5% a été obtenu avec un ajout de 10 % de SiPc (ratio massique). Par ailleurs, nous avons démontré que le SiPc peut être utilisé comme un accepteur non-fullerène, en le combinant avec le polymère P3ht dans une couche active déposée à partir de solvants non-halogénés. L'utilisation de solvants verts dans la fabrication des OPV est essentielle à la mise en œuvre commerciale de cette technologie. Nous avons exploré trois différentes configurations pour le dépôt de la couche active : hétérojonction en volume, séquence et séquence-alternée. La configuration séquence-alternée, où l'accepteur est déposé

séquentiellement au-dessus du polymère, a conduit aux meilleures performances du dispositif, à des mobilités de porteurs de charge équilibrées et à une morphologie favorable.

Les résultats présentés dans cette thèse démontrent des étapes importantes vers la mise en œuvre à grande échelle des phtalocyanines de silicium dans les OPV flexibles et à faible coût.

Acknowledgments

I would like to thank Prof. Benoît H. Lessard for giving me the opportunity to join his research group at the University of Ottawa. Thank you very much for your continuous guidance and support for my Ph.D. thesis work. I am very grateful for his patience and help during the COVID years.

I would like to thank my Co-Supervisor Dr. Salima Alem for the guidance and support throughout my studies and for providing the lab facilities at the National research council Canada (NRC). I would like to thank Dr. Ye Tao, Group leader, organic materials, and devices research group (OMD), who gave me an opportunity to work at NRC. I would like to thank Dr. Jianping Lu for the suggestions given for my research projects.

I would like to thank all group members of OMD at NRC and all group members of LRG at the University of Ottawa for their wonderful research environment. I would like to thank all collaborators Dr. Trevor Grant, Dr. Pierre Josse, Mr. Mario Vebber, Prof. Jaclyn Brusso, Prof. Timothy L. Kelly, and Dr. Chase Radford. I would like to express my thank to Mr. Eric Estwick, Mrs. Raluca Movileanu, Mr. Hiroshi Fukutani, Dr. Stephen Lang and Dr. Simona Moisa for their technical support at the NRC. I acknowledge NSERC-Green Electronics Network (GreEN) and university of ottawa for the financial support.

I would like to express my gratitude to my parents, all my family and friends. Many thanks to Arunprabaharan Subramanian and Ananthan Alagumalai for their help and discussions. Finally, I am very grateful to my wife Saranya, and my kids Kabilan, Aaradhana for their patience and sacrifice their time during my Ph.D. studies.

I would like to thank to my thesis committee for the consideration of this report.

Table of Contents

List of Figures

List of Tables

Abberivations

Chapter 1 : Introduction

1.1 Motivation

The world's population is multiplying, with predictions that we will exceed over 10 billion people by 2050. This equates to a total energy consumption of 150-200 PWh (17-23 TW).[1] Since industrial development, humanity has met its energy needs with "artificial" sources like burning fossil fuels (such as oil and gas) and nuclear materials. At the same time, renewable sources were seen as niche technologies that could not meet our growing needs. Recent studies suggest that by the end of 2050, more than 80% of U.S. electricity will be covered by renewable energy such as wind, solar, and hydroelectric generation, which is good news given the growing geopolitical challenges with fossil fuels and the risks associated with nuclear waste disposal. In the same way, Canada aims to reduce the utilization of fossil fuels and increase the use of greener energy by 62% by 2050 (Figure 1-1) compared to current levels.[2]

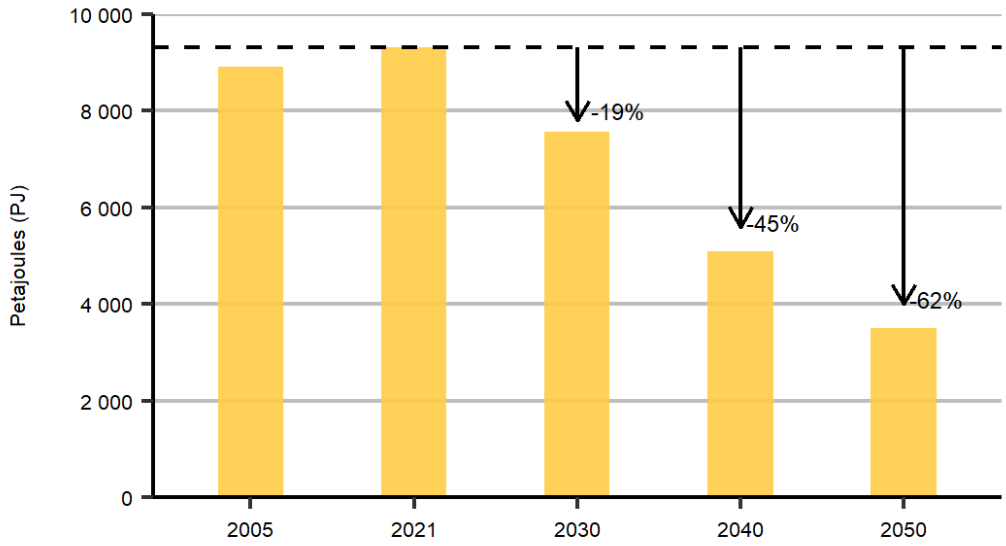

Figure 1-1 Canada's plan for adopting greener electricity by reducing fossil fuel burning for energy production in the next 30 years.[2]

The sun is the only renewable energy source that can offer enough carbon-neutral energy to meet humanity's energy needs. The amount of solar radiation that reaches the surface of the

earth is estimated to be 28000 TW.[3] This amount of energy would fulfill the annual consumption of the entire planet for 103 years. Plants and algae have had billions of years to perfect photosynthesis, the natural process by which they convert the solar energy they absorb into chemical energy.

In 1839 the French physicist Edmond Becquerel discovered the photovoltaic effect, the process by which an electric current is generated when two platinum plates are placed in an electrolyte solution and exposed to sunlight.[3] It took scientists and engineers 40 to 50 years to create the first photovoltaic device, which was based on selenium and had a PCE of 1%.[4] The major shift for this research comes in the 1950s and 1960s when Hoffman Electronics improved the efficiency of the well-known silicon solar cell from Bell Labs, from 6% to 14%. These breakthroughs have propelled research efforts in silicon photovoltaic technology where the PCE is now close to 32.3%, making it the leading solar power technology.[5]

1.2 Types of photovoltaic technologies

The first commercial solar panel was introduced in 1954, with a PCE of about 6% used almost exclusively in space applications.[4], [6] Since then, additional photovoltaic (PV) technologies have been developed, and are typically classified into three generations.[7]–[9] The first-generation consists of crystalline silicon photovoltaics (c-Si). This wafer-based PVs is subdivided into monocrystalline and polycrystalline silicon PV, which together account for more than 90% of the PV market today.[7] The average large scale PCE records are 27.6% and 23.3%, respectively, while demonstrating excellent stability. c-Si PV modules are constrained by the indirect bandgap of Si,[10] which necessitates several hundred micrometers thickness in order to absorb most of the incident light. In addition, they rely on high-purity silicon, whose production demands an enormous amount of energy. These drawbacks increase the cost and energy payback time (EPBT) of c-Si modules; it takes a longer time to pay back all the energy required for manufacturing.

The second generation of PV modules, which consists of thin-film PV modules, was developed in order to overcome the limitations and energy requirements of the c-Si PV technology. Thin-film photovoltaic cells include amorphous silicon (a-Si), Copper indium gallium diselenide (CIGS), and Cadmium telluride (CdTe). The second-generation technologies strove to reduce

material usage, which enabled low weight, some flexibility, and lower cost of solar modules. This was achieved thanks to the high absorption coefficient of CdTe, CIGS, and amorphous (a-Si), which require just a few microns thick films to absorb efficiently the incident light. Currently, these technologies represent around 9% of the PV market.[7] CdTe and CIGS have efficiencies ranging from 22.1% to 23.4% and have good stability. However, the toxicity and availability of raw materials such as: Cadmium, tellurium, indium, and gallium, may be limiting factors in some second-generation PV technologies.

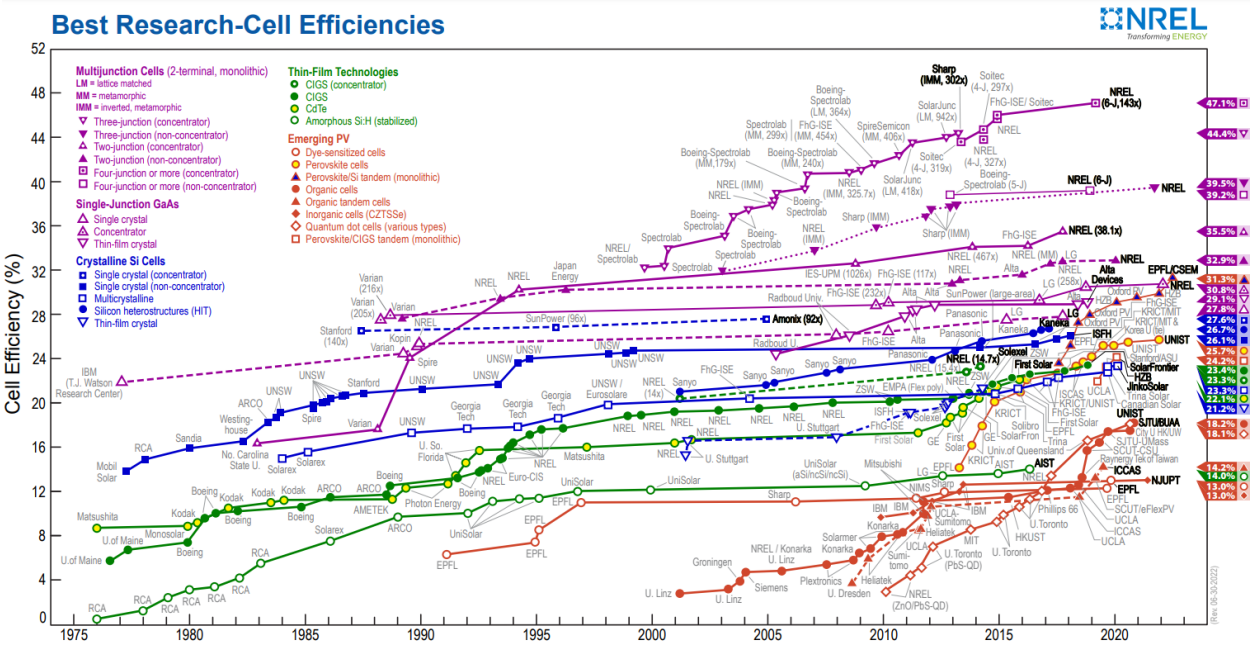

Figure 1-2 Energy efficiency chart by National renewable energy laboratory (NREL) as of early 2022. Organic photovoltaics (solid orange circles) have shown significant improvement in efficiency over the last five years.[11]

The third PV generation includes different types of PV cells: Quantum dot photovoltaics (QPV), dye-sensitized solar cells (DSSCs), organic photovoltaics (OPVs) and perovskite solar cells. These technologies have a substantially shorter energy payback time than the first and second generations of PVs because they use less material and process at lower temperatures.[12] They also feature a variety of absorbent materials, architectural designs, and engineering methodologies. Many of these thin films offer flexibility and transparency that make them very attractive to new potential applications such as window curtains, solar sails and wearable electronics. Over the past

five years, OPVs and perovskite have advanced and rapidly growing to the point where large-scale manufacturing is now possible. **Figure 1-2** shows the National renewable energy laboratory (NREL) chart of the highest confirmed PCEs for research cells for different photovoltaic technologies, plotted from 1976 to the present.

1.3 Organic photovoltaic market

OPV is an emerging and cost-effective energy technology. It can be manufactured on flexible substrates, providing lightweight and conformable power sources suitable for a wide range of emerging applications such as wearables and portable devices[13]. In addition, they provide design and process flexibility, compatible with roll-to-roll manufacturing, for integration in large-scale industrial products. The building-integrated photovoltaics (BIPV) sector has already identified OPV as a key energy technology due to the additional benefits such as the ability to offer different colors or transparency. BIPVs provide thermal insulation, noise and climate protection for buildings while converting light to current. Indoor OPV is another niche market that is predicted to grow significantly over the next decade due to the emergence of the Internet of things applications. OPVs can achieve high efficiencies under indoor lighting conditions (>25%), largely outperforming Si-based solar cells (PCE< 10%).

Global organic photovoltaics market size is projected to US $807.39 million by 2031, and the market is segmented into five distinct geographical submarkets: North America, Europe, Asia Pacific, Latin America, and the Middle East and Africa. Due to strong R&D efforts, the OPV market will account for a major role in Europe by 2027. Europe has emerged as the dominant regional market for this technology. To give just two examples, German companies BASF SE and Heliatek GmbH are excelling in the field of research and development. Additionally, governments of European countries are providing financial incentives in the form of tax subsidies and benefits to manufacturers and consumers of solar power devices, which is driving growth in the regional market. The Energy Efficiency Directive established a bold EU energy efficiency target of 32.5% by 2030.[14]

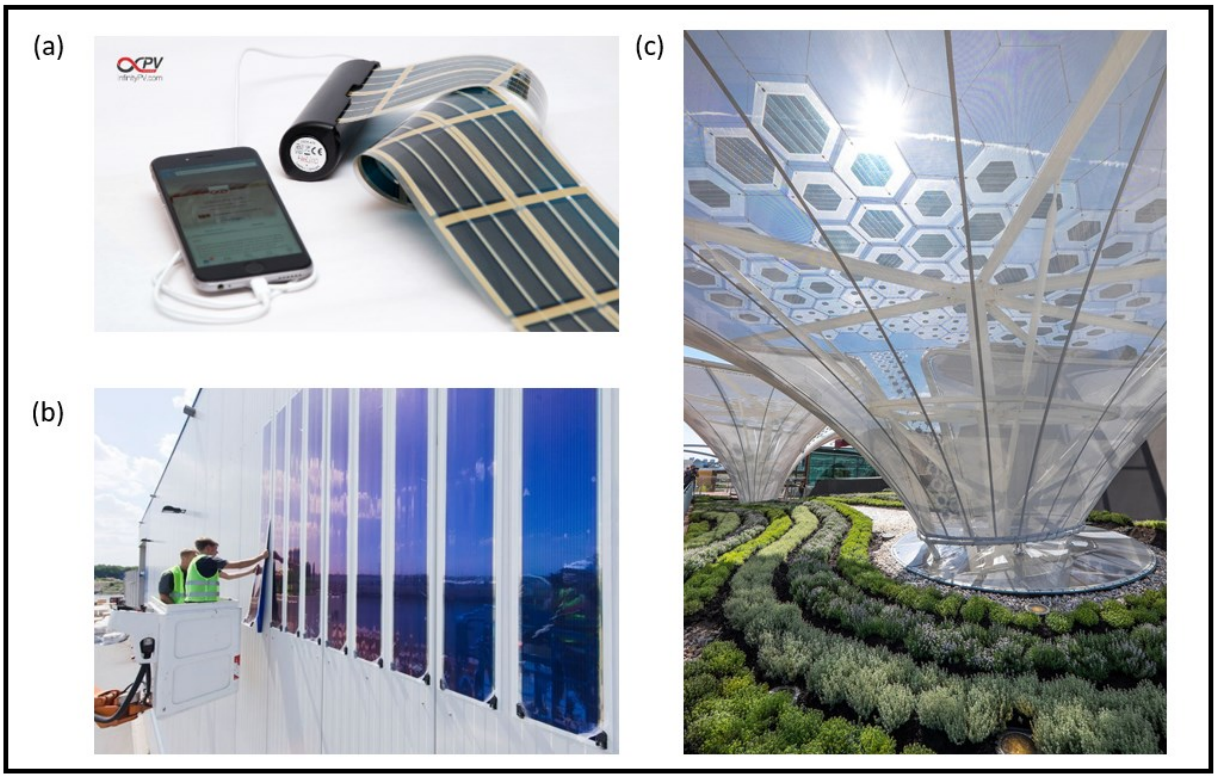

Figure 1-3 Demonstrations of OPV modules application: (a) portable charger from Infinity (b) Building integrated OPV from Heliatek (c) Commercial tree-like OPV module from BIELECTRIC OPV GmBH at the Universal Exhibition Milan 2015.[15]

There are many key players in the OPV market around the world. Companies specializing in OPV's materials, such as: Sumitomo Chemical Co. Ltd., Solarmer Energy Inc., Nano-C and Brilliant Matters, among others; and companies that produce OPV modules, such as: New Energy Technologies, Infinity PV, Heliatek GmBH, BELECTRIC OPV GmBH, among others. **Figure 1-3** displays photos of a portable mobile OPV charger and large-area OPV demonstrations (BIPV and solar tree module). Although OPV has started its industrialization phase, much work remains to be done to support the growth of the OPV market through development of more efficient and low-cost materials that can be easily synthesized and manufactured using scalable printing techniques.

1.4 Scope of thesis

This thesis mainly focuses on the fabrication of large-area solution processed OPV devices and the transition from lab-scale spin coating to scalable blade coating techniques. This thesis investigates the role of Silicon Phthalocyanines (SiPcs) as both ternary additives and non-fullerene acceptor (NFA) in blade coated, flexible OPVs. SiPcs have shown to be promising active materials in organic electronics, and that can be produced using inexpensive and simple chemical processes. Hence, this thesis demonstrates the use of low-cost SiPcs in large-area, flexible devices. This work also demonstrates a series of challenges to fulfilling the industrial requirements, such as engineering the device fabrication, optimizing the morphology of the active layer, using green solvents-based ink formulation, and enhancing the performance of devices.

The following chapters will address the outline of work included in this thesis

Chapter 1 covers the state of the art of photovoltaic technologies with an emphasis on organic photovoltaics. In **Chapter 2**, we describe the basic structure and working principle of OPV devices as well as the most used donor/acceptor materials. We also discuss the main challenges in the upscaling and mass production of OPV devices.

In **Chapter 3,** we present a detailed study investigating the use of SiPc as ternary additives in large active area OPVs, processed by spin and bade coating methods. The effect of additive concentration on morphology and charge transport characteristics is thoroughly investigated. The active layer morphology is analyzed using grazing incidence wide-angle x-ray scattering (GIWAXS) and atomic force microscopy and the charge carrier transport and recombination parameters are probed in both rigid and flexible devices.

In **Chapter 4,** we attempt to further improve the device performance using a novel ternary additive. A N-9'-heptadecanyl-2,7-carbazole functional SiPc ((CBzPho)2-SiPc) derivative is synthesized with the carbazole functional group which matches the functional group of the donor polymer, poly[[9-(1-octylnonyl)-9Hcarbazole-2,7-diyl]-2,5-thiophenediyl-2,1,3-benzothiadiazole-4,7 diyl2,5thiophenediyl] (PCDTBT). The purpose is to increase miscibility between the additive and the donor phase. The ternary OPV devices are fabricated on flexible PET substrates. The

miscibility and solid-state interaction between ternary additive and donor/acceptor blends, and charge carrier recombination dynamics are investigated and correlated to the performance of devices.

In **Chapter 5,** we demonstrate OPV devices using $(3BS)_2$-SiPc as NFA, paired with P3HT. Environmentally-friendly non –halogenated solvents are used to process the device by blade coating on flexible substrates. We explore different active layer deposition configurations such as bulk heterojunction (BHJ), Sequential layer-by-layer (Sq), and Alternate sequential layer-by-layer (Alt-Sq). The vertical distribution of donor (P3HT)-acceptor $(3BS)_2$-SiPc through the active layers, charge carrier properties are thoroughly investigated and correlated with the performance of devices.

Finally, **Chapter 6** summarizes the findings of this thesis and proposes future work and areas of interest for this exciting class of SiPcs.

Chapter 2 : Literature Review- Organic Photovoltaics

The aim of this section is to give a general overview of organic semiconductors and devices, present the working principles of OPV with an emphasis on BHJ structure, and characterization techniques. This section will also highlight recent achievements in the development of organic polymers and small molecule fullerenes as well as Phthalocyanines based organic photovoltaics.

2.1 Organic semiconductors

The photoactive layer in an OPV device is made of organic semiconducting materials, which are conjugated carbon-based compounds capable of transferring charge carriers when photoexcited. The π-π stacking and intermolecular interaction between the semiconducting molecules enables delocalized charges to hop between molecules, leading to charge transport in the solid state. Several factors contribute to the optical characteristics of organic semiconductors, such as conjugation lengths, heteroatom functionalization and solid-state arrangement. The combination of conjugation and functional group substitution determines the frontier energy levels of the molecules, such as the highest occupied molecular orbital (HOMO) and the lowest unoccupied molecular orbital (LUMO). The extension of π-π conjugation of a system leads to the splitting of both bonding and anti-bonding molecular orbitals, which eventually decreases the energy gap difference between the HOMO and LUMO of a material.[16]

2.2 OPV Working principle

An OPV device consists of one or more photoactive organic materials sandwiched between two dissimilar electrodes. In order for the solar radiation to reach the photoactive layer, one of the electrodes must be transparent. An efficient OPV device typically employs a bulk heterojunction structure, where electron donor (D) material and electron acceptor (A) material phases are dispersed within the whole active layer to create a three dimensional network of interfaces. **Figure 2-1** shows the complete process of photocurrent generation in a donor/acceptor OPV device, consisting of four steps: 1. Light absorption, 2. Exciton formation and diffusion, 3. Exciton dissociation or separation, 4. Charge transport and collection. Improving the efficiency of any of these steps can increase the overall performance of an OPV device. In the following sections, we discuss the importance and requirements of each step.

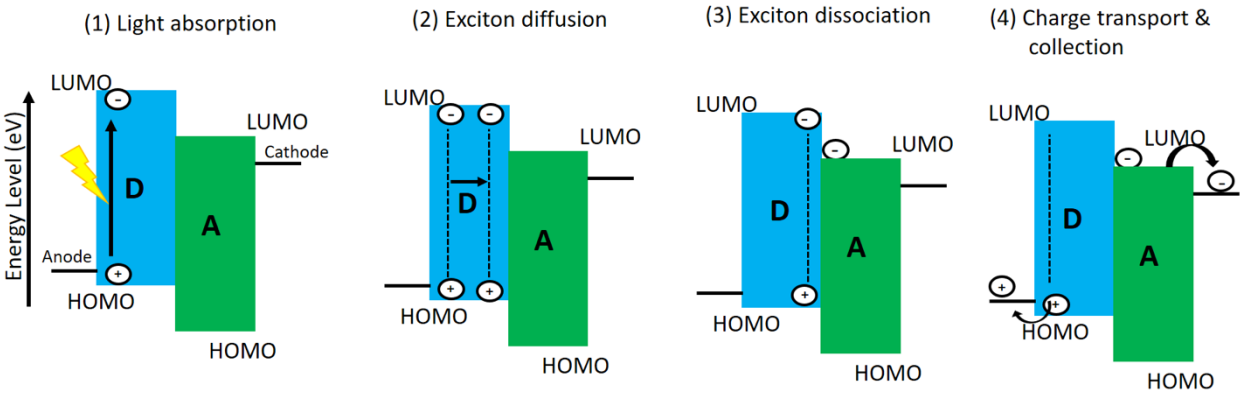

Figure 2-1 Working principles of Donor: Acceptor BHJ OPVs (1) Light absorption and exciton formation; (2) Exciton diffusion; (3) Exciton dissociation; (4) Charge carrier transport and collection.

2.2.1 Photon absorption

Sunlight represents a portion of the electromagnetic spectrum which includes ultraviolet, visible, and infrared light. The intensity and spectral distribution of solar radiation that reaches the Earth's surface is affected by the atmosphere through different processes (absorption, scattering, and reflection). About 70% of incoming solar radiation energy is distributed in the 300-900 nm range, corresponding to photon energies of 4.1 to 1.4 eV.

In most organic devices, a significant portion of the incident light is lost due to reflections and relatively high band gap of organic semiconducting materials ($hv < E_g$), where h is the plank constant, ν is the irradiation frequency and E_g is the bandgap energy of the organic materials. Only photons with similar or greater energy ($hv \geq E_g$), to the band gap energy of organic semiconductors can be absorbed.[17], [18] Therefore, it is essential to use optimal band gap materials to expand the absorption window in order to increase the efficiency of OPV.[19]–[21] A number of studies have demonstrated the ability to enhance absorption by changing molecular structure or by adding a third compound in the D-A system.[22]–[25] In some cases metal and semiconductor nanoparticles were incorporated to increase the optical density through optical spacing.[26]–[28]

2.2.2 Exciton formation and diffusion

The photo excitation of the D-A photoactive layer in OPV generates excitons (Coulomb force-bonded electron-hole pairs), which have a high binding energy (> 0.5 *eV*). Excitons diffuse through the donor and acceptor phases to reach a nearby D-A interface where they can dissociate.

However, the photogenerated excitons decay if they cannot reach a D-A interface within their diffusion length (4–20 nm).[29], [30] The intermixed BHJ concept maximizes the D-A interface area compared to planar bilayer structure and therefore reduces the decay rate of excitons. In the BHJ layer, the D and A domain sizes and crystallinity can be effectively controlled by tuning the parameters of the deposition process, such as temperature and coating speed.

2.2.3 Exciton Dissociation

Unlike in inorganic semiconductors, photogenerated excitons in organic semiconductors do not automatically separate into free charges. This is due to the low dielectric constant of organic semiconductors (typically k ~0.3 to 3) compared to inorganic (k of Si ~ 12). [31], [32] The cascade energy at D/A interface in BHJ OPV provides the driving force for excitons dissociation.[33] The separated charge carriers can either decay to the ground state through recombination processes or produce free carries in charge-separated states. Charge carriers can move freely in the respective phase of the active layer after overcoming the binding energy. The nanostructure morphology plays an important role in facilitating or hindering the charge dissociation process.[34], [35] Ultrafast charge generation (< 100 fs) has been observed in many conjugated polymer-fullerenes systems.[36]

2.2.4 Charge transport and collection

In the last step, the free charges (holes and electrons) drift towards the selective electrodes under the influence of built-in field created by their work function differences in order to generate an electrical current. For efficient charge collection from the active layer to external circuit, both the anode and cathode electrodes must form ohmic contacts with the donor and acceptor networks, respectively. The charge transport is impacted by recombination during the journey to the electrodes. Proper material design and thin film processing can mitigate the recombination losses and their impact on the performance of BHJ OPVs. Recombination loss mechanisms are discussed in more detail in section 2.3. The charge transport properties of active materials are commonly quantified by the charge carrier mobility (μ) that can be extracted by different techniques, such as space charge limited current method (SCLC), time-of-flight (TOF) or organic field-effect transistors (OFET). Balanced mobility is desired in the donor/acceptor blend of BHJ OPVs.[37]

2.3 Charge recombination losses

There are various losses that affect the efficiency of OPVs and are involved in every step of the conversion process; from capturing light to generating free-charge carriers.[38], [39] Charge carrier recombination losses within BHJ layer can be grouped into three categories (1) exciton recombination, for excitons that fail to diffuse to D/A interface, (2) geminate and (3) non-geminate recombination. The geminate or monomolecular recombination is a loss mechanism resulting from ineffective exciton dissociation or a result of immediate recombination upon dissociation (**Figures 2-2 (2)**), When geminate recombination takes place, the photocurrent reveals a strong voltage dependence caused by the electric field ionization of the charge-transfer exciton, which generates mobile carriers at high bias and suppresses their formation at low bias.[40] This generally leads to a decrease in photovoltaic performance. Ultrafast techniques such as transient absorption spectroscopy (TAS) are commonly used to probe recombination dynamics of photoexcited carriers.

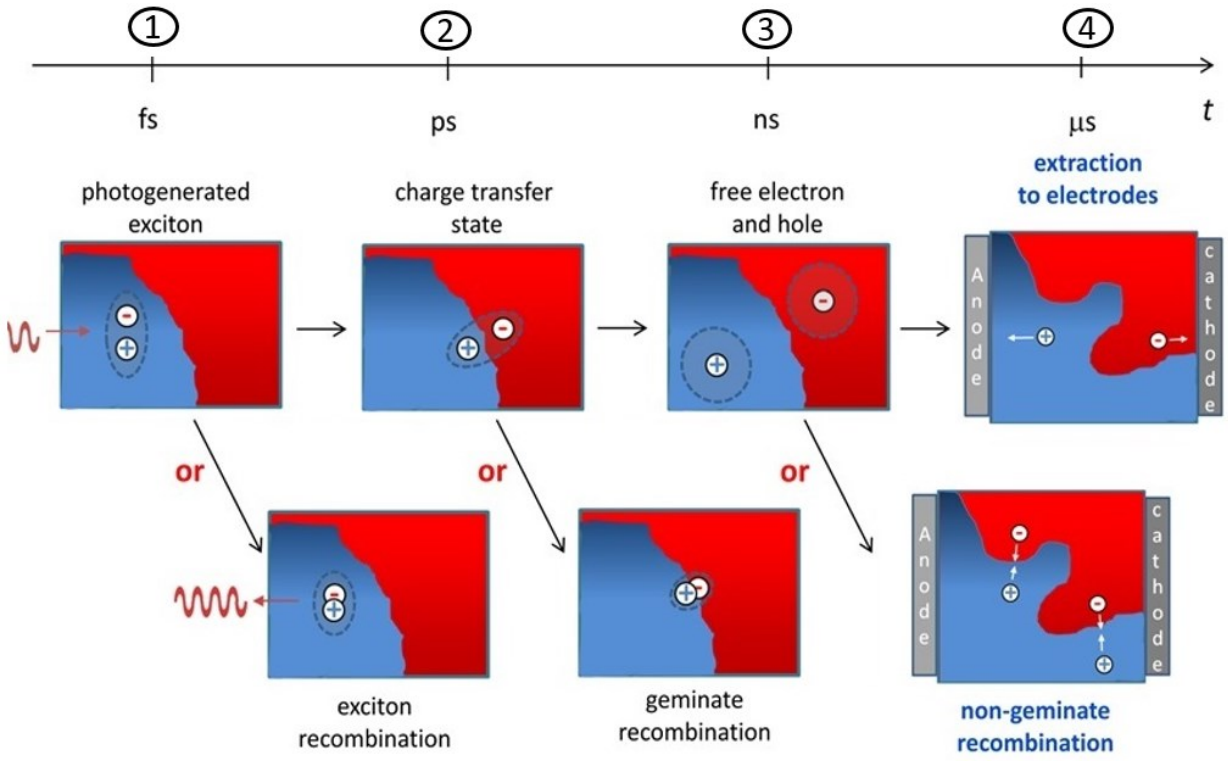

Figure 2-2 Scheme of recombination processes from geminate to non-geminate recombination[40] the time scale of mentioned for the different recombination 1. Exciton in femtoseconds (fs), 2. Geminate occurs in picoseconds (ps), and 3. Non-geminate occurs in nanoseconds (ns). Figure adapted with permission.

Following the separation of excitons, the free-charge carriers may undergo non-geminate or bimolecular recombination prior to reaching the respective electrodes (**Figures 2-2 (3)**). This refers to the recombination of any free-charge carriers that do not originate from the same singlet excitons. Bimolecular recombination (also known as Langevin recombination) is often linked to an unbalanced charge carrier mobility of holes and electrons that leads to the formation of space charge or a limited charge carrier lifetime.[41] The rate limiting step for Langevin-type recombination is the diffusion of charges of opposite sign in their respective Coulomb field[41], [42] The magnitude of Langevin recombination coefficient is given by:

$$\beta_L = \frac{q}{\varepsilon_0 \varepsilon}(\mu_{hole} + \mu_{electron}) \tag{2.1}$$

Where q is the elementary charge of the electron, ε_0 is the vacuum and ε the relative permittivity and μ_{hole}, $\mu_{electron}$ are the hole and electron mobility respectively. A free-charge carrier can also be trapped and recombine with a mobile carrier through a process called trap-assisted or Shockley-Read-Hall recombination. The recombination rate depends on the number of sites that act as traps and how fast the free-charge carrier can find the trapped carrier. [43]

The open circuit voltage (*Voc*) and the short circuit current density (*Jsc*) are strongly dependent on the presence of a specific recombination mechanism. The study of their dependency on the incident light intensity is a simple method to distinguish between bimolecular recombination and trap-assisted recombination. The light intensity dependence of the *Voc* is given by (Equation 2.2)[44], [45]

$$V_{OC} = \frac{E_{gap}}{q} - \frac{kT}{q}\ln\frac{(1-p)\beta N_c^2}{PG} \tag{2.2}$$

Where E_{gap}, is the effective energy gap between the offset of the HOMO of the electron donor and the LUMO of the electron acceptor, q is the elementary charge of the electron, k is the Boltzmann constant, T is the temperature in Kelvin, P is the dissociation probability of free carriers, β the recombination constant, N_c the density of states in the conduction band, and G the generation rate of electron-hole pairs. The slope kT/q is derived from plotting the *Voc* as a function of the logarithm

of the light intensity (P_{light}). G is the only term that is directly proportional to the light intensity. In the case of Langevin-type recombination, the slope of Voc as a function of (P_{light}) on a semi-logarithmic scale should be equal to kT/q, whereas in the presence of trap-assisted recombination, the dependence of Voc on (P_{light}) is significantly larger than kT/q. In OPV devices, Jsc typically follows a power-law dependence on P_{in} as described by the following equation (Equation 2.3).

$$J_{sc} = P_{light}^{S} \tag{2.3}$$

Where S is the scaling exponent of a power law. In general, a linear relationship between current density and light intensity ($S \sim 1$) indicates weak or no 2nd order recombination, whereas a sub-linear relationship ($S < 1$) indicates charge transport limited behavior. Unbalanced charge carrier mobility in the system typically causes S to deviate from linearity**.**

2.4 OPV device structure

2.4.1 Binary BHJ OPV

The first heterojunction OPV device was reported by C.W. Tang where a Perylenediimide (PDI) derivative as an electron acceptor and a copper phthalocyanine (CuPc) derivative as an electron donor (**Figure 2-3 a**) were successively evaporated, enabling the formation of the donor/acceptor interface for the dissociation of the excitons into free electrons and holes. The resulting bilayer device provided about 1% of PCE. The performance of typical bilayer architecture is limited by the short exciton diffusion length and the small D-A interface. These limitations were overcome with the introduction of the bulk heterojunction (BHJ) concept in 1995. Heeger et al. reported the first BHJ device based on a blend of a conjugated polymer electron donor poly(2-methoxy-5-(2'-ethyl-hexyloxy)-1,4-phenylene vinylene) (MEH-PPV) and a soluble fullerene-based electron acceptor [6,6]-phenyl-C_{61}-butyric acid (PC61BM).[46] By casting a thin film from a polymer/fullerene solution, an interpenetrating network with increased donor/acceptor interfacial area was formed and led to a significant increase of exciton separation sites (**Figure 2-3 b**). Polymer and small molecule BHJ systems have become popular since the introduction of the concept and are used in several top-performing OPVs.[47]–[52] All-polymer[53], [54] and all-small molecule BHJ devices,[55] as well as planar heterojunction (PHJ) devices produced by

physical vapor deposition (PVD) methods[56] remain active research areas with competitive PCEs.

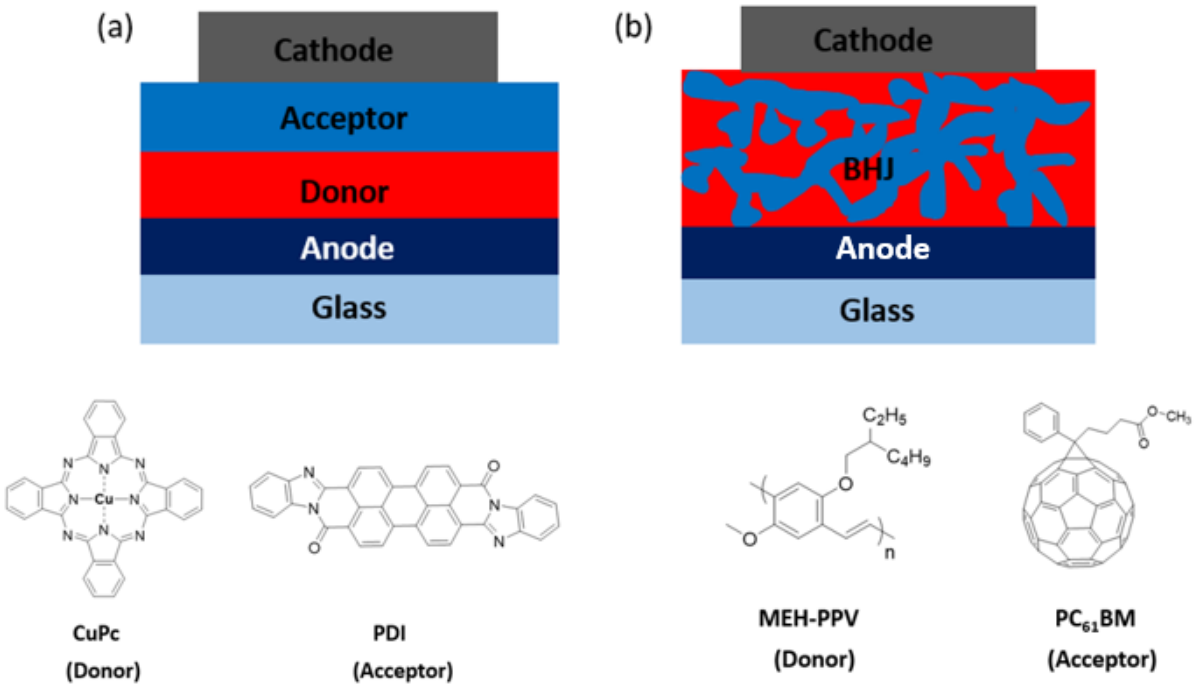

Figure 2-3 Basic (a) planar heterojunction and (b) bulk heterojunction OPV devices stacks the semiconductors along with metal electrodes. Where the used donor/acceptor in PHJ and in BHJ are CuPc/PDI and MEH-PPV/PC61BM respectively.

Many processing parameters can influence the morphology of the BHJ film and ultimately the interfacial area and the pathways for the charge carriers have to take to get to the respective electrodes.[57] These parameters include material composition, choice of solvents, drying time, solution concentration, donor/acceptor mass ratio, and thermal treatments.

The BHJ active layer can be deposited by different deposition techniques, such as spin coating or scalable coating/printing techniques, such as blade coating, slot die coating, inkjet printing, screen-printing, and flexographic printing. Interlayers, which are thin layers stacked between the active layer and the electrodes, act as charge selective extraction layers, such as the hole transporting layer (HTL) and the electron transport layer (ETL). ETL and HTL can be deposited using solution-processable techniques or by thermal evaporation. In an OPV device, the

top electrode, commonly deposited by PVD, defines the device area where all the layers of the device structure overlap. Indium tin oxide (ITO) sputtered on a substrate (glass or polyethylene terephthalate (PET)), is commonly used as a transparent electrode.

Two device geometries are generally used in the fabrication of OPVs, namely conventional and inverted structures as illustrated in **Figure 2-4**. Both the conventional and inverted structures favors lab-scale devices to explore new materials and device physics.[58] In conventional structure, poly (3, 4-ethylenedioxythiophene)-poly styrene sulfonate (PEDOT: PSS)[45], [59] is normally used as HTL and lithium fluoride (LiF)[60], calcium (Ca)[61], or bathocuproine (BCP) are used as ETL with aluminum (Al) as top electrode. In an inverted configuration, zinc oxide (ZnO) or titanium dioxide (TiO_2) is generally used as ETL, deposited on the transparent ITO electrode. For the hole transport layer, molybdenum oxide (MoO_3) is mostly thermal evaporated on the active layer with silver (Ag) as the top electrode.[62], [63] The inverted configuration shows better stability than conventional configuration and it is widely used in the scalable process because of high oxidative stability and solution-processability of silver electrode.[64]

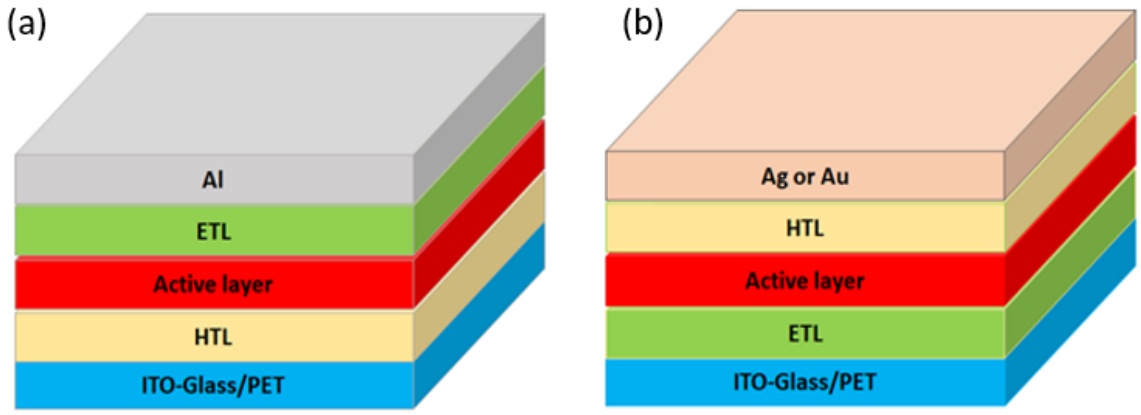

Figure 2-4 Common OPV devices configurations (a) conventional structure consists of ITO/glass or PET/HTL/Active layer/ ETL/ Al (b) inverted structure consists of ITO/glass or PET/ETL/Active layer/ HTL/ Ag or Au.

2.4.2 Ternary organic Photovoltaics

Adding a third component into a binary BHJ blend can improve the performance of OPVs.[65] [66] Several different promising ternary additives have emerged: dye sensitizers[67], donor polymer[68], small molecule[69], and quantum dot sensitizers. [22],[23] Typically, the ternary additive improves the PCE of the BHJ OPV by enhancing photon absorption. It is important to note that in some cases only a small amount of a ternary additive is needed which does not affect the morphology of the BHJ blend. [70], [71] Also, depending on the characteristics of additive molecules, they can interact with the donor and acceptor compounds in several ways to enhance the device performance. The morphology of ternary blends can be classified into four types (**Figure 2-5**). First, the third material could be embedded with either the donor phase or the acceptor phase, which are highly dependent upon the respective material's surface energy. The second possibility of ternary morphology is that the added material (dye, small molecule,) can diffuse into the donor-acceptor interfaces. The third mechanism is that ternary additives can accommodate between donor and acceptor phases and act as parallel-like structures. Another possibility of ternary morphology is to form alloy-like structures. [66]

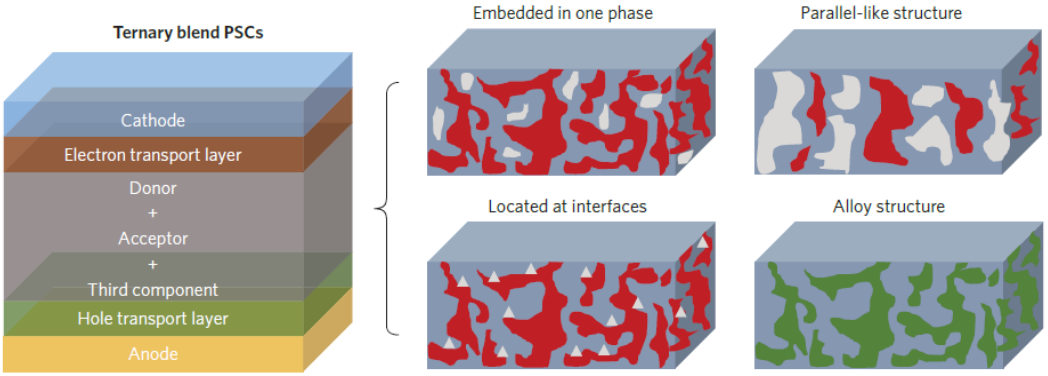

Figure 2-5 schematic diagram of ternary blend OPVs with four different active layer morphologies include the third component embedded in one donor or acceptor phase, generating a parallel-like structure with the main donor or acceptor and an alloy with either the donor or acceptor material.[66]

2.5 OPV device characterisation

2.5.1 I-V characterisation

The most common way to evaluate the performance of a solar cell is to measure the current-voltage (*I-V*) characteristic. This characteristic is recorded in dark and under illumination. The AM 1.5 global (G) spectrum (1000 Wm^{-2}) is defined as the standard terrestrial solar spectrum for solar cell testing **(Figure 2-6).** This is equivalent to solar irradiation at a zenith angle of 48.2º and represents the annual average for mid-latitudes.[72] Solar simulators are engineered to mimic incident light from the sun (AM1.5G) and are used for testing photovoltaic devices.

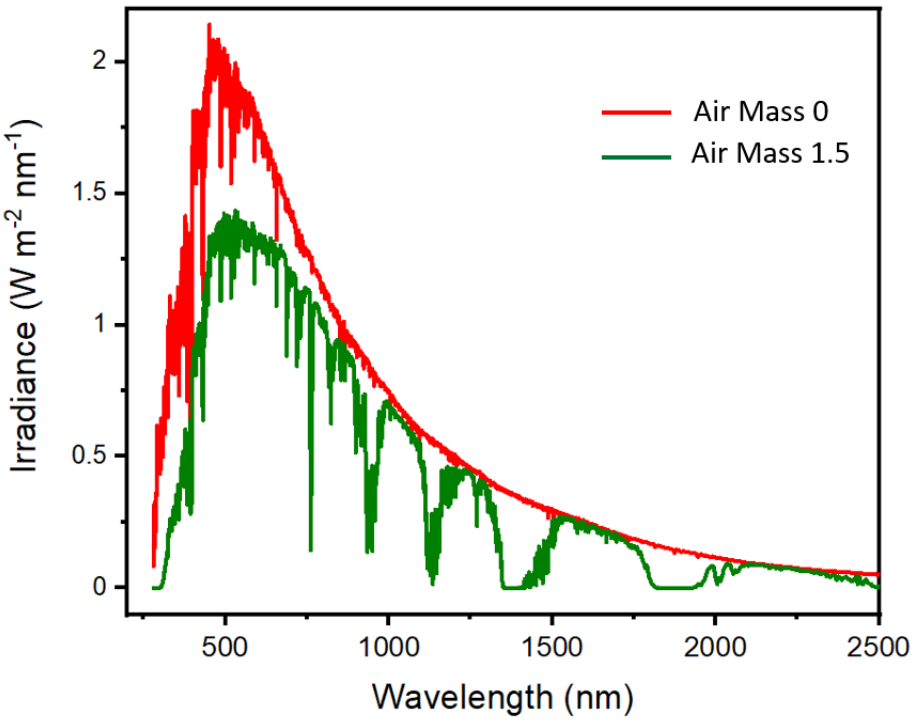

Figure 2-6 Sunlight irradiance at Air Mass 0 (red curve) and standard Air Mass 1.5 (green curve) correspond to a zenith angle of 48.2º. Where, half of irradiance covers in the visible range from 400 nm to 750 nm.[72]

The I-V characteristic under illumination provides the parameters required to estimate the PCE of the device. The typical curve is presented in **Figure 2-7b.** The equivalent circuit that describes the operation of a solar cell is presented in **Figure 2-7a**. I_{ph} refers to the photocurrent generated under light illumination. The series resistance (R_S) is often associated with the resistance of the bulk layer and electrodes and the resistance of contacts/interfaces. R_S can be estimated from

the inverse slope at positive voltage > V_{OC}.[73], [74] Shunt resistance (R_{SH}) is associated with the leakage current[75], [76] and recombination losses and can be derived by the inverse slope around 0V. Under illumination, the *I-V* curve of ideal cells can be expressed by equation 2.5:

$$I = I_0 \left(e^{\frac{qv}{nkt}} - 1\right) - I_L \tag{2.5}$$

Where *I* denotes the current flow, I_L the photogenerated current, I_0 the diode saturation current, *q* is the elementary charge, *V* is the voltage across the device, *k* is the Boltzmann constant, *T* is the absolute temperature of the OPV device, *n* is the diode ideality factor.

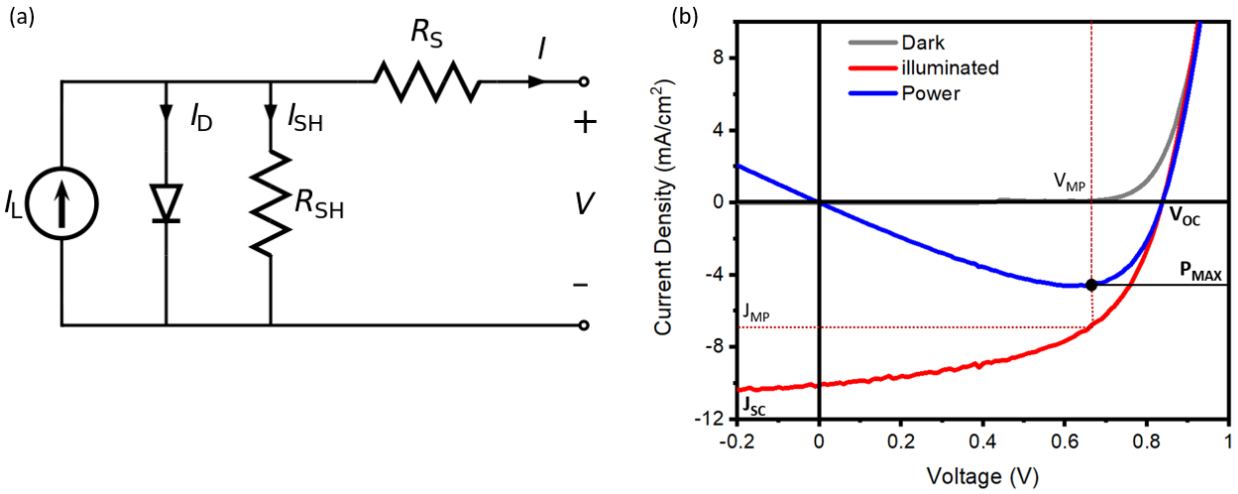

Figure 2-7 (a) Schematic representation of the equivalent circuit of a photovoltaic cell,[77] (b) A typical current-voltage curve, where FF measures ratio between power maximum (P_{MAX}) and theoretical power defined by the product J_{SC} and V_{OC}.

The key photovoltaic parameters are open circuit voltage (V_{OC}), short-circuit current density (J_{SC}), fill factor (*FF*), and the PCE.[78] The V_{OC} is the difference of electrical potentials under the open circuit condition (*I* = 0 A) and depends on the energy gap between the HOMO level of the donor and LUMO level of the acceptor in BHJ devices.[79] The J_{SC} is defined as the current density in the external circuit when the external load is short-circuited (V = 0V). *FF* measures the quality of the solar cells and is defined by the ratio of the maximum power point (P_{max}) available from the solar cells to the theoretical power defined by the product J_{SC} and V_{OC} as described

(Equation 2.6). P_{max} defined by product of current and voltage at maximum power point (J_{MP} and V_{MP}).

$$FF = \frac{P_{MAX}}{V_{OC} * J_{SC}} \tag{2.6}$$

The PCE is defined as the ratio of the output power to the incident light power. It can be calculated from

$$PCE = \frac{V_{OC} * J_{SC} * FF}{P_{light}} \tag{2.7}$$

Where J_{SC} is in A/m^2, V_{OC} is in V, and P_{light} is the incident solar radiation in W/m^2.

2.5.2 Incident photon to electron conversion efficiency

Incident photon to electron conversion efficiency or external quantum efficiency (EQE) indicates the amount of incident photons that are converted to photocurrent under short circuit conditions as a function of wavelength. IPCE is calculated using the following formula:

$$IPCE = \frac{1240 * ISC}{\lambda * P_{in}} * 100\% \tag{2.8}$$

λ is the wavelength and P_{in} is the incident photon intensity of each wavelength. I_{SC} is the short circuit current obtained from the device. The shape of the EQE curve is highly dependent on the light absorption profile of the device as well as the absorption coefficient of active materials. The integration of an EQE spectrum is typically proportional to J_{SC}.

2.6 Industrial relevance and challenges

The efficiency of OPV cells has significantly improved over the last 5 years, reaching 18-19%.[49] However, the commercial viability of OPV technology additionally depends on their stability and their production cost. Therefore, it is important to optimize some relevant factors, such as the cost and stability of materials as well as the manufacturing process of the devices. The

development of efficient OPV cells has been the primary focus of the research. As a result, efficiencies have reached record highs, but at the expense of using complex synthetic materials that have poor scalability, high air sensitivity, and, ironically, are prone to photodegradation.[80], [81] Another generally overlooked issue is the use of halogenated solvents in the fabrication process, which is prohibited in industrial production due to their detrimental impact on the environment and human health. The mass deployment of silicon PV and the economies of scale have hindered the adoption of OPV technologies. It was perceived that the low performance of devices was the main reason, consequently, research efforts over the last decade to focus on this metric at all costs. Krebs and co-workers were among the few groups who focused on the development of large-area modules for OPV with emphasis on scalability and mass production with an impact on the PCEs.[82]–[84] Despite the fact that high PCEs are now achievable, the OPV research community need to focus on developing low-cost efficient materials and scalable processes.

2.6.1 Thin film deposition: Moving from spin coating to Blade coating

The main advantage of organic semiconductor materials is the simple solution processing which, allows the use of printing/coating methods, facilitating the fabrication of large area films. However, most of the "champion devices" reported in the literature are made in laboratory settings using the spin coating deposition technique and have a small active area (< 0.1 cm^2). Although the improvement in device efficiency is very important for the advancement of the OPV field, it is also important to consider the route from laboratory to large-scale production. There are various large-scale deposition techniques available, including spray coating, blade coating, slot die coating and ink jet printing. The ink preparation varies for each technique due to different requirements in viscosities.[85] It is best to use scalable deposition techniques in research laboratories and study important factors like the rheological properties of the ink, shear forces applied during ink deposition, as well as drying times of the thin films because they have a significant impact on the film thickness and morphology and consequently on the device performance. In the following sections, we will describe the two deposition techniques used in research labs for the fabrication of OPVs.

2.6.2 Spin coating

Spin coating is the most commonly used deposition technique in the fabrication of OPV devices. Low capital cost, use of a small volume of solutions and reproducible results have made the spin coater a reliable deposition tool, which can be found in every OPV research lab around the world. Unfortunately, the process and drying kinetics of spin coating do not translate to roll-to-roll printing techniques. The spin coating operation involves depositing a solution on a substrate spinning at a high speed (**Figure 2.8a**). The angular velocity of the substrates leads to the ejection of the solvent, leaving behind a thin film.[86] This implies an inherent batch process where the shear forces on the solution are radial, originating from the center of the substrate. A large amount of solution (>90%) is ejected and wasted during the spin coating. Solution recycling techniques can be employed, but it is challenging to maintain the purity of the recycled solution, and this is nearly impossible in a laboratory setting.

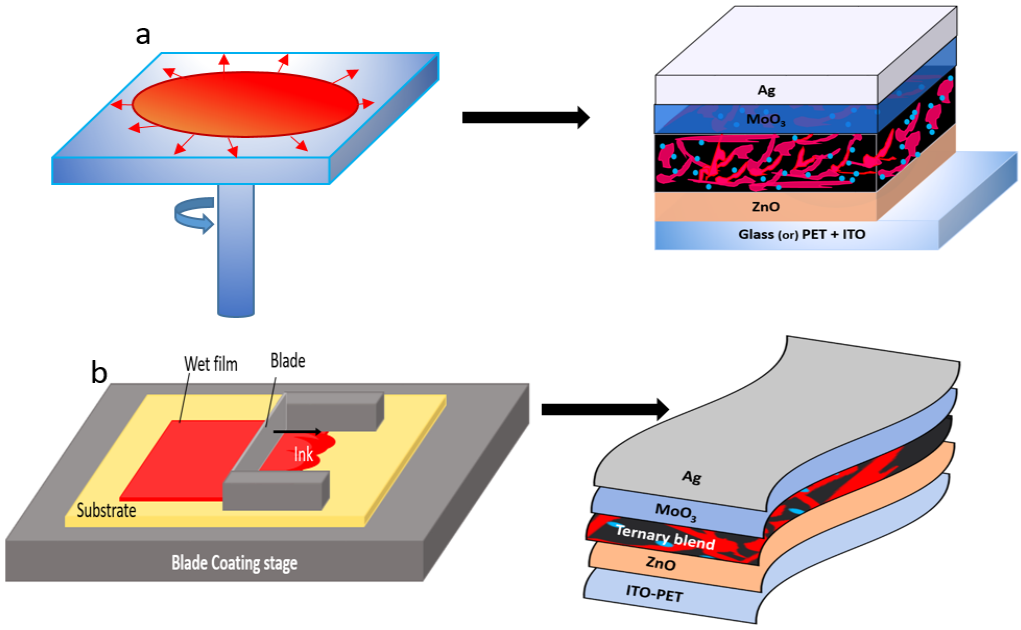

Figure 2-8 Schematic diagram of a) spin coating and b) blade coating process and the respective inverted device prepared on glass or PET/ITO substrates.

The thickness and morphology of spin-coated films are highly dependent on many parameters, including rotation and drying speed, solvent volatility, ink concentration, viscosity and diffusivity, and material molecular weight. The thickness of the film, *d*, is generally represented using an empirical equation.

$$d = k\omega^{\alpha}$$

Where ω is the angular velocity while k and α are empirical constants related to the physical properties of the solvent, material, and substrate.[85]

2.6.3 Blade coating

Blade coating is a simple one-dimensional, directional deposition technique, less frequently used in the fabrication of OPVs. The blade or applicator is placed at a fixed distance from the substrate, which is positioned on a (blade) stage as illustrated in **Figure 2.8b.** The formulated ink is deposited between the applicator and the substrate. A uniform thin film can be formed by moving linearly across the substrate at a constant speed. The wet film thickness depends on the gap between the blade and the substrate and coating speed.[87] But other parameters, such as the surface energy of the substrate, the surface tension of the ink, viscosity, and substrate temperature influence the formation and the thickness of the film. The thickness of the dry film, denoted by *d*, can be calculated from the empirical relationship.

$$d = \frac{1}{2}\, g \left(\frac{c}{\rho} \right)$$

Where *g* is the gap width between the substrate and the blade, *c* is the concentration of the solution g/ cm^3, and ρ is the density of the material in the final film in g / cm^3.[85]

The blade coating method is favourable for the fabrication of large-area devices and the process can be easily translated to slot die coating, a continuous roll-to-roll printing technique. Therefore, the films obtained by blade coating are representative of those produced through mass production, making this technique favourable to spin coating.

2.6.4 Use of green solvents

The state-of-the-art BHJ OPV devices are mostly processed by highly toxic halogenated solvents. Processing high-performance devices using green solvents is a necessary step toward their commercialization. In BHJ structure devices, the selection of processing solvent is limited since it is necessary to take into consideration both the miscibility of donor and acceptor as well as the solubility of individual molecules. **Figure 2.9** organizes possible solvents for OPVs

processing into a hierarchy, ranging from hazardous halogenated aromatics (bottom) toward polar media (top).[88]

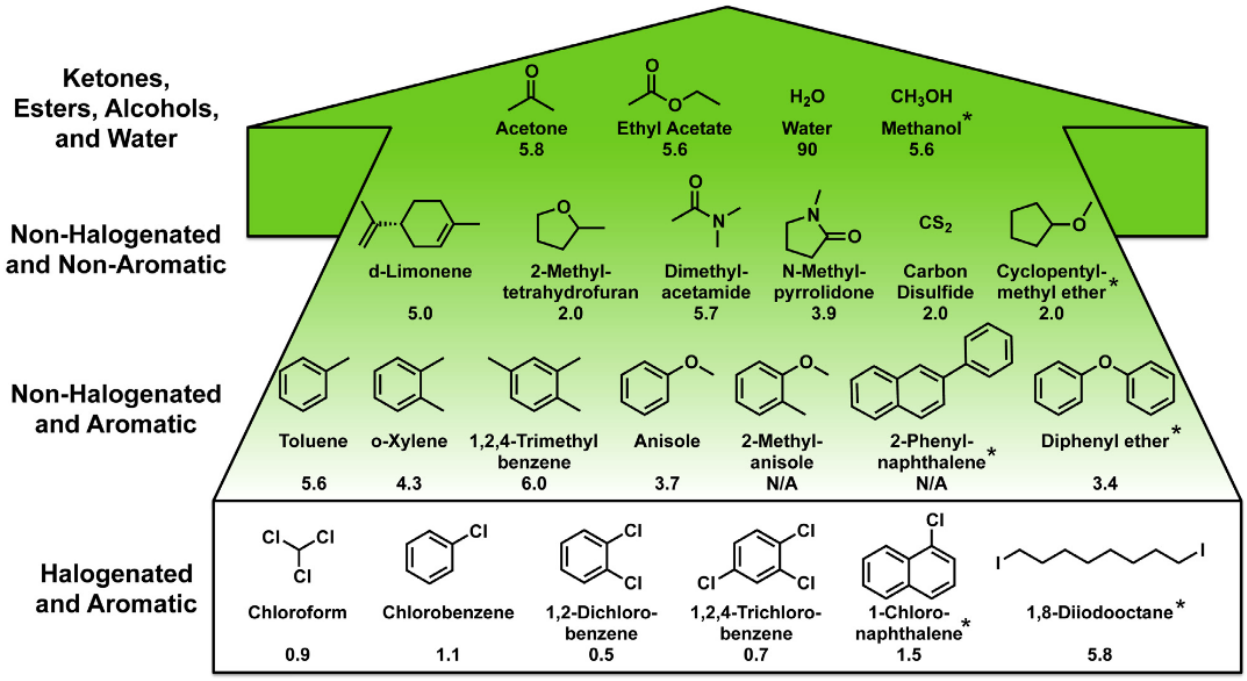

Figure 2-9 General classification of solvents used in the fabrication of BHJ solar cells, median lethal dose (LD50) values of organic solvents (in g/kg for rats by oral administration) give a relative assessment of toxicity.[88]

Wan et.al have recently demonstrated high-performance OPV (PCE ~ 16%) based on donor polymer PM6 and low bandgap NFA (BF-OC), where the active layer was sequentially (layer-by-layer) deposited by spin coating using non-halogenated solvent (o-Xylene).[89] In the field of OPV, the employment of scalable printing techniques with green solvents has been given very little attention, despite the fact that it is one of the key drivers for their mass-production and commercialization. This is a critical area of research which requires further attention.

2.7 Overview of OPV photoactive materials

Over the last three decades, a plethora of organic materials have been developed for OPV devices.[90]–[92] The introduction of the concept of polymer/fullerene bulk heterojunction in 1992 first directed OPV research towards the development of conjugated donor polymers. Since the 2010s, non-fullerene acceptors (NFA), including polymers and small molecules, have become the focus of many research efforts, in order to overcome the weak light absorption of the fullerenes

which limits their contribution to the photogeneration process. The current state-of-the-art NFA-based BHJ OPVs are approaching the performance of silicon solar cells, with PCEs ~ 19%. Although all-polymer and all-small molecule based BHJ OPVs have been demonstrated[93], the large majority of studies use polymers as donors and small molecules as acceptors.

2.7.1 Donor Polymers

Poly(3-hexylthiophene (P3HT) is an electron-donor polymer, which has been extensively used in the photoactive layer of OPVs.[94] The popularity of P3HT results from its comparatively easy synthesis, low cost and possibility of large-scale manufacturing. However, P3HT-based OPV devices typically have low PCE (<6%), mainly due to the wide bandgap of P3HT (~1.9 eV) which limits the absorption of low-energy photons. In order to expand the absorption range, considerable efforts have been directed towards the synthesis of conjugated polymer donors with low optical bandgaps (~ 1.4 eV).[95] The chemical structures of the most commonly used commercially available polymer donors, including P3HT, are shown in **Figure 2-10**. Optical and electronic properties of conjugated polymers have been optimized through the "push-pull" polymer design which consists of alternating electron-rich and electron-deficient units.[96] The intrinsic optical and electronic characteristics of push-pull conjugated polymers can be tuned by controlling the intramolecular charge transfer from donor unit to acceptor unit through the rational selection of

the two moieties. PBDB-T, PTQ10 and PTB7 polymers have emerged as top performing donor materials, capable of achieving PCEs greater than 17%.[97]

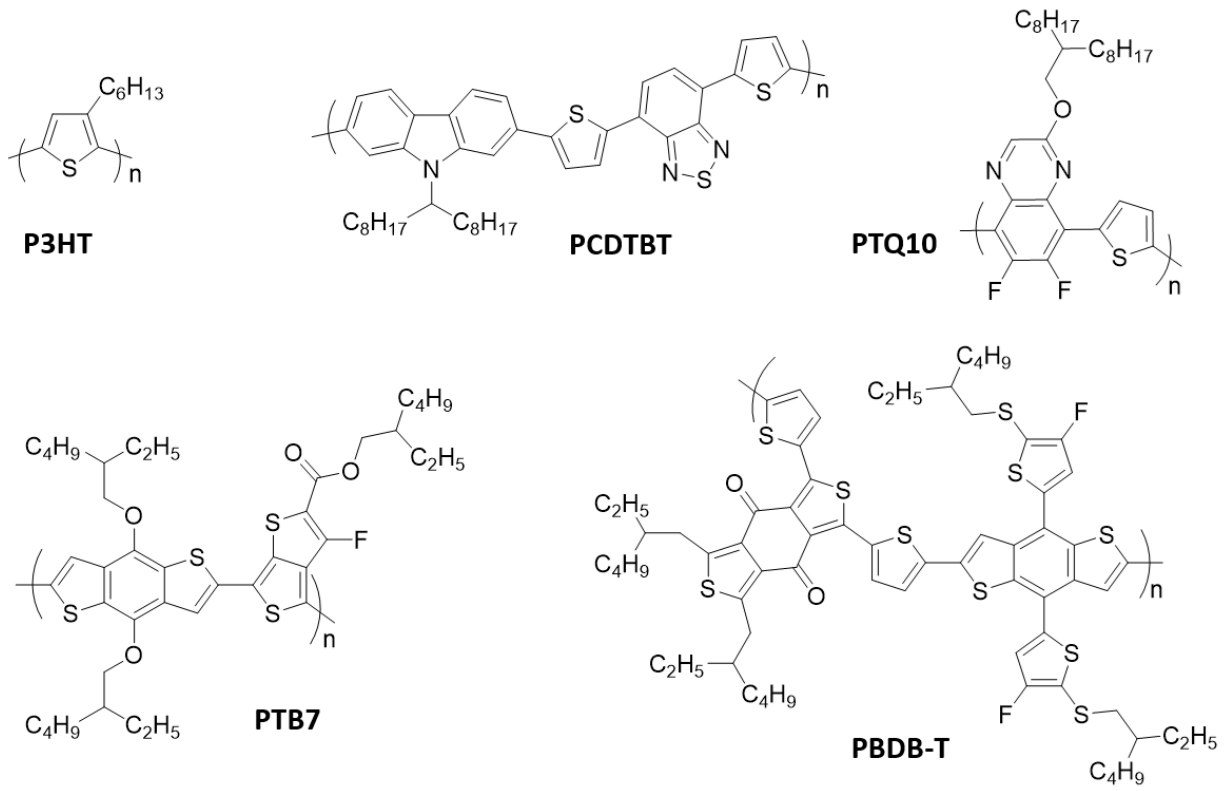

Figure 2-10 Molecular structures of some commercially available polymer donors (P3HT, PCDTBT, PTQ10, PTB7, and PBDB=T)

2.7.2 Small molecule acceptors

The fullerene derivative $PC_{61}BM$ is one of the most popular electron-accepting semiconductors in BHJ OPVs. $PC_{61}BM$ is a soluble form of fullerene C_{60}, also known as Buckminsterfullerene, and was first reported by Fred Wudl and co-workers in 1995.[98] $PC_{61}BM$ has been shown to have a high electron mobility ($\mu_e \sim 0.001\text{-}1\ cm^2v^{-1}s^{-1}$),[99], [100] and the ability to form controllable domain size with polymers in a BHJ structure for effective photocurrent generation. However, it has a low absorption in the visible region which limits the current density (J_{SC}) and a deep LUMO which limits the open circuit voltage (V_{OC}). Alternative fullerene compounds have been introduced to overcome these limitations. These include [6,6]-Phenyl-C_{71}-butyric acid methyl ester ($PC_{71}BM$), which has a lower symmetry, allowing broader absorption,

[101] and Indene-C60 bisadduct (ICBA) acceptor with a shallower LUMO energy level, demonstrating increased V_{OC} when blended with P3HT.[102] Another class of acceptor molecules are perylene diimide (PDI) derivatives, of which a representative (monomer) is depicted in **Figure 2.11**. PDIs, well-studied organic dyes, have substantial absorption in the visible spectrum and outstanding electrical properties, including high charge carrier mobility.[103] PDIs-based OPVs have relatively low PCEs compared to devices made with fullerenes due to the strong tendency of molecular aggregation and high degree of phase separations.[104]–[106] Nazari et al. synthesized a series of N-annulated PDI based on benzyl substitution and achieved PCEs of 4.9% and 5.8% when mixed with PTB7-Th and TTFQx-T1 polymers, respectively.[107] Laventure et al. demonstrated the highest Voc (1.12 V) using a blend of N-annulated PDI and PTB7-Th polymer, processed with the green solvent 1,2,4-trimethylbenzene (TMB).[108] The same research group has reported N-H annulated PDI synthesis and achieved a PCE of 6.3 % with quinoxaline-based polymer TTFQx-T.[109] These different studies show that PDI dimer and tetramer have shown promising results in OPVs.

NFAs are commonly designed to absorb at longer wavelengths than donor polymers in order to enhance spectral coverage in OPV devices. Typically, an electron-rich core flanked by two electron-poor moieties in a push-pull structure is used to achieve low bandgap material with red-shifted absorption. In 2015, Lin et al. synthesized a high performing NFA, ITIC, composed of an indacenodithienothiophene core surrounded by two dicyanovinylindanone groups. The ITIC paired with Poly([2,6′-4,8-di(5-ethylhexylthienyl)benzo[1,2-b;3,3-b]dithiophene]{3-fluoro-2[(2-ethylhexyl)carbonyl]thieno[3,4-b]thiophenediyl}) (PTB7-Th) exhibit PCE of 6.8%.[110] In addition, the same NFA shows high V_{OC} (~ 1 V) and PCEs above 12%, when combined with the wide bandgap ($E_g = 1.92\ eV$) poly[(thiophene)-alt-(6,7-difluoro-2-(2-hexyldecyloxy)quinoxaline)] (PTQ10) polymer.[111] PCEs over 10% were also achieved by different derivatives of ITIC: methylated (ITIC-M),[47] chlorinated (ITIC-2Cl),[112] and fluorinated (ITIC-2F)[113]. The development of ITIC addressed many of the drawbacks of fullerene acceptors, providing high electron mobility, absorption up to 700 nm, and a LUMO of 3.8 eV. Other commercially available NFAs include O-IDTBR, which has been shown to achieve a PCE greater than 6% in P3HT-based devices processed by printing techniques,[114] and Y6 with a PCE of 18%[49]. Recently, Chui et al. synthesized and reported ternary OPV with a new NFA (eC9-2Cl) paired with the wide bandgap

polymer donor (PBQx-TF) and achieved a high record PCE of 19%[115] for single junction OPVs. Chemical structures of some commercially available acceptors used in BHJ OPVs are shown in **Figure 2-11**.

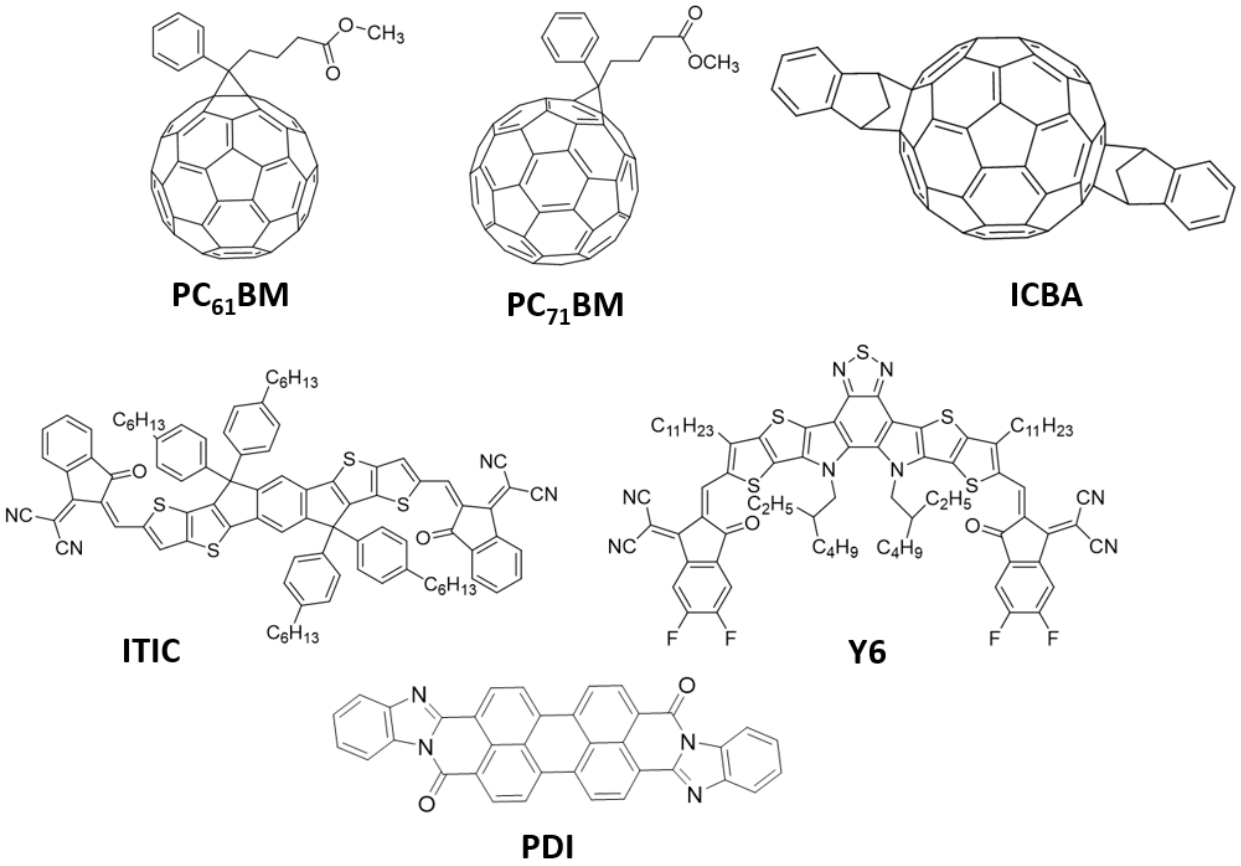

Figure 2-11 Molecular structures of some commercially available fullerene and non-fullerene acceptor materials ($PC_{61}BM$, $PC_{71}BM$, ICBA, ITIC, PDI, and Y6).

2.7.3 Silicon Phthalocyanines in OPV

Organic dye molecules could be potential low-cost materials for solution processable OPVs, where they can be used as donors, acceptors, or additives. Several functionalized dye molecules have previously been reported in OPV applications including squaraine,[116] BODIPY,[117] PDI,[118] PBI, porphyrins,[119] and of greater interest to this thesis: phthalocyanines.

Metal and Metalloid phthalocyanines (MPcs) are planar conjugated macrocycles which chelates a metal inclusion (**Figure 2.12a**). MPcs have a characteristic dark blue/green color due to the high degree of conjugation of their core. They are produced annually on the kiloton scale and used as commercial dyes.[120] Their electronic properties can be easily tuned through functionalization, either at the peripheral or/and axial positions (**Figure 2.12b).** The functional groups can facilitate tuning the physical and chemical properties of MPcs such as electronic energy level HOMO/LUMO, solubility, crystallization, nucleation, and solid-state interactions. MPcs have been widely studied in different optoelectronic devices such as organic light emitting diodes (OLED),[121]–[123] Organic thin-film transistor (OTFT),[124] and OPVs.[125] MPcs have also been used in other PV technologies such as DSSC,[126] and as interfacial layers in Perovskite solar cells.[127] The first bilayer OPV device, reported by Tang, was fabricated using copper MPc (CuPc) paired with PDI as acceptor material. Most divalent MPcs such as CuPc or zinc MPc (ZnPc) are used as donor material, paired with either fullerene C_{60} or PDI derivatives.[128] CuPc and ZnPc in planar OPVs have achieved a PCE up to 3.6% and 4.5 % respectively.[129], [130]

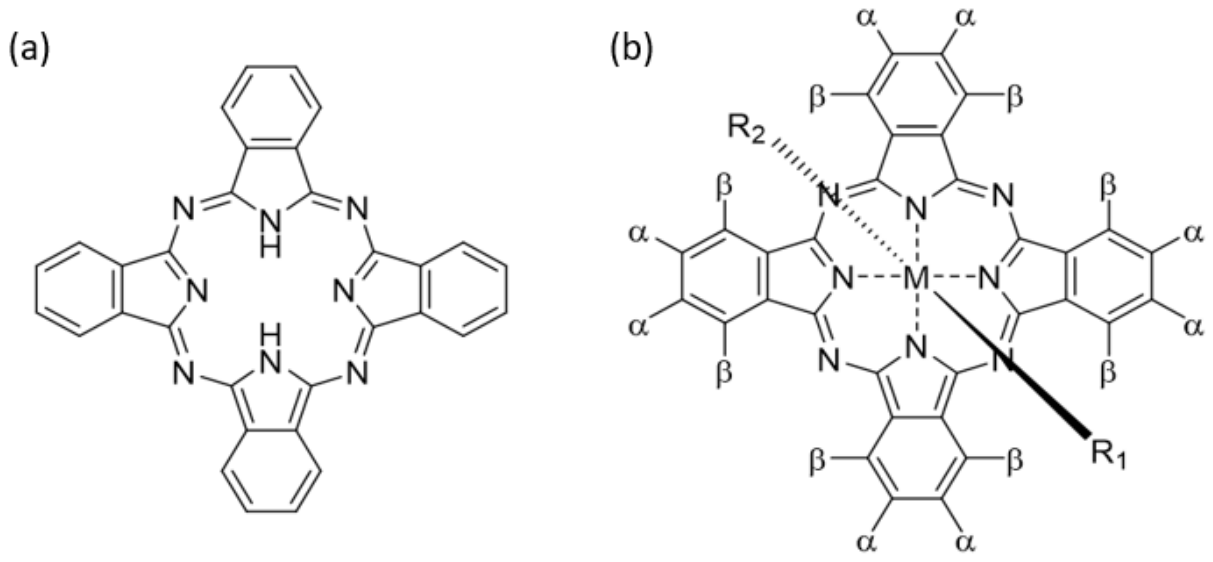

Figure 2-12 a) Metal-free Phthalocyanine, and (b) common structure for metal (M) peripheral (α, β) and axial (R1, R2) substituted Phthalocyanine

Silicon Phthalocyanines (R_2-SiPc) are an exciting class of MPcs which have emerged over the last decade. SiPc is tetravalent, which leads to two axial groups that are perpendicular to the MPc plane and are effective handles for the functionalization of the R_2-SiPc. R_2-SiPc therefore has better solubility due to the easy substitution of soluble functional groups in axial positions. The versatility of the axial groups for the R_2-SiPc has made them exciting active materials for both planar and BHJ OPVs.[131]–[134] Wheeler et.al (1984) were the first to report the synthesis of the R_2-SiPc derivative and its photophysical properties. Honda et al. reported the first integration of R_2-SiPcs in OPVs in 2009. They investigated bis (tri-n-hexylsilyl oxide) silicon phthalocyanine ($(3HS)_2$-SiPc), as a ternary additive in P3HT:PC_{61}BM based BHJ OPVs. They found that adding as little as 10 wt.% $(3HS)_2$-SiPc produced a 50% increase in *Jsc* and a 20% increase in PCE. The bulky axial groups of $(3HS)_2$-SiPc suppressed the formation of dye aggregations in the ternary film. The improvement in performance results from the combination of effective cascade energy transfer,[132], [135], [136] as a result of $(3HS)_2$-SiPc migration to the P3HT:PC_{61}BM interface, an additional EQE contribution from $(3HS)_2$-SiPc in an extended wavelength range of 650-700 nm.[137] Other studies have since investigated different axial groups of R_2-SiPcs to enhance the morphology and the performance of OPVs. Xu et al, designed an asymmetric R_2-SiPc additive with hexyl groups compatible with the P3HT and benzyl groups compatible with the PC_{61}BM, resulting in a 30% increase in PCE in comparison to the binary BHJ OPV device.[138] They showed that the optimal R_2-SiPcs are selectively located at P3HT/PC_{61}B interface, suppressing bimolecular recombination in the ternary blend films.

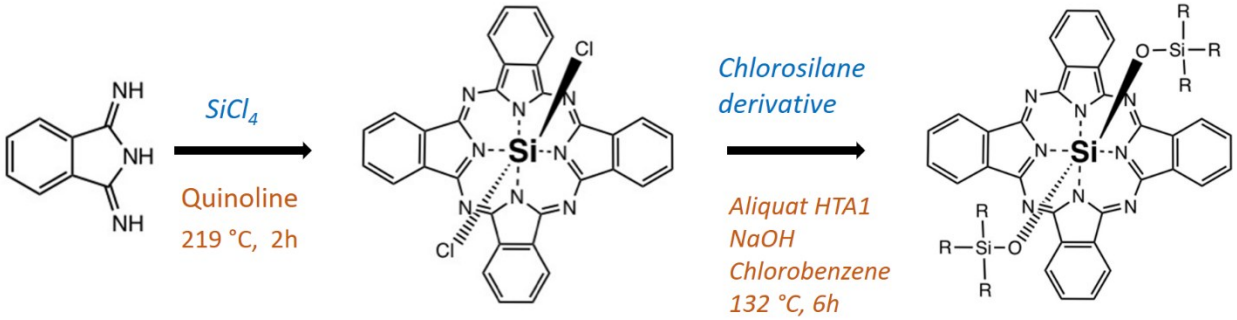

Figure 2-13 Synthetic pathways for Cl2-SiPc and commonly utilized R2-SiPc derivatives reported in literature.[139]

Ke et al. have developed a novel series of pyrene-substituted silicon Phthalocyanines (SiPc-Pys) with various lengths of alkyl chain tethers. UV–vis and EQE results show efficient near-IR sensitization up to 800 nm, which clearly establishes the influence of the pyrene substitution. This results in an increase of over 20% in J_{SC} and over 50% in the PCE for the dye-sensitized ternary device. In addition, the optical and electrical characteristics of the compound indicated that the length of the alkyl chains that are located between the core and the pyrene ligands controls the intermolecular and intramolecular interactions in the solid state. [133], [140] Lessard et al. (2014) reported a multifunctional R_2-SiPc derivative-based OPV with enhanced photogeneration that improved photon-to-electron conversion. Devices demonstrate long stability as a result of cross-linking of the azide group which freezes the optimal morphology.[141]

Dang et al studied bis(tri-nbutylsilyl oxide) silicon phthalocyanine ($(3BS)_2$-SiPc) and bis(tri-n-isopropylsilyl oxide) silicon phthalocyanine ($(3TS)_2$-SiPc), and investigated the effect of the length of the alkyl chain of $(3BS)_2$-SiPc on its properties.[142] Both $(3BS)_2$-SiPc and $(3TS)_2$-SiPc were able to increase J_{SC} when added to P3HT/PC_{61}BM based devices. In addition, thin film X-ray diffraction (XRD) studies revealed that the shorter alkyl chain derivatives have a tendency to form smaller crystalline domains, increasing the possibilities of migration at the P3HT/PC_{61}BM interface. Honda et al. studied a silicon naphthalocyanine (SiNc) based ternary additive that was further functionalized with tri-n-hexylsilyl axial substituents, achieving an extended EQE contribution around 750-800 nm and an improved Jsc for P3HT:PC_{61}BM and P3HT:N2200 blend devices.[134], [143] Furthermore, Lim et al. demonstrated that the addition of tert-butyl-functional groups to silicon 2,3-naphthalocyanine bis(trihexylsilyloxide) improved the dye's solubility in the P3HT:PC_{61}BM blend, allowing the use of higher dye concentration.[144] This increased the NIR absorption of the ternary additive resulting in up to 40% increase in the photogeneration current and a maximum PCE of 4.5%, compared to the PCE of 3.8% of baseline P3HT:PC_{61}BM device.

Although R_2-SiPcs have been primarily used as ternary additives in BHJ-based OPVs, their excellent electron mobility has also motivated their use as non-fullerene acceptors (NFA). Dong et al. reported the use of bis(tri-n-isopropylsilyl oxide) ($(3TS)_2$-SiPc) as NFA in combination with P3HT donor polymer and achieved a PCE up to 1.1%. In a different study, Zysman-Colman et al

achieved a PCE of 2.7%, using a blend of PTB7 and highly soluble carboxylate substituted R2-SiPc.

Vebber et al. reported the use of an axially substituted R_2-SiPc derivative $(3BS)_2$-SiPc with a combination of PTB7 polymer. They obtained a high V_{OC} (~1.07 V) and retained 80% of the PCE when compared to their PCBM counterpart.[145] Recently, Grant et al. used axially substituted R2-SiPc in combination with P3HT and PDDB-T donor polymers, demonstrating PCEs of 3.4 % and 3.6 % respectively and V_{OC}s above 1.1 V.[146] In another report, the same authors have used $(3PS)_2$-SiPc as an NFA with P3HT, showing a record PCE over 4.3%.[147] The morphology of these devices were significantly improved through optimal phase separation due to the unique crystallization property of $(3PS)_2$-SiPc. Vebber et al. studied thermodynamic properties of axial substituted SiPcs ($(R_3SiO)_2$-SiPc), paired with P3HT in OPV devices. The relationship between the critical radius, nucleation rate, and device performance was established. The smaller critical radius of active films shows a higher device performance (PCE of 4.4%).[148] This study reveals the importance of axial chain lengths of SiPc in thin film formation with different drying kinetics, which is a highly important factor in the scalability of the process.

However, all of the devices reported in the aforementioned studies have a small active area and are spin-coated on glass substrates. In **Chapters 3-5** of this thesis, I will discuss the investigations of R_2-SiPc as a ternary additive and as a NFA in OPVs processed by a large-scale deposition method: blade coating.

2.14 References

[1] Y. Abd El Aziz, *Renewables 2022 Global Status Report Germany Factsheet*. 2022.

[2] Canadian Energy Regulator, "CER – Canada's Energy Future 2021 - Key Findings," 2021, [Online]. Available: https://www.cer-rec.gc.ca/en/data-analysis/canada-energy-future/2021/key-findings.html.

[3] N. Gasparini, "Controlling charge carrier recombination in ternary organic solar cells," p. 167, 2017.

[4] D. M. Chapin, C. S. Fuller, and G. L. Pearson, "A new silicon p-n junction photocell for converting solar radiation into electrical power [3]," *J. Appl. Phys.*, vol. 25, no. 5, pp. 676–677, 1954, doi: 10.1063/1.1721711.

[5] "National Renewable Energy Laboratory, https://www.nrel.gov/pv/assets/pdfs/best-research-cell-efficiencies-rev220630.pdf," p. 2020, 2020.

[6] H. Spanggaard and F. C. Krebs, "A brief history of the development of organic and polymeric photovoltaics," *Sol. Energy Mater. Sol. Cells*, vol. 83, no. 2–3, pp. 125–146, 2004, doi: 10.1016/j.solmat.2004.02.021.

[7] P. R. I. F. O. R. S. E. S. ISE, "Photovoltaics Report," no. September, 2012.

[8] J. Jean, P. R. Brown, R. L. Jaffe, T. Buonassisi, and V. Bulović, "Pathways for solar photovoltaics," *Energy Environ. Sci.*, vol. 8, no. 4, pp. 1200–1219, 2015, doi: 10.1039/c4ee04073b.

[9] D. M. Bagnall and M. Boreland, "Photovoltaic technologies," *Energy Policy*, vol. 36, no. 12, pp. 4390–4396, 2008, doi: 10.1016/j.enpol.2008.09.070.

[10] G. A. R. Benatto, F. C. Krebs, J. W. Andreasen, E. Wang, and ..., *Large scale roll-to-roll produced organic photovoltaic devices: manufacturing, lifetime and environmental impact*. 2017.

[11] "Best Research-Cell Efficiencies," p. 2020, 2020.

[12] N. Espinosa, M. Hösel, D. Angmo, and F. C. Krebs, "Solar cells with one-day energy payback for the factories of the future," *Energy Environ. Sci.*, vol. 5, no. 1, pp. 5117–5132, 2012, doi: 10.1039/c1ee02728j.

[13] "Organic PV Solar Cells Market Size, Regional Outlook, Application Growth Potential, Competitive Market Growth & Forecast, 2022 – 2028." https://www.gminsights.com/industry-analysis/organic-pv-solar-cells-market#.

[14] "Organic PV Solar Cells Market Size, Regional Outlook, Application Growth Potential, Competitive Market Growth & Forecast, 2022 – 2028," *Global Market Insights*, 2021. https://www.gminsights.com/industry-analysis/organic-pv-solar-cells-market#.

[15] S. Berny *et al.*, "Solar trees: First large-scale demonstration of fully solution coated, semitransparent, flexible organic photovoltaic modules," *Adv. Sci.*, vol. 3, no. 5, pp. 1–7, 2015, doi: 10.1002/advs.201500342.

[16] J. L. Bré das, J. P. Calbert, D. A. da Silva Filho, and J. Cornil, "Organic semiconductors: A theoretical characterization of the basic parameters governing charge transport," 2002. [Online]. Available: www.pnas.orgcgidoi10.1073pnas.092143399.

[17] J. D. Servaites, M. A. Ratner, and T. J. Marks, "Practical efficiency limits in organic photovoltaic cells: Functional dependence of fill factor and external quantum efficiency," *Appl. Phys. Lett.*, vol. 95, no. 16, pp. 1–4, 2009, doi: 10.1063/1.3243986.

[18] M. C. Scharber *et al.*, "Design rules for donors in bulk-heterojunction solar cells - Towards 10 % energy-conversion efficiency," *Adv. Mater.*, vol. 18, no. 6, pp. 789–794, 2006, doi: 10.1002/adma.200501717.

[19] H. Zhong *et al.*, "Fused dithienogermolodithiophene low band gap polymers for high-performance organic solar cells without processing additives," *J. Am. Chem. Soc.*, vol. 135, no. 6, pp. 2040–2043, 2013, doi: 10.1021/ja311700u.

[20] K. Colladet *et al.*, "Low band gap donor-acceptor conjugated polymers toward organic solar cells applications," *Macromolecules*, vol. 40, no. 1, pp. 65–72, 2007, doi: 10.1021/ma061760i.

[21] D. Mo *et al.*, "Chlorination of Low-Band-Gap Polymers: Toward High-Performance Polymer Solar Cells," *Chem. Mater.*, vol. 29, no. 7, pp. 2819–2830, 2017, doi: 10.1021/acs.chemmater.6b04828.

[22] G. Itskos *et al.*, "Optical properties of organic semiconductor blends with near-infrared quantum-dot sensitizers for light harvesting applications," *Adv. Energy Mater.*, vol. 1, no. 5, pp. 802–812, 2011, doi: 10.1002/aenm.201100182.

[23] J. N. De Freitas, I. R. Grova, L. C. Akcelrud, E. Arici, N. S. Sariciftci, and A. F. Nogueira,

"The effects of CdSe incorporation into bulk heterojunction solar cells," *J. Mater. Chem.*, vol. 20, no. 23, pp. 4845–4853, 2010, doi: 10.1039/c0jm00191k.

[24] Y. Zhu *et al.*, "Improved performances of PCDTBT:PC71BM BHJ solar cells through incorporating small molecule donor," *Phys. Chem. Chem. Phys.*, vol. 17, no. 40, pp. 26777–26782, 2015, doi: 10.1039/c5cp03888j.

[25] B. Ananda Rao *et al.*, "Effect of incorporation of squaraine dye on the photovoltaic response of bulk heterojunction solar cells based on P3HT:PC70BM blend," *ACS Sustain. Chem. Eng.*, vol. 2, no. 7, pp. 1743–1751, 2014, doi: 10.1021/sc500276u.

[26] J. Gilot, I. Barbu, M. M. Wienk, and R. A. J. Janssen, "The use of ZnO as optical spacer in polymer solar cells: Theoretical and experimental study," *Appl. Phys. Lett.*, vol. 91, no. 11, 2007, doi: 10.1063/1.2784961.

[27] T. K. S. Wong, "Effect of embedded nanoparticle surface chemistry on plasmonic organic photovoltaic devices," *Mater. Renew. Sustain. Energy*, vol. 6, no. 1, pp. 1–16, 2017, doi: 10.1007/s40243-017-0087-3.

[28] X. G. Mbuyise, E. A. A. Arbab, and G. T. Mola, "The effect of a trimetallic nanocomposite in the solar absorber layer of organic solar cells," *RSC Adv.*, vol. 9, no. 11, pp. 6070–6076, 2019, doi: 10.1039/c8ra08725c.

[29] B. C. Thompson and J. M. J. Fréchet, "Polymer-fullerene composite solar cells," *Angew. Chemie - Int. Ed.*, vol. 47, no. 1, pp. 58–77, 2008, doi: 10.1002/anie.200702506.

[30] S. R. Scully and M. D. McGehee, "Effects of optical interference and energy transfer on exciton diffusion length measurements in organic semiconductors," *J. Appl. Phys.*, vol. 100, no. 3, 2006, doi: 10.1063/1.2226687.

[31] T. M. Clarke and J. R. Durrant, "Charge photogeneration in organic solar cells," *Chem. Rev.*, vol. 110, no. 11, pp. 6736–6767, 2010, doi: 10.1021/cr900271s.

[32] A. W. Hains, Z. Liang, M. A. Woodhouse, and B. A. Gregg, "Molecular semiconductors in organic photovoltaic cells," *Chem. Rev.*, vol. 110, no. 11, pp. 6689–6735, 2010, doi: 10.1021/cr9002984.

[33] T. M. Burke and M. D. McGehee, "How high local charge carrier mobility and an energy cascade in a three-phase bulk heterojunction enable >90% quantum efficiency," *Adv. Mater.*, vol. 26, no. 12, pp. 1923–1928, 2014, doi: 10.1002/adma.201304241.

[34] G. Grancini *et al.*, "Hot exciton dissociation in polymer solar cells," *Nat. Mater.*, vol. 12,

no. 1, pp. 29–33, 2013, doi: 10.1038/nmat3502.

[35] B. P. Lyons, N. Clarke, and C. Groves, "The relative importance of domain size, domain purity and domain interfaces to the performance of bulk-heterojunction organic photovoltaics," *Energy Environ. Sci.*, vol. 5, no. 6, pp. 7657–7663, 2012, doi: 10.1039/c2ee21327c.

[36] N. S. Sariciftci, L. Smilowitz, A. J. Heeger, and F. Wudl, "Photoinduced electron transfer from a conducting polymer to buckminsterfullerene," *Science (80-.).*, vol. 258, no. 5087, pp. 1474–1476, 1992, doi: 10.1126/science.258.5087.1474.

[37] Y. Firdaus *et al.*, "Key Parameters Requirements for Non-Fullerene-Based Organic Solar Cells with Power Conversion Efficiency >20%," *Adv. Sci.*, vol. 6, no. 9, 2019, doi: 10.1002/advs.201802028.

[38] P. Schilinsky, C. Waldauf, and C. J. Brabec, "Recombination and loss analysis in polythiophene based bulk heterojunction photodetectors," *Appl. Phys. Lett.*, vol. 81, no. 20, pp. 3885–3887, 2002, doi: 10.1063/1.1521244.

[39] S. R. Cowan, A. Roy, and A. J. Heeger, "Recombination in polymer-fullerene bulk heterojunction solar cells," *Phys. Rev. B - Condens. Matter Mater. Phys.*, vol. 82, no. 24, pp. 1–10, 2010, doi: 10.1103/PhysRevB.82.245207.

[40] J. Kurpiers *et al.*, "Probing the pathways of free charge generation in organic bulk heterojunction solar cells," *Nat. Commun.*, vol. 9, no. 1, pp. 1–11, 2018, doi: 10.1038/s41467-018-04386-3.

[41] L. J. A. Koster, V. D. Mihailetchi, and P. W. M. Blom, "Bimolecular recombination in polymer/fullerene bulk heterojunction solar cells," *Appl. Phys. Lett.*, vol. 88, no. 5, pp. 1–3, 2006, doi: 10.1063/1.2170424.

[42] M. M. Mandoc, F. B. Kooistra, J. C. Hummelen, B. De Boer, and P. W. M. Blom, "Effect of traps on the performance of bulk heterojunction organic solar cells," *Appl. Phys. Lett.*, vol. 91, no. 26, pp. 91–94, 2007, doi: 10.1063/1.2821368.

[43] M. Kuik, L. J. A. Koster, G. A. H. Wetzelaer, and P. W. M. Blom, "Trap-assisted recombination in disordered organic semiconductors," *Phys. Rev. Lett.*, vol. 107, no. 25, pp. 1–5, 2011, doi: 10.1103/PhysRevLett.107.256805.

[44] L. J. A. Koster, V. D. Mihailetchi, R. Ramaker, and P. W. M. Blom, "Light intensity dependence of open-circuit voltage of polymer:fullerene solar cells," *Appl. Phys. Lett.*, vol.

86, no. 12, pp. 1–3, 2005, doi: 10.1063/1.1889240.

[45] I. Riedel, J. Parisi, V. Dyakonov, L. Lutsen, D. Vanderzande, and J. C. Hummelen, "Effect of temperature and illumination on the electrical characteristics of polymer-fullerene bulk-heterojunction solar cells," *Adv. Funct. Mater.*, vol. 14, no. 1, pp. 38–44, 2004, doi: 10.1002/adfm.200304399.

[46] A. J. Yu, G.; Gao, J.; Hummelen, J. C.; Wudl, F.; Heeger, "Polymer Photovoltaic Cells : Enhanced Efficiencies via a Network of Internal Donor-Acceptor Heterojunctions," *Science (80-.).*, vol. 270, pp. 1789–1791, 1995.

[47] S. Li *et al.*, "Energy-Level Modulation of Small-Molecule Electron Acceptors to Achieve over 12% Efficiency in Polymer Solar Cells," *Adv. Mater.*, vol. 28, no. 42, pp. 9423–9429, 2016, doi: 10.1002/adma.201602776.

[48] K. Narayanaswamy *et al.*, "Impact of A-D-A Structured Dithienosilole and Phenoxazine based Small Molecular Material for Bulk Heterojunction and Dopant-free Perovskite Solar Cells," *Chem. – A Eur. J.*, 2019, doi: 10.1002/chem.201903599.

[49] Q. Liu *et al.*, "18% Efficiency organic solar cells," *Sci. Bull.*, vol. 65, no. 4, pp. 272–275, 2020, doi: 10.1016/j.scib.2020.01.001.

[50] Y. Cui *et al.*, "Over 16% efficiency organic photovoltaic cells enabled by a chlorinated acceptor with increased open-circuit voltages," *Nat. Commun.*, vol. 10, no. 1, pp. 1–8, 2019, doi: 10.1038/s41467-019-10351-5.

[51] Y. Lin *et al.*, "17% Efficient Organic Solar Cells Based on Liquid Exfoliated WS2 as a Replacement for PEDOT:PSS," *Adv. Mater.*, vol. 31, no. 46, 2019, doi: 10.1002/adma.201902965.

[52] L. Hong *et al.*, "Eco-Compatible Solvent-Processed Organic Photovoltaic Cells with Over 16% Efficiency," *Adv. Mater.*, vol. 31, no. 39, pp. 1–7, 2019, doi: 10.1002/adma.201903441.

[53] Y. Xia, *Polymer / polymer blends in organic photovoltaic and photodiode devices*, no. 1974. 2018.

[54] A. Facchetti, "Polymer donor-polymer acceptor (all-polymer) solar cells," *Mater. Today*, vol. 16, no. 4, pp. 123–132, 2013, doi: 10.1016/j.mattod.2013.04.005.

[55] S. D. Collins, N. A. Ran, M. C. Heiber, and T. Q. Nguyen, "Small is Powerful: Recent Progress in Solution-Processed Small Molecule Solar Cells," *Adv. Energy Mater.*, vol. 7,

no. 10, 2017, doi: 10.1002/aenm.201602242.

[56] A. Venkateswararao and K. T. Wong, "Small molecules for vacuum-processed organic photovoltaics: Past, current status, and prospect," *Bull. Chem. Soc. Jpn.*, vol. 94, no. 3, pp. 812–838, 2021, doi: 10.1246/BCSJ.20200330.

[57] H. Hoppe and N. S. Sariciftci, "Morphology of polymer/fullerene bulk heterojunction solar cells," *J. Mater. Chem.*, vol. 16, no. 1, pp. 45–61, 2006, doi: 10.1039/b510618b.

[58] S. Almosni *et al.*, "Material challenges for solar cells in the twenty-first century: directions in emerging technologies," *Sci. Technol. Adv. Mater.*, vol. 19, no. 1, pp. 336–369, 2018, doi: 10.1080/14686996.2018.1433439.

[59] Z. Li *et al.*, "Toward Improved Lifetimes of Organic Solar Cells under Thermal Stress: Substrate-Dependent Morphological Stability of PCDTBT:PCBM Films and Devices," *Sci. Rep.*, vol. 5, no. October, pp. 1–9, 2015, doi: 10.1038/srep15149.

[60] T. Plint, B. H. Lessard, and T. P. Bender, "Assessing the potential of group 13 and 14 metal/metalloid phthalocyanines as hole transport layers in organic light emitting diodes," *J. Appl. Phys.*, vol. 119, no. 14, 2016, doi: 10.1063/1.4945377.

[61] A. K. K. Kyaw *et al.*, "Intensity dependence of current-voltage characteristics and recombination in high-efficiency solution-processed small-molecule solar cells," *ACS Nano*, vol. 7, no. 5, pp. 4569–4577, 2013, doi: 10.1021/nn401267s.

[62] S. Alem, J. Lu, R. Movileanu, T. Kololuoma, A. Dadvand, and Y. Tao, "Solution-processed annealing-free ZnO nanoparticles for stable inverted organic solar cells," *Org. Electron.*, vol. 15, no. 5, pp. 1035–1042, 2014, doi: 10.1016/j.orgel.2014.02.024.

[63] J. H. Chang, Y. H. Chen, H. W. Lin, Y. T. Lin, H. F. Meng, and E. C. Chen, "Highly efficient inverted rapid-drying blade-coated organic solar cells," *Org. Electron.*, vol. 13, no. 4, pp. 705–709, 2012, doi: 10.1016/j.orgel.2011.12.025.

[64] J. S. Yu *et al.*, "Silver front electrode grids for ITO-free all printed polymer solar cells with embedded and raised topographies, prepared by thermal imprint, flexographic and inkjet roll-to-roll processes," *Nanoscale*, vol. 4, no. 19, pp. 6032–6040, 2012, doi: 10.1039/c2nr31508d.

[65] S. Yu *et al.*, "Performance Enhancement of Ternary Polymer Solar Cells Induced by Tetrafluorotetracyanoquinodimethane Doping," *Chem. Mater.*, vol. 31, no. 18, pp. 7650–7656, 2019, doi: 10.1021/acs.chemmater.9b02520.

[66] L. Lu, M. A. Kelly, W. You, and L. Yu, "Status and prospects for ternary organic photovoltaics," *Nat. Photonics*, vol. 9, no. 8, pp. 491–500, 2015, doi: 10.1038/nphoton.2015.128.

[67] L. Zhu, R. Wang, J. Qiao, and F. Wu, "Enhanced photovoltaic performance of ternary solar cells by doping a new squaraine derivative," *Dye. Pigment.*, vol. 132, pp. 20–26, 2016, doi: 10.1016/j.dyepig.2016.04.038.

[68] L. Lu, T. Xu, W. Chen, E. S. Landry, and L. Yu, "Ternary blend polymer solar cells with enhanced power conversion efficiency," *Nat. Photonics*, vol. 8, no. 9, pp. 716–722, 2014, doi: 10.1038/nphoton.2014.172.

[69] H. Cha *et al.*, "Complementary absorbing star-shaped small molecules for the preparation of ternary cascade energy structures in organic photovoltaic cells," *Adv. Funct. Mater.*, vol. 23, no. 12, pp. 1556–1565, 2013, doi: 10.1002/adfm.201201913.

[70] A. Diacon, L. Derue, C. Lecourtier, O. Dautel, G. Wantz, and P. Hudhomme, "Cross-linkable azido C60-fullerene derivatives for efficient thermal stabilization of polymer bulk-heterojunction solar cells," *J. Mater. Chem. C*, vol. 2, no. 35, pp. 7163–7167, 2014, doi: 10.1039/c4tc01178c.

[71] A. Diaz de Zerio Mendaza *et al.*, "A fullerene alloy based photovoltaic blend with a glass transition temperature above 200 °C," *J. Mater. Chem. A*, vol. 5, no. 8, pp. 4156–4162, 2017, doi: 10.1039/c6ta08106a.

[72] C. and P. H. Riordan, "What is an Air mass 1.5 spectrum ?," *IEEE Conf. Photovolt. Spec.*, vol. 2, no. 2, pp. 1085–1088, 1990, doi: 10.1109/PVSC.1990.111784.

[73] S. Han, W. S. Shin, M. Seo, D. Gupta, S. J. Moon, and S. Yoo, "Improving performance of organic solar cells using amorphous tungsten oxides as an interfacial buffer layer on transparent anodes," *Org. Electron.*, vol. 10, no. 5, pp. 791–797, 2009, doi: 10.1016/j.orgel.2009.03.016.

[74] R. A. Street, K. W. Song, and S. Cowan, "Influence of series resistance on the photocurrent analysis of organic solar cells," *Org. Electron.*, vol. 12, no. 2, pp. 244–248, 2011, doi: 10.1016/j.orgel.2010.11.012.

[75] C. M. Proctor and T. Q. Nguyen, "Effect of leakage current and shunt resistance on the light intensity dependence of organic solar cells," *Appl. Phys. Lett.*, vol. 106, no. 8, 2015, doi: 10.1063/1.4913589.

[76] K. Li *et al.*, "Breakdown mechanisms and reverse current-voltage characteristics of organic bulk heterojunction solar cells and photodetectors," *J. Appl. Phys.*, vol. 115, no. 22, 2014, doi: 10.1063/1.4883501.

[77] J. L. Gray, *The Physics of the Solar Cell, in Handbook of Photovoltaic Science and Engineering,*. John Wiley and Sons, 2011.

[78] N. W. Scarratt, "The Fabrication and Scale-Up of Organic Photovoltaic Devices via Ultrasonic Spray Coating," no. September, 2015.

[79] N. K. Elumalai and A. Uddin, "Open circuit voltage of organic solar cells: An in-depth review," *Energy Environ. Sci.*, vol. 9, no. 2, pp. 391–410, 2016, doi: 10.1039/c5ee02871j.

[80] N. Gasparini *et al.*, "Exploiting Ternary Blends for Improved Photostability in High-Efficiency Organic Solar Cells," *ACS Energy Lett.*, vol. 5, no. 5, pp. 1371–1379, 2020, doi: 10.1021/acsenergylett.0c00604.

[81] J. W. Ha, C. E. Song, H. S. Kim, D. H. Ryu, W. S. Shin, and D. H. Hwang, "Highly Efficient and Photostable Ternary Organic Solar Cells Enabled by the Combination of Non-Fullerene and Fullerene Acceptors with Thienopyrrolodione-based Polymer Donors," *ACS Appl. Mater. Interfaces*, vol. 12, no. 46, pp. 51699–51708, 2020, doi: 10.1021/acsami.0c14367.

[82] F. C. Krebs, "Roll-to-roll fabrication of monolithic large-area polymer solar cells free from indium-tin-oxide," *Sol. Energy Mater. Sol. Cells*, vol. 93, no. 9, pp. 1636–1641, 2009, doi: 10.1016/j.solmat.2009.04.020.

[83] F. C. Krebs, "Polymer solar cell modules prepared using roll-to-roll methods: Knife-over-edge coating, slot-die coating and screen printing," *Sol. Energy Mater. Sol. Cells*, vol. 93, no. 4, pp. 465–475, 2009, doi: 10.1016/j.solmat.2008.12.012.

[84] J. E. Carlé, T. R. Andersen, M. Helgesen, E. Bundgaard, M. Jorgensen, and F. C. Krebs, "A laboratory scale approach to polymer solar cells using one coating/printing machine, flexible substrates, no ITO, no vacuum and no spincoating," *Sol. Energy Mater. Sol. Cells*, vol. 108, pp. 126–128, 2013, doi: 10.1016/j.solmat.2012.09.008.

[85] F. C. Krebs, "Fabrication and processing of polymer solar cells: A review of printing and coating techniques," *Sol. Energy Mater. Sol. Cells*, vol. 93, no. 4, pp. 394–412, 2009, doi: 10.1016/j.solmat.2008.10.004.

[86] K. Norrman, A. Ghanbari-Siahkali, and N. B. Larsen, "Studies of spin-coated polymer films," *Annu. Reports Prog. Chem. - Sect. C*, vol. 101, pp. 174–201, 2005, doi:

10.1039/b408857n.

[87] L. Wengeler, M. Schmitt, K. Peters, P. Scharfer, and W. Schabel, "Comparison of large scale coating techniques for organic and hybrid films in polymer based solar cells," *Chem. Eng. Process. Process Intensif.*, vol. 68, pp. 38–44, 2013, doi: 10.1016/j.cep.2012.03.004.

[88] C. McDowell and G. C. Bazan, "Organic solar cells processed from green solvents," *Curr. Opin. Green Sustain. Chem.*, vol. 5, pp. 49–54, 2017, doi: 10.1016/j.cogsc.2017.03.007.

[89] J. Wan *et al.*, "All-Green Solvent-Processed Planar Heterojunction Organic Solar Cells with Outstanding Power Conversion Efficiency of 16%," *Adv. Funct. Mater.*, vol. 32, no. 5, pp. 1–8, 2022, doi: 10.1002/adfm.202107567.

[90] A. Armin *et al.*, "A History and Perspective of Non-Fullerene Electron Acceptors for Organic Solar Cells," *Adv. Energy Mater.*, vol. 11, no. 15, 2021, doi: 10.1002/aenm.202003570.

[91] A. Venkateswararao, S. W. Liu, and K. T. Wong, "Organic polymeric and small molecular electron acceptors for organic solar cells," *Mater. Sci. Eng. R Reports*, vol. 124, pp. 1–57, 2018, doi: 10.1016/j.mser.2018.01.001.

[92] J. Hou, O. Inganas, R. H. Friend, and F. Gao, "Organic solar cells based on non-fullerene acceptors," *Nat. Mater.*, vol. 17, no. 2, pp. 119–128, 2018, doi: 10.1038/NMAT5063.

[93] Y. Wang, M. Chang, B. Kan, X. Wan, C. Li, and Y. Chen, "All-Small-Molecule Organic Solar Cells Based on Pentathiophene Donor and Alkylated Indacenodithiophene-Based Acceptors with Efficiency over 8%," *ACS Appl. Energy Mater.*, vol. 1, no. 5, pp. 2150–2156, 2018, doi: 10.1021/acsaem.8b00205.

[94] A. T. Kleinschmidt, S. E. Root, and D. J. Lipomi, "Poly(3-hexylthiophene) (P3HT): Fruit fly or outlier in organic solar cell research?," *J. Mater. Chem. A*, vol. 5, no. 23, pp. 11396–11400, 2017, doi: 10.1039/c6ta08317j.

[95] D. H. Lim, J. W. Ha, H. Choi, S. C. Yoon, B. R. Lee, and S. J. Ko, "Recent progress of ultra-narrow-bandgap polymer donors for NIR-absorbing organic solar cells," *Nanoscale Adv.*, vol. 3, no. 15, pp. 4306–4320, 2021, doi: 10.1039/d1na00245g.

[96] C. Duan, F. Huang, and Y. Cao, "Recent development of push-pull conjugated polymers for bulk-heterojunction photovoltaics: Rational design and fine tailoring of molecular structures," *J. Mater. Chem.*, vol. 22, no. 21, pp. 10416–10434, 2012, doi: 10.1039/c2jm30470h.

[97] Z. Zheng, H. Yao, L. Ye, Y. Xu, S. Zhang, and J. Hou, "PBDB-T and its derivatives: A family of polymer donors enables over 17% efficiency in organic photovoltaics," *Mater. Today*, vol. 35, no. May, pp. 115–130, 2020, doi: 10.1016/j.mattod.2019.10.023.

[98] J. C. Hummelen, B. W. Knight, F. Lepeq, F. Wudl, J. Yao, and C. L. Wilkins, "Preparation and Characterization of Fulleroid and Methanofullerene Derivatives," *J. Org. Chem.*, vol. 60, no. 3, pp. 532–538, 1995, doi: 10.1021/jo00108a012.

[99] A. Armin, S. Shoaee, Q. Lin, P. L. Burn, and P. Meredith, "On the unipolarity of charge transport in methanofullerene diodes," *npj Flex. Electron.*, vol. 1, no. 1, pp. 1–5, 2017, doi: 10.1038/s41528-017-0012-y.

[100] A. Devižis, D. Hertel, K. Meerholz, V. Gulbinas, and J. E. Moser, "Time-independent, high electron mobility in thin PC61BM films: Relevance to organic photovoltaics," *Org. Electron.*, vol. 15, no. 12, pp. 3729–3734, 2014, doi: 10.1016/j.orgel.2014.10.028.

[101] F. Zhang *et al.*, "Influence of PC60BM or PC70BM as electron acceptor on the performance of polymer solar cells," *Sol. Energy Mater. Sol. Cells*, vol. 97, pp. 71–77, 2012, doi: 10.1016/j.solmat.2011.09.006.

[102] Y. He, H. Y. Chen, J. Hou, and Y. Li, "Indene - C60 bisadduct: A new acceptor for high-performance polymer solar cells," *J. Am. Chem. Soc.*, vol. 132, no. 4, pp. 1377–1382, 2010, doi: 10.1021/ja908602j.

[103] C. Li and H. Wonneberger, "Perylene imides for organic photovoltaics: Yesterday, today, and tomorrow," *Adv. Mater.*, vol. 24, no. 5, pp. 613–636, 2012, doi: 10.1002/adma.201104447.

[104] V. Kamm *et al.*, "Polythiophene:perylene diimide solar cells - The impact of alkyl-substitution on the photovoltaic performance," *Adv. Energy Mater.*, vol. 1, no. 2, pp. 297–302, 2011, doi: 10.1002/aenm.201000006.

[105] T. Ye, R. Singh, H. J. Butt, G. Floudas, and P. E. Keivanidis, "Effect of local and global structural order on the performance of perylene diimide excimeric solar cells," *ACS Appl. Mater. Interfaces*, vol. 5, no. 22, pp. 11844–11857, 2013, doi: 10.1021/am4035416.

[106] R. Singh, E. Aluicio-Sarduy, Z. Kan, T. Ye, R. C. I. Mackenzie, and P. E. Keivanidis, "Fullerene-free organic solar cells with an efficiency of 3.7% based on a low-cost geometrically planar perylene diimide monomer," *J. Mater. Chem. A*, vol. 2, no. 35, pp. 14348–14353, 2014, doi: 10.1039/c4ta02851a.

[107] M. Nazari *et al.*, "Benzyl and fluorinated benzyl side chains for perylene diimide non-fullerene acceptors," *Mater. Chem. Front.*, vol. 2, no. 12, pp. 2272–2276, 2018, doi: 10.1039/c8qm00487k.

[108] A. Laventure, S. Stanzel, A. J. Payne, B. H. Lessard, and G. C. Welch, "A ring fused N-annulated PDI non-fullerene acceptor for high open circuit voltage solar cells processed from non-halogenated solvents," *Synth. Met.*, vol. 250, no. March, pp. 55–62, 2019, doi: 10.1016/j.synthmet.2019.02.010.

[109] A. Laventure, S. Stanzel, A. J. Payne, B. H. Lessard, and G. C. Welch, "N-Annulated perylene diimide dimers and tetramer non-fullerene acceptors: impact of solvent processing additive on their thin film formation behavior," *J. Chem. Technol. Biotechnol.*, vol. 97, no. 4, pp. 844–851, 2022, doi: 10.1002/jctb.6894.

[110] Y. Lin *et al.*, "An electron acceptor challenging fullerenes for efficient polymer solar cells," *Adv. Mater.*, vol. 27, no. 7, pp. 1170–1174, 2015, doi: 10.1002/adma.201404317.

[111] Z. Xu *et al.*, "Understanding the Morphology of High-Performance Solar Cells Based on a Low-Cost Polymer Donor," *ACS Appl. Mater. Interfaces*, vol. 12, no. 8, pp. 9537–9544, 2020, doi: 10.1021/acsami.9b22666.

[112] H. Zhang *et al.*, "Over 14% Efficiency in Organic Solar Cells Enabled by Chlorinated Nonfullerene Small-Molecule Acceptors," *Adv. Mater.*, vol. 30, no. 28, pp. 1–7, 2018, doi: 10.1002/adma.201800613.

[113] W. Zhao *et al.*, "Molecular Optimization Enables over 13% Efficiency in Organic Solar Cells," *J. Am. Chem. Soc.*, vol. 139, no. 21, pp. 7148–7151, 2017, doi: 10.1021/jacs.7b02677.

[114] N. Gasparini *et al.*, "Burn-in Free Nonfullerene-Based Organic Solar Cells," *Adv. Energy Mater.*, vol. 7, no. 19, 2017, doi: 10.1002/aenm.201700770.

[115] Y. Cui *et al.*, "Single-Junction Organic Photovoltaic Cell with 19% Efficiency," *Adv. Mater.*, vol. 33, no. 41, pp. 1–8, 2021, doi: 10.1002/adma.202102420.

[116] G. Chen, H. Sasabe, T. Igarashi, Z. Hong, and J. Kido, "Squaraine dyes for organic photovoltaic cells," *J. Mater. Chem. A*, vol. 3, no. 28, pp. 14517–14534, 2015, doi: 10.1039/c5ta01879j.

[117] N. Y. Doumon, L. Yang, and F. Rosei, "Ternary organic solar cells: A review of the role of the third element," *Nano Energy*, vol. 94, no. December 2021, 2022, doi:

10.1016/j.nanoen.2021.106915.

[118] K. Weng *et al.*, "Ternary organic solar cells based on two compatible PDI-based acceptors with an enhanced power conversion efficiency," *J. Mater. Chem. A*, vol. 7, no. 8, pp. 3552–3557, 2019, doi: 10.1039/c8ta12034j.

[119] J. Rawson, A. C. Stuart, W. You, and M. J. Therien, "Tailoring porphyrin-based electron accepting materials for organic photovoltaics," *J. Am. Chem. Soc.*, vol. 136, no. 50, pp. 17561–17569, 2014, doi: 10.1021/ja5097418.

[120] P. Gregory, *Industrial applications of phthalocyaninesTitle*. 2000.

[121] A. J. Pearson *et al.*, "Silicon phthalocyanines as dopant red emitters for efficient solution processed OLEDs," *J. Mater. Chem. C*, vol. 5, no. 48, pp. 12688–12698, 2017, doi: 10.1039/c7tc03946h.

[122] T. Plint, B. H. Lessard, and T. P. Bender, "Assessing the potential of group 13 and 14 metal/metalloid phthalocyanines as hole transport layers in organic light emitting diodes," *J. Appl. Phys.*, vol. 119, no. 14, 2016, doi: 10.1063/1.4945377.

[123] E. Zysman-Colman *et al.*, "Solution-Processable Silicon Phthalocyanines in Electroluminescent and Photovoltaic Devices," *ACS Appl. Mater. Interfaces*, vol. 8, no. 14, pp. 9247–9253, 2016, doi: 10.1021/acsami.5b12408.

[124] O. A. Melville *et al.*, "Contact Engineering Using Manganese, Chromium, and Bathocuproine in Group 14 Phthalocyanine Organic Thin-Film Transistors," *ACS Appl. Electron. Mater.*, vol. 2, no. 5, pp. 1313–1322, 2020, doi: 10.1021/acsaelm.0c00104.

[125] B. H. Lessard, T. M. Grant, R. White, E. Thibau, Z. H. Lu, and T. P. Bender, "The position and frequency of fluorine atoms changes the electron donor/acceptor properties of fluorophenoxy silicon phthalocyanines within organic photovoltaic devices," *J. Mater. Chem. A*, vol. 3, no. 48, pp. 24512–24524, 2015, doi: 10.1039/c5ta07173a.

[126] B. Lim *et al.*, "Silicon-naphthalo/phthalocyanine-hybrid sensitizer for efficient red response in dye-sensitized solar cells," *Org. Lett.*, vol. 15, no. 4, pp. 784–787, 2013, doi: 10.1021/ol303436q.

[127] S. Zhang *et al.*, "Interface engineering via phthalocyanine decoration of perovskite solar cells with high efficiency and stability," *J. Power Sources*, vol. 438, no. August, p. 226987, 2019, doi: 10.1016/j.jpowsour.2019.226987.

[128] J. Kim, I. Heo, D. Park, S. J. Ahn, S. Y. Jang, and S. Yim, "Efficient solvent-assisted

external treatment for planar heterojunction small-molecule organic solar cells," *J. Mater. Chem. A*, vol. 2, no. 26, pp. 10250–10256, 2014, doi: 10.1039/c4ta01154f.

[129] X. Z. Zhu *et al.*, "Enhancement of device efficiency in CuPc/C60 based organic photovoltaic cells by inserting an InCl3 layer," *Synth. Met.*, vol. 162, no. 24, pp. 2212–2215, 2012, doi: 10.1016/j.synthmet.2012.10.021.

[130] J. Meiss *et al.*, "Fluorinated zinc phthalocyanine as donor for efficient vacuum-deposited organic solar cells," *Adv. Funct. Mater.*, vol. 22, no. 2, pp. 405–414, 2012, doi: 10.1002/adfm.201101799.

[131] B. H. Lessard, J. D. Dang, T. M. Grant, D. Gao, D. S. Seferos, and T. P. Bender, "Bis(tri- n -hexylsilyl oxide) silicon phthalocyanine: A unique additive in ternary bulk heterojunction organic photovoltaic devices," *ACS Appl. Mater. Interfaces*, vol. 6, no. 17, pp. 15040–15051, 2014, doi: 10.1021/am503038t.

[132] S. Honda, H. Ohkita, H. Benten, and S. Ito, "Selective dye loading at the heterojunction in polymer/fullerene solar cells," *Adv. Energy Mater.*, vol. 1, no. 4, pp. 588–598, 2011, doi: 10.1002/aenm.201100094.

[133] L. Ke *et al.*, "Panchromatic ternary/quaternary polymer/fullerene BHJ solar cells based on novel silicon naphthalocyanine and silicon phthalocyanine dye sensitizers," *J. Mater. Chem. A*, vol. 5, no. 6, pp. 2550–2562, 2017, doi: 10.1039/c6ta08729a.

[134] H. Xu, H. Ohkita, T. Hirata, H. Benten, and S. Ito, "Near-IR dye sensitization of polymer blend solar cells," *Polymer (Guildf).*, vol. 55, no. 12, pp. 2856–2860, 2014, doi: 10.1016/j.polymer.2014.04.045.

[135] S. Ito, H. Ohkita, H. Benten, and S. Honda, "Spectroscopic analysis of NIR-dye sensitization in bulk heterojunction polymer solar cells," *Ambio*, vol. 41, no. SUPPL.2, pp. 132–134, 2012, doi: 10.1007/s13280-012-0268-3.

[136] S. Honda, S. Yokoya, H. Ohkita, H. Benten, and S. Ito, "Light-harvesting mechanism in polymer/fullerene/dye ternary blends studied by transient absorption spectroscopy," *J. Phys. Chem. C*, vol. 115, no. 22, pp. 11306–11317, 2011, doi: 10.1021/jp201742v.

[137] S. Honda, T. Nogami, H. Ohkita, H. Benten, and S. Ito, "Improvement of the light-harvesting efficiency in polymer/fullerene bulk heterojunction solar cells by interfacial dye modification," *ACS Appl. Mater. Interfaces*, vol. 1, no. 4, pp. 804–810, 2009, doi: 10.1021/am800229p.

[138] H. Xu, H. Ohkita, Y. Tamai, H. Benten, and S. Ito, "Interface Engineering for Ternary Blend Polymer Solar Cells with a Heterostructured Near-IR Dye," *Adv. Mater.*, vol. 27, no. 39, pp. 5868–5874, 2015, doi: 10.1002/adma.201502773.

[139] T. M. Grant, D. S. Josey, K. L. Sampson, T. Mudigonda, T. P. Bender, and B. H. Lessard, "Boron Subphthalocyanines and Silicon Phthalocyanines for Use as Active Materials in Organic Photovoltaics," *Chem. Rec.*, vol. 19, no. 6, pp. 1093–1112, 2019, doi: 10.1002/tcr.201800178.

[140] L. Ke *et al.*, "A Series of Pyrene-Substituted Silicon Phthalocyanines as Near-IR Sensitizers in Organic Ternary Solar Cells," *Adv. Energy Mater.*, vol. 6, no. 7, pp. 1–13, 2016, doi: 10.1002/aenm.201502355.

[141] T. M. Grant, T. Gorisse, O. Dautel, G. Wantz, and B. H. Lessard, "Multifunctional ternary additive in bulk heterojunction OPV: Increased device performance and stability," *J. Mater. Chem. A*, vol. 5, no. 4, pp. 1581–1587, 2017, doi: 10.1039/c6ta08593h.

[142] M. T. Dang, T. M. Grant, H. Yan, D. S. Seferos, B. H. Lessard, and T. P. Bender, "Bis(tri-n-alkylsilyl oxide) silicon phthalocyanines: A start to establishing a structure property relationship as both ternary additives and non-fullerene electron acceptors in bulk heterojunction organic photovoltaic devices," *J. Mater. Chem. A*, vol. 5, no. 24, pp. 12168–12182, 2017, doi: 10.1039/c6ta10739g.

[143] S. Ito, T. Hirata, D. Mori, H. Benten, H. Ohkita, and S. Honda, "Near-infrared dye sensitization of polymer/polymer thin-film solar cells," *Mol. Cryst. Liq. Cryst.*, vol. 578, no. 1, pp. 19–25, 2013, doi: 10.1080/15421406.2013.802971.

[144] B. Lim, J. T. Bloking, A. Ponec, M. D. McGehee, and A. Sellinger, "Ternary bulk heterojunction solar cells: Addition of soluble NIR dyes for photocurrent generation beyond 800 nm," *ACS Appl. Mater. Interfaces*, vol. 6, no. 9, pp. 6905–6913, 2014, doi: 10.1021/am5007172.

[145] M. C. Vebber, N. A. Rice, J. L. Brusso, and B. H. Lessard, "Variance-resistant PTB7 and axially-substituted silicon phthalocyanines as active materials for high-Voc organic photovoltaics," *Sci. Rep.*, vol. 11, no. 1, pp. 1–8, 2021, doi: 10.1038/s41598-021-94704-5.

[146] T. M. Grant, K. L. C. Kaller, T. J. Coathup, N. A. Rice, K. Hinzer, and B. H. Lessard, "High Voc solution-processed organic solar cells containing silicon phthalocyanine as a non-fullerene electron acceptor," *Org. Electron.*, vol. 87, no. June, p. 105976, 2020, doi:

10.1016/j.orgel.2020.105976.

[147] T. M. Grant, C. Dindault, N. A. Rice, S. Swaraj, and B. H. Lessard, "Synthetically facile organic solar cells with >4% efficiency using P3HT and a silicon phthalocyanine non-fullerene acceptor," *Mater. Adv.*, vol. 2, no. 8, pp. 2594–2599, 2021, doi: 10.1039/d1ma00165e.

[148] M. C. Vebber, N. A. Rice, J. L. Brusso, and B. H. Lessard, "Thermodynamic Property-Performance Relationships in Silicon Phthalocyanine-Based Organic Photovoltaics," *ACS Appl. Energy Mater.*, vol. 5, no. 3, pp. 3426–3435, 2022, doi: 10.1021/acsaem.1c04013.

Chapter 3 : Changes in Optimal Ternary Additive Loading when Processing Large Area Organic Photovoltaics by Spin vs Blade Coating Methods

This Chapter work was published in the journal "Solar RRL": *Chithiravel Sundaresan, Salima Alem, Chase L. Radford, Trevor M. Grant, Timothy L. Kelly, Jianping Lu, Ye Tao, and Benoît H. Lessard. Sol. RRL2021,5, (2100432), DOI: 10.1002/solr.202100432.*

Context

At the start of my thesis, I aimed to demonstrate large-area OPV device engineering, I utilized silicon Phthalocyanines as ternary additives in PCDTBT: PCBM-based photovoltaic devices. As outlined in Chapter 2, the ternary additive concept in BHJ OPV is one of the straightforward methods to enhance the performance of OPV devices by increasing charge generation. Although few studies reported ternary OPV using SiPc, all were prepared by spin coating method, which limits the large-scale fabrication and the integration of flexible substrates. Therefore, I was interested in investigating the performance of PCDTBT: $PC_{71}BM$ OPV by adding SiPc as a third material in large active area flexible devices, using the blade coating technique. I have thoroughly investigated the optimal loading of ternary additives, morphology of thin films, and charge carrier transport in blade coated films.

Contributions

I performed all the device fabrication, blade-coated active layer optimization, electrical characterization, and data analysis. Dr. Trevor Grant performed chemical synthesis of SiPc which was previously reported. C. L. Radford and Prof. T. L. Kelly performed GIWAXS studies. Dr. Jianping and Dr. Ye Tao, have given valuable suggestions and provided the lab facility at the National research council Canada. Prof. Benoit Lessard and Dr. Salima Alem supervised the whole project. I wrote the first draft of the manuscript with major input from BHL and SA. All of the authors were involved in the process of editing, correcting, and finalizing the manuscript.

3.1. Abstract

As we move towards roll-to-roll processing of organic photovoltaics (OPVs) it is important to validate the process and the ink formulations. We demonstrate a poly[[9-(1-octylnonyl)-9Hcarbazole-2,7-diyl]-2,5-thiophenediyl-2,1,3-benzothiadiazole-4,7 diyl2,5thiophenediyl]: [6,6]-phenyl C71 butyric acid methyl ester (PCDTBT: PC71BM) based OPV with an increase of power conversion efficiency (PCE) from 4.6% up to 5.4% by incorporating bis(tri-hexylsiloxy) silicon phthalocyanine ((3HS)2-SiPc) NIR absorbing ternary additives on ITO/PET flexible substrate with active area of 1 cm^2. under simulated AM 1.5G one sun irradiation. which is up to 15% increment with compared to baseline devices. Maximum PCE of the ternary OPVs was obtained with 5 wt% of $(3HS)_2$-SiPc added when processing the active layer by spin-coating, while the addition of 10 wt% of $(3HS)_2$-SiPc was required for maximization of PCE when processing the films by blade coating. This study demonstrates the importance of processing conditions when optimizing the concentration of ternary additives in BHJ OPVs.

3.2. Introduction

Organic photovoltaics (OPVs) presents an opportunity for low-cost energy generation and niche applications such as collapsible electronics, solar sails and weather resistant and curved solar roofs.[1] In recent years OPV device performance has been consistently improving with recent power conversion efficiencies (PCE) greater than 18%.[2], [3] Unfortunately, these devices rely almost exclusively on materials that are synthetically challenging to produce and have limited large scale potential.[4] In addition, the most promising OPV devices are fabricated by spin-coating with small active areas (< 0.07 cm^2). While spin-coating is an inexpensive and reproducible thin film processing technique, it is very wasteful and does not scale to roll to roll (R2R) processes. Poly[[9-(1-octylnonyl)-9H-carbazole-2,7-diyl]-2,5-thiophenediyl-2,1,3-benzothiadiazole-4,7 diyl2,5thiophenediyl]: [6,6]-phenyl C_{71} butyric acid methyl ester (PCDTBT: $PC_{71}BM$) based bulk heterojunction (BHJ) OPV have been found to strike a balance between high stability, low cost, ease of synthesis, and ease of large-scale manufacturing.[5], [6] Unfortunately, the performance of PCDTBT:$PC_{71}BM$ based OPV is limited by the poor absorption of the active layer in the NIR region. This issue can be addressed by using a ternary additive, as has been effectively demonstrated with some other BHJ systems.[7],[8] For example, Silicon phthalocyanines (SiPc) are synthetically simple conjugated macrocycles that are chemically stable

and absorb light in the NIR region. SiPcs have found application in n-type organic thin film transistors[9], [10]organic light-emitting diodes[11]–[13] and recently as non-fullerene acceptors and/or ternary additives in poly(hexyl thiophene) (P3HT) based OPVs.[14]–[16] Originally proposed by Honda et al.[17], [18] and others,[19] it was determined that the addition of as little as 3-10 wt% of bis(tri-n-hexylsilyl oxide) silicon phthalocyanine ($(3HS)_2$-SiPc) would increase the photocurrent generation in the 685 nm range resulting in an increase in short circuit current (J_{SC}) and PCE of up to 25% and 20%, respectively for a P3HT/$PC_{61}BM$ based OPV device. The authors found that at low additive loadings the $(3HS)_2$-SiPc would migrate to the P3HT/$PC_{61}BM$ interface providing an energy cascade between the P3HT and the $PC_{61}BM$ but when the additive loading increased the $(3HS)_2$-SiPc would crystalize and form its own phase leading to a drop in device performance.[20]–[22] Recently, Vebber et al. demonstrated that matching the solubility of the SiPc additive with that of the P3HT leads to optimized OPV performance further emphasizing the subtle effect of SiPc solubilizing groups and their interaction with P3HT/$PC_{61}BM$[23] during film formation. While promising, the devices in all these studies were fabricated by spin coating using relatively small device areas which suggests that the resulting morphology might differ when moving to scalable processing techniques such as blade coating. Furthermore, the use of $(3HS)_2$-SiPc ternary additives has yet to be studied with the use of PCDTBT and $PC_{71}BM$ or on flexible substrates.

In this study we aim to approach large scale production by reporting the first $(3HS)_2$-SiPc/PCDTBT/$PC_{71}BM$ ternary BHJ OPV devices, its processing by blade coating, its integration onto flexible substrates and with relatively large device area of 1 cm^2. We report the effect of additive concentration on morphology and charge transport characteristics as a function of spin coating versus blade coating processing. GIWAXS and TOF-SIMS provides additional information on the resulting film morphology and the role of the $(3HS)_2$-SiPc additives on final device performance.

3.3. Experimental section

Materials

PCDTBT (Mn = 36 kDa. Mw=110 kDa) and $PC_{71}BM$ (purity >99%) were purchased from PCAS Canada Inc. and Nano-C, respectively, and used without any further purification. ZnO

nanoparticles used for electron transport interlayer, were prepared according to our previous procedure. [24] MoO_3 used for hole extraction interlayer, was purchased from Sigma-Aldrich and used with no further purification. Bis(tri-n-hexylsilyl oxide) silicon phthalocyanine ($(3HS)_2$-SiPc) was prepared according to previous reports.[25]

Device fabrication

The spin coated devices were prepared on top of 4 cm x 4 cm pre-patterned indium tin oxide (ITO)-coated glass substrates, purchased from Kintek company. The sheet resistance and thickness of the ITO are 12 Ω/sq and 150 nm, respectively. The ITO substrates were first cleaned in an ultrasonic bath sequentially for 5 min in detergent solution, deionized water (DI), acetone (purity 99.5%), and isopropyl alcohol (IPA, purity 99.999%). The ITO was blown dry with a nitrogen air gun, then UV/ozone cleaned for 15 minutes. ZnO nanoparticles solution was spin coated onto the ITO at 5000 rpm for 50 s and then annealed at 110 °C for 5 min resulting in a 15 nm thick film. The active layer of binary and ternary films were afterwards spin coated with a spin speed of 800 rpm for 60 s, resulting in a film thickness of ~ 75 nm. Binary solution of PCDTBT:$PC_{71}BM$ was prepared with a weight ratio of 1:3 and a total concentration of 16 mg/ml in 1,2-dichlorobenzene (o-DCB, HPLC grade) and was stirred at 100 °C for 24 h. Ternary solutions were prepared by adding $(3HS)_2$-SiPc into the binary solution with different weight content from 3 wt.% to 25 wt.% and stirred for an additional 24 h at 70 °C. The device structure was completed by a vacuum deposition (base pressure ~ 3 $x10^{-7}$ Torr) of 10 nm of MoO_3 and 100 nm of silver.
The blade coated devices were fabricated on 12 cm x 15 cm ITO-coated polyethyleneterapthalate (PET) substrates, purchased from Sigma Aldrich, with a PET thickness of 125 μm. The sheet resistance and thickness of the ITO are 60 Ω/sq and 130 nm, respectively. ITO-coated PET sheets were patterned using a screen printable etching paste (SolarEtch® AXS Type 20), deposited using an EKRA X1-SL flatbed screen printer with a 350 mesh stainless steel screen. After curing the paste for 10 min at 120 °C, the underlying ITO was etched, and then the paste was removed with deionized water. The ITO sheets were afterward thoroughly cleaned in detergent and DI water, sonicated in acetone and IPA for 5 min, and blown dry with a nitrogen air gun. The cleaned ITO/PET sheets were treated with an oxygen plasma for 30s. ZnO nanoparticles solution was afterward blade coated at a speed of 2.5 mm/s with a gap of 300 μm and dried at 110 °C for 10 min on a hotplate. The same binary and ternary solutions were blade coated at a speed of 15 mm/s with a gap of 300 μm, resulting in dry layer thicknesses of 75-80 nm. The structure is completed

by vacuum deposition (base pressure ~ 3 x10^{-7} Torr) of bilayer (MoO_3/Ag) electrode. All the devices have an active area of 1 cm^2.

The spin-coating and blade-coating depositions were carried out in air. The thickness of films was measured by a Dektak profilometer and a ZYGO NewView 7300 optical profiler.

Electrical Characterization

The photovoltaic parameters were extracted from the current density-voltage (*J-V*) characteristics measured in air with a Keithley 2400 digital source meter under AM 1.5G irradiation of 100 mW/cm^2 (ScienceTech SS 500W solar simulator). The light intensity was adjusted using a calibrated Si photodiode with a KG-5 filter purchased from PV measurements Inc. The external quantum efficiency (EQE) spectrum was measured using a Jobin-Yvon Triax spectrometer, a Jobin-Yvon xenon light source, a Merlin lock-in amplifier, a calibrated Si UV detector, and an SR570 low noise current amplifier. The short-circuit current density (J_{SC}) of all the spin coated or blade coated devices reported in this study were verified from the wavelength integration of the product of the EQE curve and the standard AM 1.5G solar spectrum.

GIWAXS Measurements

GIWAXS experiments were performed at the Canadian Light Source (CLS) using the Hard X-ray Micro Analysis (HXMA) beam line. A photon energy of 12.69 keV was selected using a Si(111) monochromator. The beam size was defined by slits having a 0.2 mm vertical gap and a 0.3 mm horizontal gap, and the angle of incidence was set to 0.06°. The sample was deposited on a ⟨100⟩ silicon wafer by either spin-coating or blade-coating. GIWAXS patterns were collected with a Rayonix SX165 CCD detector (80 μm pixel size; 16.3 cm diameter), which was placed 220 mm from the sample center. The GIWAXS data were calibrated against a silver behenate standard and analyzed using the GIXSGUI software package.[26] Both polarization and solid-angle corrections were applied.

Time-of-flight secondary ion spectroscopy (TOF-SMIS)

The samples were examined using an ION-TOF (GmbH) TOF-SIMS IV equipped with a Bi cluster liquid metal ion source. A pulsed 25 keV Bi_3^+ cluster primary ion beam was used to bombard the sample surface to generate secondary ions. The negative secondary ions were extracted from the sample surface, mass separated and detected *via* a reflectron-type of time-of-flight analyzer, allowing parallel detection of ion fragments having a mass/charge ratio (m/z) up

to ~900 within each cycle (100 µs). A pulsed, low energy electron flood gun was used to neutralize sample surface charging.

In order to depth profile the samples, a 3 keV Cs+ ion beam was used to sputter the surface in an area of 200 µm × 200 µm and negative ion mass spectra were collected at 128 × 128 pixels over a smaller area (128 µm ×128 µm) within the sputtered area. The depth profile data was obtained by sputtering the surface with the Cs+ beam for 2 s followed by a 0.5 s pause before Bi3 + was used to analyse the newly generated surface.

3.4. Results and Discussion

The UV-Vis absorption spectra of PCDTBT: $PC_{71}BM$ binary film and PCDTBT: $PC_{71}BM$: $(3HS)_2$-SiPc ternary films with different $(3HS)_2$-SiPc contents are shown in **Figure 3.1c**. When increasing the relative amount of $(3HS)_2$-SiPc in the PCDTBT: $PC_{71}BM$ films, we observe a strong increase in absorption at 685 nm together with a small increase at 350 nm, which corresponds to the absorption of the Q and soret bands respectively for $(3HS)_2$-SiPc (**Figure S3.1**).[27] The absorption spectra between 400-600 nm does not change with the addition of less than 10 wt% of $(3HS)_2$-SiPc. For the sample with 10 wt% of $(3HS)_2$-SiPc we see a small increase in the absorption between 400-600 nm which is due to the slight overall increases of active layer thickness. These results suggest a complimentary absorption coverage between $(3HS)_2$-SiPc additive and PCDTBT: $PC_{71}BM$.

Solar cell characterization

PCDTBT: $PC_{71}BM$:$(3HS)_2$-SiPc ternary devices were fabricated with the addition of $(3HS)_2$-SiPc at six different concentrations 3, 5, 10, 15, 20 and 25 wt.% relative to PCDTBT/$PC_{71}BM$ using an inverted structure depicted in **Figure 3.1b**. Two sets of devices were prepared by spin coating and blade coating ZnO layer and active layer, using rigid and flexible substrates respectively (**Figure 3.2e** and 3.**2f**). **Figure 3.2a** and **2.3b** shows the corresponding J-V characteristics, demonstrating the noticeable impact of the addition of the $(3HS)_2$-SiPc on electrical characteristics of the devices for both deposition techniques. The average PCE of the spin-coated baseline (without additive) device is 4.7±0.1% , which is lower than our previous reported PCE of PCDTBT:PC71BM- inverted devices. This is due to the variation batch-to-batch of PCDTBT polymer. The baseline of blade coated devices shows an average PCE of 4.6±0.1%, which is

comparable to spin-coated devices in this series of experiments. In addition, the baseline devices were fabricated by spin coating method on both rigid (glass/ITO) and flexible (PET/ITO) substrates to compare the device performance. (**Figure S3.2, Table S3.1**). Film thickness of both blade-coated and spin-coated active layers was optimized to ~75 nm to achieve the highest PCE.[28]

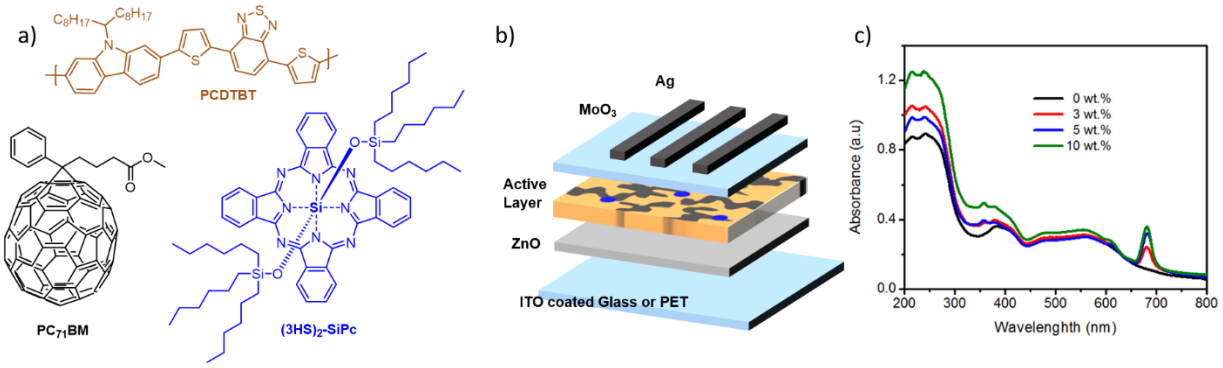

Figure 3-1. a) Chemical structure of PCDTBT, $PC_{71}BM$ and bis(tri-n-hexylsilyl oxide) silicon phthalocyanine ($(3HS)_2$-SiPc) used as the active layer in ternary OPVs. b) Inverted OPV device structure. c) UV-Vis absorption spectra of PCDTBT: $PC_{71}BM$ binary film and ternary films with different ($(3HS)_2$-SiPc loadings.

The highest performing ternary device processed by spin coating exhibited an average PCE 5.4±0.2% with a max PCE of 5.6% at 5 wt % of $(3HS)_2$-SiPc. However, the blade coated ternary devices required a 10 wt % of $(3HS)_2$-SiPc loading to achieve the highest PCE (5.3±0.1%). We surmise that the difference in optimal loading of $(3HS)_2$-SiPc is likely due to the different drying processes between spin and blade coating.[29]–[31]

The effect of additive loading on the PV performance for both blade coated, and spin coated devices can easily be compared in **Figure 3.3** (Table S1, ESI). The improved performance is mainly due to the increased J_{SC}, in both blade coated, and spin coated devices, resulting from the additional photocurrent generation due to the absorption of $(3HS)_2$-SiPc at 685nm. Similar to when paired with P3HT, the use of 5wt% leads to the most significant increase in device J_{SC}.[17], [18] This contribution is clearly seen in EQE spectra for both spin-coated (**Figure 3.2c**) and blade-coated (**Figure 3.2d**) devices. The EQE values at 685 nm increases linearly with the concentration of $(3HS)_2$-SiPc, while the contribution between 400-600 nm slightly increases up 10 wt% of

$(3HS)_2$-SiPc content before decreasing for higher contents (>10 wt%). However, it is interesting to note that the EQE values at 685 nm are higher in blade coated devices compared to the spin-coated devices suggesting a favourable morphology with better PCDTBT:$PC_{71}BM$ interfacial coverage by $(3HS)_2$-SiPc.[20]–[22], [32]

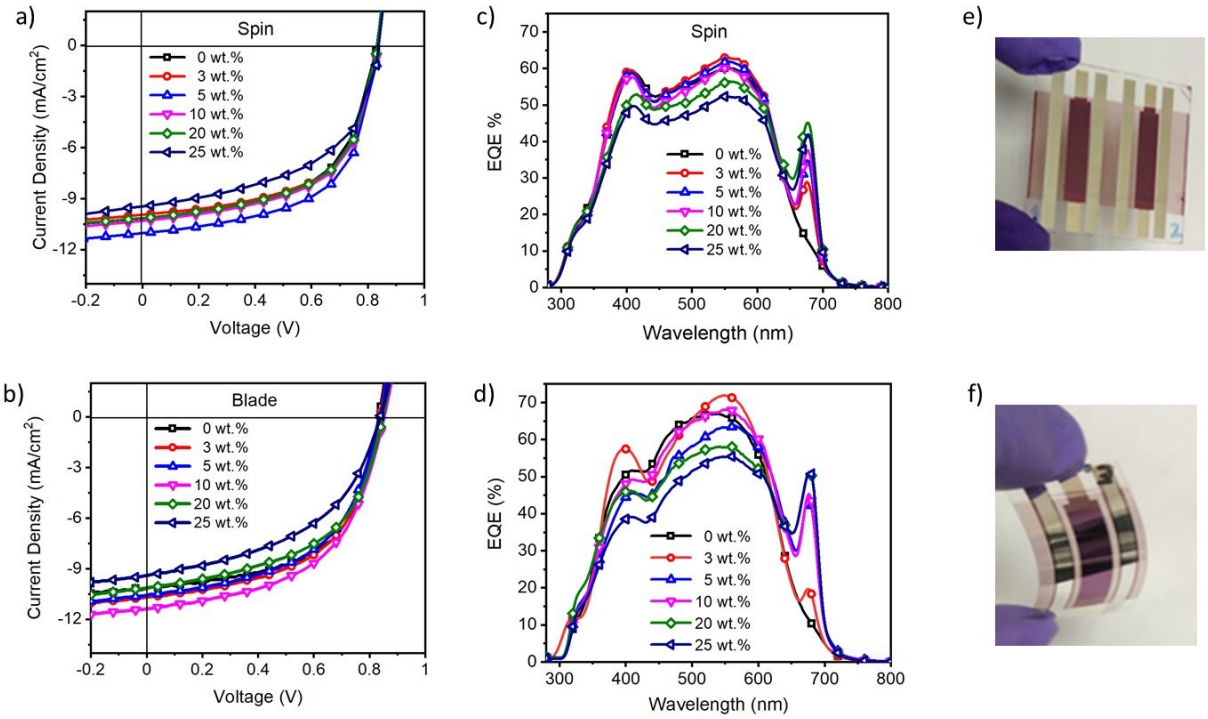

Figure 3-2. J-V characteristics of PCDTBT: $PC_{71}BM$:$(3HS)_2$-SiPc ternary BHJ OPV devices fabricated by (a) spin coating (b) blade coating; along with the corresponding EQE curves (c and d, respectively), and pictures of the resulting devices with (e) a spin coated active layer on glass/ITO substrates and (f) a blade coated active layer on flexible PET/ITO substrates.

Charge generation and transport properties.

To gain insight on the effect of $(3HS)_2$-SiPc loading, charge carrier mobilities of the binary and ternary devices were evaluated by space charge-limited current (SCLC) method. Single carrier devices with the following architectures were fabricated: ITO/ PEDOT: PSS/PCDTBT: $PC_{71}BM$: $(3HS)_2$-SiPc /MoO3/Au for hole-only devices and ITO/ZnO/PCDTBT: $PC_{71}BM$: $(3HS)_2$-SiPc /LiF/Al for electron-only devices. We expect $(3HS)_2$-SiPc to predominantly exhibit electron transport due to its reported performance in organic thin film transistors.[33] In fact SiPc derivatives in general are mostly n-type semiconductors [34][35]. However, there are some

examples of their hole transport properties.[13] Based on our previous work, we surmise the hole mobility of $(3HS)_2$-SiPc is lower than that of PCDTBT. **Table 3.1** summarizes electron mobility (μ_e) and hole mobility (μ_h) values in the spin-coated PCDTBT:$PC_{71}BM$:$(3HS)_2$-SiPc blends with 0%, 10% and 20% of $(3HS)_2$-SiPc content.

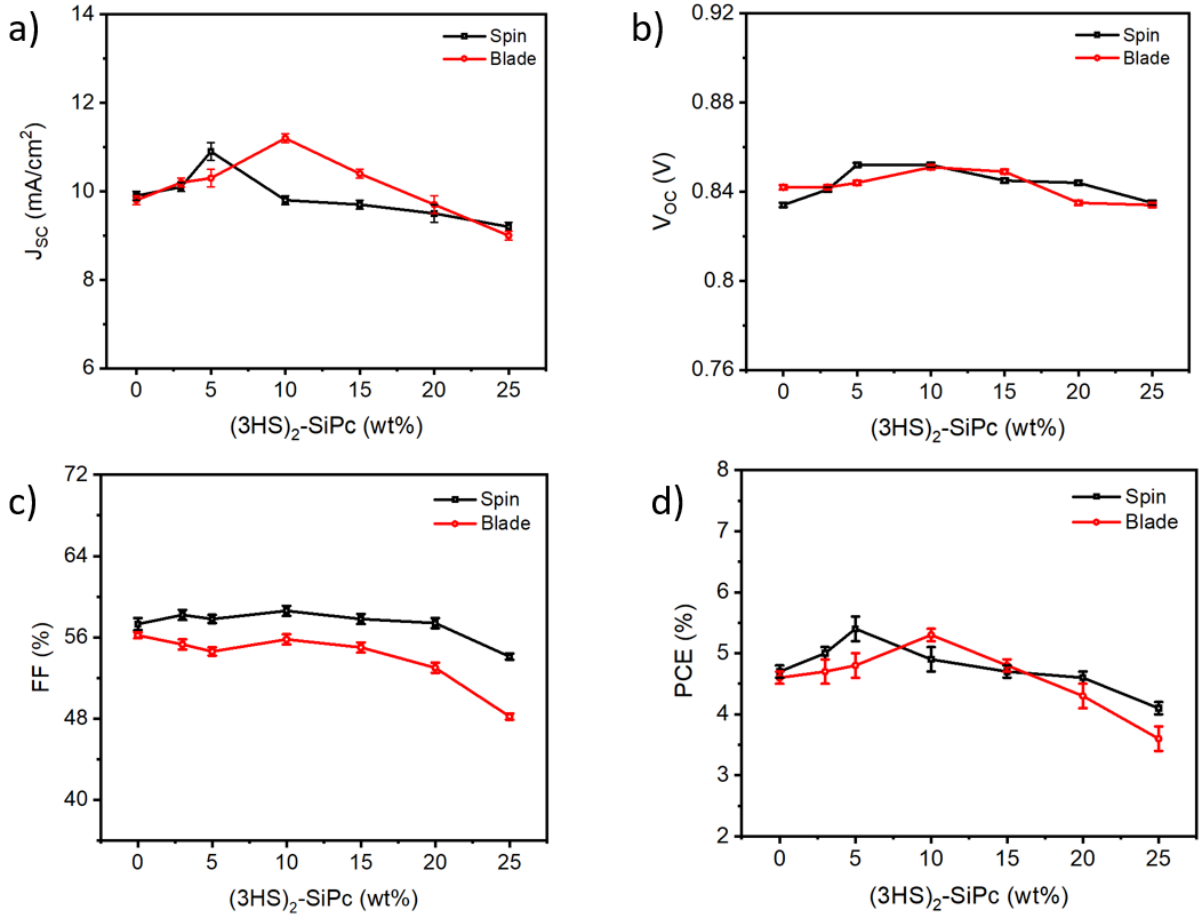

Figure 3-3. Graphical representation of PCDTBT: $PC_{71}BM$ ternary OPV devices processed by spin coating (spin) and blade coating (blade) are compared. The resulting device a) Short-circuit current density (J_{SC}); b) Open circuit voltage (V_{OC}); c) Fill factor (FF) and d) power conversion efficiency (PCE) is plotted as a function of $(3HS)_2$-SiPc additive concentration. Error bars denote the standard deviation of at least four data points.

The mobilities were calculated using Mott–Gurney's SCLC model where the current density (*J*) is defined by:

$$J = \frac{9}{8}\varepsilon_0\varepsilon_r\mu\frac{V^2}{L^3} \quad (3.1)$$

where ε_0 is the permittivity of free space, ε_r is the relative dielectric constant of the active layer, L is the thickness of the active layer. The J–V characteristics of SCLC devices are shown in **Figure S3.3**. It is observed that with increasing the content of $(3HS)_2$-SiPc from 0% to 10 wt%, the electron mobility increased from 1.7 x 10^{-4} $cm^2v^{-1}s^{-1}$ to 2.3 x 10^{-4} $cm^2v^{-1}s^{-1}$. Whereas, the hole mobility decreased from 4.7 x 10^{-4} $cm^2v^{-1}s^{-1}$ to 2.3 x 10^{-4} $cm^2v^{-1}s^{-1}$. At 20% of $(3HS)_2$-SiPc loading, we observe a decrease in both electron and hole mobilities. These results demonstrate that the addition of a small amount of $(3HS)_2$-SiPc can have a significant effect on the charge carriers transport in the films. It is also important to note that at 5 wt% and 10 wt% of $(3HS)_2$-SiPc loadings, the hole and electron mobilities are balanced, suggesting that greater device performance is likely due to reduced recombination losses.[36], [37] The dynamics of charge recombination in PCDTBT:$PC_{71}BM$: $(3HS)_2$-SiPc films are investigated through the analysis of J_{SC} and V_{OC} under various light intensities (**Figure S3.4**). The slope (α) of $ln(J_{SC}) \propto ln(P_{light})$ for the baseline device is 0.89 while the addition of $(3HS)_2$-SiPc (>3 wt%) led to an increase in α value to close to unity (0.92); implying a negligible bimolecular recombination in these devices [38][36]. In addition, the ternary devices show a weak dependence of V_{OC} on P_{light} with a slope of 1.06 *kT/q* compared to 1.15 *kT/q* for the binary device. *k, T* and *q* refer to Boltzmann constant, absolute temperature and elementary charge, respectively. This implies a more suppressed trap-assisted recombination in the ternary devices.[39]–[41] From the above results, it can be reasonably concluded that balanced charge transport and more suppressed charge recombination in the ternary devices are among the reasons for the enhanced OPV performance.

Table 3-1. Space charge limited current (SCLC) mobilities obtained for PCDTBT: $PC_{71}B$ M:$(3HS)_2$-SiPc) single carrier devices.

PCDTBT:$PC_{71}BM$: $(3HS)_2$-SiPc [a)]	$(3HS)_2$-SiPc (wt. %)	μ_e [$cm^2V^{-1}s^{-1}$]	μ_h [$cm^2V^{-1}s^{-1}$]	μ_h/μ_e
1:3:0	0	1.7×10^{-4}	4.7×10^{-4}	2.7
1:3:0.2	5	2.0×10^{-4}	2.4×10^{-4}	1.2
1:3:0.4	10	2.3×10^{-4}	2.3×10^{-4}	1.1
1:3:0.8	20	1.2×10^{-4}	2.1×10^{-4}	1.7

a) Active layers with and without additive were spin cast at 800 rpm for all devices. Active layer thickness was obtained by profilometry for mobility calculation.

To further explore the effect of adding $(3HS)_2$-SiPc in PCDTBT:$PC_{71}BM$ devices, we determined the maximum exciton generation rate (G_{max}) and exciton dissociation probability (P_{diss}) of the devices with the best performance. The photocurrent density (J_{ph}) versus the effective voltage (V_{eff}) plots for PCDTBT:$PC_{71}BM$:$(3HS)_2$-SiPc devices at different $(3HS)_2$-SiPc weight ratios are shown in **Figure S3.5** J_{ph} is the difference between the current densities under illumination at 100 mW/cm^2 and in the dark, while V_{eff} is defined as a difference between the comprensation voltage (V_0) and the applied voltage.[42] V_0 is the voltage at which the net photocurrent (J_{ph}) is zero and is determined from the competition between the diffusion and the drift of the photogenerated carriers.[43] Assuming that all of the photogenerated excitons are dissociated and contributed to the current in the saturated regime due to the sufficiently high electric field, the values of G_{max} can be obtained by $G_{max} = J_{sat}/qL$, where J_{sat} is the saturation current density at elevated V_{eff} (3.8 V), q is the electronic charge and L is the thickness of the active layer. **Table 3.2** summarizes the values at different $(3HS)_2$-SiPc weight ratios. It is noticeable that the value of G_{max} increased when $(3HS)_2$-SiPc is added to the PCDTBT:$PC_{71}BM$ blend. The maximum values of 10.6×10^{21} cm^{-3} s^{-1} and 11.2×10^{21} cm^{-3} s^{-1} were achieved with 5 wt% and 10% $(3HS)_2$-SiPc ternary blend, respectively in spin coated and blade coated devices. This implies an enhanced exciton generation likely due to the increased light absorption.

Table 3-2: Charge generation parameters of spin coated and blade coated PCDTBT: $PC_{71}BM$:$(3HS)_2$-SiPc ternary devices with different $(3HS)_2$-SiPc contents

$(3HS)_2$-SiPc (wt. %)	Spin coated			Blade coated		
	J_{sat} [a)] (mA/cm^2)	G_{max} [a)] (cm^{-3}s^{-1})	P_{diss} [a)] (%)	J_{sat} [a)] (mA/cm^2)	G_{max} [a)] (cm^{-3}s^{-1})	P_{diss} [a)] (%)
0	12.05	10.0 x 10^{21}	83.7	12.33	10.3 x 10^{21}	83.7
3	12.11	10.1 x 10^{21}	84.9	12.45	10.4 x 10^{21}	84.0
5	12.78	10.6 x 10^{21}	88.3	12.82	10.7 x 10^{21}	84.7
10	12.01	10.0 x 10^{21}	83.9	13.40	11.2 x 10^{21}	85.2
20	11.93	9.9 x 10^{21}	83.3	13.55	10.2 x 10^{21}	80.4

a) J_{sat} is the saturation current density, P_{diss} is the charge dissociation probability, G_{max} is the charge carrier generation.

The P_{diss} can be obtained by $P_{diss} = J_{ph}/J_{sat}$ under any bias. Under short circuit condition, the value of P_{diss} increased from 83.7% for the binary spin coated device to a maximum of 88.3% for the ternary device with 5 wt% of $(3HS)_2$-SiPc and increased from 83.7% to 85.2% in blade coated devices (**Table 3.2**); indicating a greater exciton dissociation and charge collection efficiency.[44]

Nanoscale morphology and phase segregation

In order to further understand the improved photovoltaic performance and effect of $(3HS)_2$-SiPc loading, we performed grazing-incidence wide-angle x-ray scattering (GIWAXS) on the corresponding thin films. We analyzed ternary blended films of PCDTBT: $PC_{71}BM$:$(3HS)_2$-SiPc films with 0-20 wt% $(3HS)_2$-SiPc content that was prepared by both spin coating (**Figure 3.4**) and blade coating (**Figure 3.5**). Both the two-dimensional GIWAXS patterns and the corresponding out-of-plane and in-plane line cuts are shown. As-cast, PCDTBT is often weakly ordered; [45], [46] the same is true here, and the polymer displays a weak preference for face-on packing. This is evidenced by a weak π-stacking reflection around q = 1.5 Å^{-1} in the out-of-plane direction, although this is largely overshadowed by an isotropic ring due to scattering from $PC_{71}BM$ (q = 1.3 Å^{-1}, Figure 4a, 5a). For the spin-coated films, the scattering pattern does not change significantly with the addition of 5 wt% $(3HS)_2$-SiPc (**Figure 3.4**). Higher additive loadings (10 wt.% and 20 wt%) lead to an increase in the width of the PCDTBT π-stacking peak, indicating a reduction in

the crystalline coherence length. This is accompanied by the appearance of a new peak in the out-of-plane line cuts at q = 0.46 Å^{-1}, corresponding to the (001) reflection of the (3HS)$_2$-SiPc. This suggests that small amounts of (3HS)$_2$-SiPc do not phase separate or otherwise impact the film morphology, but that larger loadings tend to form (3HS)$_2$-SiPc crystallites and may also disrupt the crystallization of the polymer component. [47], [48] This crystallite-mediated disruption of the polymer packing is consistent with the lower hole mobilities observed for the higher (3HS)$_2$-SiPc loadings (**Table 3.2**). When the films are prepared by blade coating, the changes in the GIWAXS patterns with the increased addition of (3HS)$_2$-SiPc are more pronounced. For the blade-coated films, the (3HS)$_2$-SiPc (100) peak at q = 0.46 Å^{-1} starts to appear for films with a 10 wt.% (3HS)$_2$-SiPc loading, and this peak becomes more intense and distinct as the loading increases to 20 wt.% (**Figure 3.5**). At 20 wt.% there is also a peak at q = 1.65 Å^{-1} ($\chi \sim 55°$) that corresponds to the (211) plane of (3HS)$_2$-SiPc.

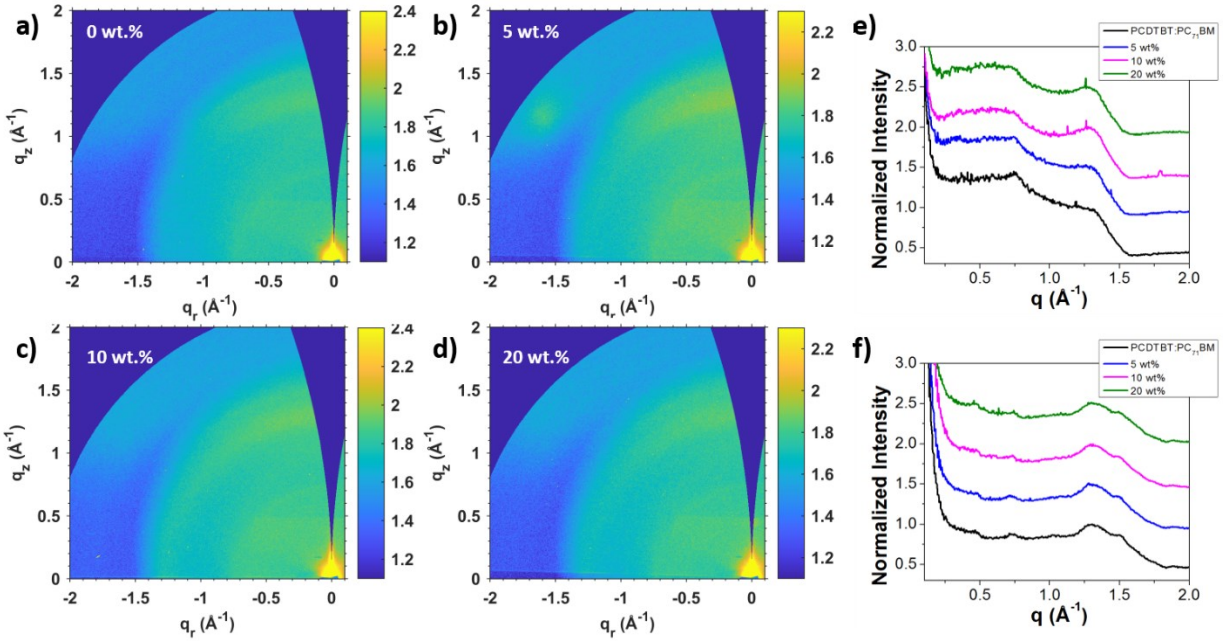

Figure 3-4. 2D-GIWAXS patterns for PCDTBT: PC$_{71}$BM films processed by spin coating with different (3HS)$_2$-SiPc content (a) without additive, (b) 5 wt.%, (c) 10 wt.%, (d) 20 wt.%, (e-f) corresponding in-plane and out-of-plane line cuts of blend films, respectively.

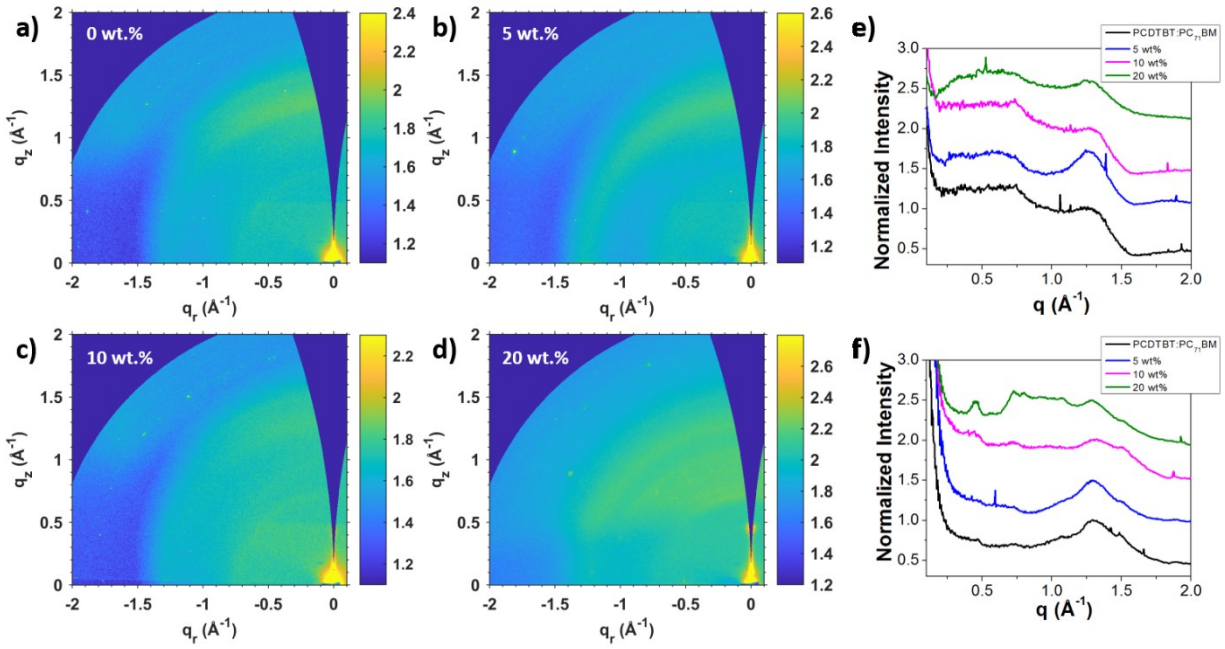

Figure 3-5. 2D-GIWAXS patterns for PCDTBT: $PC_{71}BM$ films processed by blade coating with different $(3HS)_2$-SiPc content (a) without additive, (b) 5 wt.%, (c) 10 wt.%, (d) 20 wt.%, (e-f) corresponding in-plane and out-of-plane line cuts of blend films, respectively

The spot-like nature of both the (100) and (211) reflections shows that the $(3HS)_2$-SiPc crystallites are highly oriented relative to the substrate, with the phthalocyanine rings tilted ~ 55° relative to the surface. At 20 wt.% $(3HS)_2$-SiPc loadings the PCDTBT peaks also begin to broaden, implying that the crystallization of the $(3HS)_2$-SiPc begins to disrupt the polymer packing. These results are in correlation with AFM data (Figure S5), where either spin-coated or blade-coated ternary films with 20% $(3HS)_2$-SiPc content exhibit larger features size (up to 65 nm) and higher root-mean-square (rms) roughness (> 1 nm). Overall, these data are consistent with the OPV results. Higher $(3HS)_2$-SiPc loadings disrupt the polymer packing, leading to a drop in the hole mobility (Table 2); however, small loadings (5% and 10% in spin-coated and blade-coated devices, respectively) have less of an impact on the polymer. At these low loadings, the $(3HS)_2$-SiPc additive can contribute to photocurrent generation without impeding hole transport.

Vertical stratification of ternary films

Binary and ternary films with 10 wt.% $(3HS)_2$-SiPc loading was prepared by spin coating and blade coating on GaAs wafers and analyzed by time-of-flight secondary ion mass spectroscopy (TOF-SIMS). GaAs substrates were used to avoid interfering with the Si^- signal originating from the $(3HS)_2$-SiPc. **Figure S3.7** represents the characteristic TOF-SIMS plots that show the relative intensity of various detected species as a function of sputtering time (film depth). With the addition of $(3HS)_2$-SiPc (10 wt%) we see a uniform increase in Si^- throughout both blade and spin-coated films suggesting a uniform distribution throughout the film. These results indicate that the addition of $(3HS)_2$-SiPc has no effect on the vertical composition distribution in both spin and blade-coated films and that the $(3HS)_2$-SiPc is well distributed across the film thickness.

3.5. Conclusion

We report the use of $(3HS)_2$-SiPc as a ternary additive in PCDTBT: $PC_{71}BM$ bulk heterojunction photovoltaic devices leading to increased power conversion efficiency due to the increased absorption in the 685 nm range. We also identify that the addition of $(3HS)_2$-SiPc also leads to the balanced hole and electron mobility through the blended films. We found that device performance fluctuated with the concentration of $(3HS)_2$-SiPc in the film and that the optimal loading was different when the films were processed using blade coating versus spin coating. Further investigation into the resulting films by AFM and GIWAXS suggests that at elevated $(3HS)_2$-SiPc concentration we observe increased crystallization and the formation of a third phase which coincides with a drop in performance. TOF-SIMS demonstrates a consistent vertical phase separation for both spin-coated and blade-coated films. Overall, these results suggest that the optimization of the concentration of ternary additives needs to be performed as a function of processing conditions, i.e the optimal solution concentration to obtain high-performance OPVs by spin coating is not necessarily the same when engineering OPV devices by blade coating.

3.6. References

[1] D. J. Lipomi and Z. Bao, "Stretchable, elastic materials and devices for solar energy conversion," *Energy Environ. Sci.*, vol. 4, no. 9, pp. 3314–3328, 2011.

[2] Y. Cui *et al.*, "Single-Junction Organic Photovoltaic Cells with Approaching 18% Efficiency," *Adv. Mater.*, vol. 32, no. 19, pp. 1–7, 2020.

[3] Q. Liu *et al.*, "18% Efficiency organic solar cells," *Sci. Bull.*, vol. 65, no. 4, pp. 272–275, 2020.

[4] A. Wadsworth *et al.*, "Critical review of the molecular design progress in non-fullerene electron acceptors towards commercially viable organic solar cells," *Chem. Soc. Rev.*, vol. 48, no. 6, pp. 1596–1625, 2019.

[5] S. Alem *et al.*, "Effect of mixed solvents on PCDTBT:PC70BM based solar cells," *Org. Electron.*, vol. 12, no. 11, pp. 1788–1793, 2011.

[6] S. Alem, N. Graddage, J. Lu, T. Kololuoma, R. Movileanu, and Y. Tao, "Flexographic printing of polycarbazole-based inverted solar cells," *Org. Electron.*, vol. 52, no. October 2017, pp. 146–152, 2018.

[7] T. Ameri, P. Khoram, J. Min, and C. J. Brabec, "Organic ternary solar cells: A review," *Adv. Mater.*, vol. 25, no. 31, pp. 4245–4266, 2013.

[8] Q. An, F. Zhang, J. Zhang, W. Tang, Z. Deng, and B. Hu, "Versatile ternary organic solar cells: A critical review," *Energy Environ. Sci.*, vol. 9, no. 2, pp. 281–322, 2016.

[9] O. A. Melville, T. M. Grant, and B. H. Lessard, "Silicon phthalocyanines as N-type semiconductors in organic thin film transistors," *J. Mater. Chem. C*, vol. 6, no. 20, pp. 5482–5488, 2018.

[10] O. A. Melville, T. M. Grant, B. Mirka, N. T. Boileau, J. Park, and B. H. Lessard, "Ambipolarity and Air Stability of Silicon Phthalocyanine Organic Thin-Film Transistors," *Adv. Electron. Mater.*, vol. 5, no. 8, pp. 1–7, 2019.

[11] A. J. Pearson *et al.*, "Silicon phthalocyanines as dopant red emitters for efficient solution processed OLEDs," *J. Mater. Chem. C*, vol. 5, no. 48, pp. 12688–12698, 2017.

[12] E. Zysman-Colman *et al.*, "Solution-Processable Silicon Phthalocyanines in Electroluminescent and Photovoltaic Devices," *ACS Appl. Mater. Interfaces*, vol. 8, no. 14, pp. 9247–9253, 2016.

[13] T. Plint, B. H. Lessard, and T. P. Bender, "Assessing the potential of group 13 and 14 metal/metalloid phthalocyanines as hole transport layers in organic light emitting diodes," *J. Appl. Phys.*, vol. 119, no. 14, 2016.

[14] T. M. Grant, T. Gorisse, O. Dautel, G. Wantz, and B. H. Lessard, "Multifunctional ternary additive in bulk heterojunction OPV: Increased device performance and stability," *J. Mater. Chem. A*, vol. 5, no. 4, pp. 1581–1587, 2017.

[15] T. M. Grant, K. L. C. Kaller, T. J. Coathup, N. A. Rice, K. Hinzer, and B. H. Lessard, "High Voc solution-processed organic solar cells containing silicon phthalocyanine as a non-fullerene electron acceptor," *Org. Electron.*, vol. 87, no. June, p. 105976, 2020.

[16] T. M. Grant, D. S. Josey, K. L. Sampson, T. Mudigonda, T. P. Bender, and B. H. Lessard, "Boron Subphthalocyanines and Silicon Phthalocyanines for Use as Active Materials in Organic Photovoltaics," *Chem. Rec.*, vol. 19, no. 6, pp. 1093–1112, 2019.

[17] S. Honda, T. Nogami, H. Ohkita, H. Benten, and S. Ito, "Improvement of the light-harvesting efficiency in polymer/fullerene bulk heterojunction solar cells by interfacial dye modification," *ACS Appl. Mater. Interfaces*, vol. 1, no. 4, pp. 804–810, 2009.

[18] S. Honda, H. Ohkita, H. Benten, and S. Ito, "Multi-colored dye sensitization of polymer/fullerene bulk heterojunction solar cells," *Chem. Commun.*, vol. 46, no. 35, pp. 6596–6598, 2010.

[19] B. H. Lessard, J. D. Dang, T. M. Grant, D. Gao, D. S. Seferos, and T. P. Bender, "Bis(tri- n -hexylsilyl oxide) silicon phthalocyanine: A unique additive in ternary bulk heterojunction organic photovoltaic devices," *ACS Appl. Mater. Interfaces*, vol. 6, no. 17, pp. 15040–15051, 2014.

[20] S. Honda, H. Ohkita, H. Benten, and S. Ito, "Selective dye loading at the heterojunction in polymer/fullerene solar cells," *Adv. Energy Mater.*, vol. 1, no. 4, pp. 588–598, 2011.

[21] S. Ito, H. Ohkita, H. Benten, and S. Honda, "Spectroscopic analysis of NIR-dye sensitization in bulk heterojunction polymer solar cells," *Ambio*, vol. 41, no. SUPPL.2, pp. 132–134, 2012.

[22] S. Honda, S. Yokoya, H. Ohkita, H. Benten, and S. Ito, "Light-harvesting mechanism in polymer/fullerene/dye ternary blends studied by transient absorption spectroscopy," *J. Phys. Chem. C*, vol. 115, no. 22, pp. 11306–11317, 2011.

[23] M. C. Vebber, T. M. Grant, J. L. Brusso, and B. H. Lessard, "Bis(trialkylsilyl oxide) Silicon

Phthalocyanines: Understanding the Role of Solubility in Device Performance as Ternary Additives in Organic Photovoltaics," *Langmuir*, vol. 36, no. 10, pp. 2612–2621, 2020.

[24] S. Alem, J. Lu, R. Movileanu, T. Kololuoma, A. Dadvand, and Y. Tao, "Solution-processed annealing-free ZnO nanoparticles for stable inverted organic solar cells," *Org. Electron.*, vol. 15, no. 5, pp. 1035–1042, 2014.

[25] M. T. Dang, T. M. Grant, H. Yan, D. S. Seferos, B. H. Lessard, and T. P. Bender, "Bis(tri-n-alkylsilyl oxide) silicon phthalocyanines: A start to establishing a structure property relationship as both ternary additives and non-fullerene electron acceptors in bulk heterojunction organic photovoltaic devices," *J. Mater. Chem. A*, vol. 5, no. 24, pp. 12168–12182, 2017.

[26] Z. Jiang, "GIXSGUI: A MATLAB toolbox for grazing-incidence X-ray scattering data visualization and reduction, and indexing of buried three-dimensional periodic nanostructured films," *J. Appl. Crystallogr.*, vol. 48, pp. 917–926, 2015.

[27] T. M. Grant, N. A. Rice, L. Muccioli, F. Castet, and B. H. Lessard, "Solution-Processable n-Type Tin Phthalocyanines in Organic Thin Film Transistors and as Ternary Additives in Organic Photovoltaics," *ACS Appl. Electron. Mater.*, vol. 1, no. 4, pp. 494–504, 2019.

[28] T. Y. Chu *et al.*, "Highly efficient polycarbazole-based organic photovoltaic devices," *Appl. Phys. Lett.*, vol. 95, no. 6, pp. 48–51, 2009.

[29] P. Cheng *et al.*, "Comparison of additive amount used in spin-coated and roll-coated organic solar cells," *J. Mater. Chem. A*, vol. 2, no. 45, pp. 19542–19549, 2014.

[30] K. Zhao *et al.*, "Highly efficient polymer solar cells with printed photoactive layer: Rational process transfer from spin-coating," *J. Mater. Chem. A*, vol. 4, no. 41, pp. 16036–16046, 2016.

[31] L. Wengeler, *Coating and drying processes for functional films in polymer solar cells: From laboratory to pilot scale*. 2014.

[32] H. Xu, H. Ohkita, Y. Tamai, H. Benten, and S. Ito, "Interface Engineering for Ternary Blend Polymer Solar Cells with a Heterostructured Near-IR Dye," *Adv. Mater.*, vol. 27, no. 39, pp. 5868–5874, 2015.

[33] R. R. Cranston *et al.*, "Thin-film engineering of solution-processable n-type silicon phthalocyanines for organic thin-film transistors," *ACS Appl. Mater. Interfaces*, 2021.

[34] B. King *et al.*, "Silicon phthalocyanines for N-type organic thin-film transistors:

Development of structure−property relationships," *ACS Appl. Electron. Mater.*, 2021.

[35] O. A. Melville *et al.*, "Contact Engineering Using Manganese, Chromium, and Bathocuproine in Group 14 Phthalocyanine Organic Thin-Film Transistors," *ACS Appl. Electron. Mater.*, vol. 2, no. 5, pp. 1313–1322, 2020.

[36] A. K. K. Kyaw *et al.*, "Intensity dependence of current-voltage characteristics and recombination in high-efficiency solution-processed small-molecule solar cells," *ACS Nano*, vol. 7, no. 5, pp. 4569–4577, 2013.

[37] M. M. Mandoc, W. Veurman, L. J. A. Koster, B. De Boer, and P. W. M. Blom, "Origin of the reduced fill factor and photocurrent in MDMO-PPV:IPCNEPV all-polymer solar cells," *Adv. Funct. Mater.*, vol. 17, no. 13, pp. 2167–2173, 2007.

[38] P. Schilinsky, C. Waldauf, and C. J. Brabec, "Recombination and loss analysis in polythiophene based bulk heterojunction photodetectors," *Appl. Phys. Lett.*, vol. 81, no. 20, pp. 3885–3887, 2002.

[39] L. Zhang, B. Lin, B. Hu, X. Xu, and W. Ma, "Blade-Cast Nonfullerene Organic Solar Cells in Air with Excellent Morphology, Efficiency, and Stability," *Adv. Mater.*, vol. 30, no. 22, pp. 1–8, 2018.

[40] F. Etzold *et al.*, "Ultrafast exciton dissociation followed by nongeminate charge recombination in PCDTBT:PCBM photovoltaic blends," *J. Am. Chem. Soc.*, vol. 133, no. 24, pp. 9469–9479, 2011.

[41] G. Namkoong, J. Kong, M. Samson, I. W. Hwang, and K. Lee, "Active layer thickness effect on the recombination process of PCDTBT:PC71BM organic solar cells," *Org. Electron.*, vol. 14, no. 1, pp. 74–79, 2013.

[42] P. Bi and X. Hao, "Versatile Ternary Approach for Novel Organic Solar Cells: A Review," *Sol. RRL*, vol. 3, no. 1, pp. 1–34, 2019.

[43] V. D. Mihailetchi, L. J. A. Koster, J. C. Hummelen, and P. W. M. Blom, "Photocurrent generation in polymer-fullerene bulk heterojunctions," *Phys. Rev. Lett.*, vol. 93, no. 21, pp. 19–22, 2004.

[44] D. Credgington, F. C. Jamieson, B. Walker, T. Q. Nguyen, and J. R. Durrant, "Quantification of geminate and non-geminate recombination losses within a solution-processed small-molecule bulk heterojunction solar cell," *Adv. Mater.*, vol. 24, no. 16, pp. 2135–2141, 2012.

[45] J. Griffin *et al.*, "Organic photovoltaic devices with enhanced efficiency processed from non-halogenated binary solvent blends," *Org. Electron.*, vol. 21, pp. 216–222, 2015.

[46] X. Lu *et al.*, "Bilayer order in a polycarbazole-conjugated polymer," *Nat. Commun.*, vol. 3, 2012.

[47] Q. Liang *et al.*, "Reducing the confinement of PBDB-T to ITIC to improve the crystallinity of PBDB-T/ITIC blends," *J. Mater. Chem. A*, vol. 6, no. 32, pp. 15610–15620, 2018.

[48] C. L. Radford, R. D. Pettipas, and T. L. Kelly, "Watching Paint Dry: Operando Solvent Vapor Annealing of Organic Solar Cells," *J. Phys. Chem. Lett.*, vol. 11, no. 15, pp. 6450–6455, 2020.

Chapter 4 : Design of Ternary Additive for Organic Photovoltaics: A Cautionary Tale

This Chapter work was published in the journal "RSC advances": *Chithiravel Sundaresan, Pierre Josse, Mario C. Vebber, Jaclyn Brusso, Jianping Lu, Ye Tao, Salima Alem, and Benoît H. Lessard. RSC Adv. 2022, 12 (16),10029–10036. DOI: 10.1039/d2ra00540a.*

Context

I showed in Chapter 3 that the PCE of PCDTBT: $PC_{71}BM$ BHJ devices increased up to 5.5% when incorporating $(3HS)_2$-SiPc as a ternary additive. To further improve the performance of devices, I investigated a newly designed and synthesised SiPc derivative as a ternary additive in PCDTBT: $PC_{71}BM$-based devices. We believed that enhancing the miscibility between ternary additive and donor polymer domains would potentially improve the nanomorphology. I investigated surface energy of blade coated films by contact angle measurements. I have optimised the thickness of blade coated active layer with various additive contents by tuning the blade speed and the substrate temperature. I also investigated the charge recombination in ternary films by probing the light intensity dependence of photocurrent and photovoltage. Overall, the results highlighted the impact of solubility, miscibility and nanomorphology of the ternary additive on OPVs performance.

Contributions

I performed all the device fabrication, blade-coated active layer optimization, electrical characterization, and data analysis. I performed UV-Vis spectra recording for solution and thin films of SiPc. Dr. Pierre Josse performed the chemical synthesis of SiPc. Mario Vebber performed for the cyclic voltammetry. Dr. Jianping and Dr. Ye Tao, have given suggestions for molecule synthesis and provided the lab facility at the National research council Canada. Prof. Benoit Lessard and Dr. Salima Alem supervised the project. I wrote the first draft of the manuscript with major input from BHL and SA. All of the authors were involved in the process of editing, correcting, and finalizing the manuscript.

4.1. Abstract

Silicon Phthalocyanines as ternary additives are a promising way to increase the performance of organic photovoltaics. The miscibility of the additive and the donor polymer play a significant role in the enhancement of the device performance, therefore, ternary additives can be designed to better interact with the conjugated polymer. We synthesized N-9'-heptadecanyl-2,7-carbazole functional SiPc ($(CBzPho)_2$-SiPc), a ternary additive with increased miscibility in poly[[9-(1-octylnonyl)-9Hcarbazole-2,7-diyl]-2,5-thiophenediyl-2,1,3-benzothiadiazole-4,7 diyl2,5thiophenediyl] (PCDTBT). The resulting additive was included into PCDTBT and [6,6]-phenyl C71 butyric acid methyl ester as bulk ($PC_{71}BM$) heterojunction OPV devices as ternary additive. While the $(CBzPho)_2$-SiPc demonstrated strong EQE >30% contribution in the range of 650-730 nm, the overall performance was reduced because $(CBzPho)_2$-SiPc acted as hole traps due to its high-lying HOMO energy level. This study demonstrates the importance of the solubility, miscibility, and energy level engineering of the ternary additive when designing organic photovoltaic devices.

4.2. Introduction

Organic photovoltaics (OPVs) are proving to be an exciting, flexible, semitransparent light harvesting technology with the potential to reduce power requirements and provide clean energy. The typical OPV requires complimentary donor/acceptor semiconductors to harvest photons and convert them into current. A strategy to improve device performance is to use functional ternary additives, which can be added to existing donor-acceptor systems while providing additional functionality such as increased stability or increased photogeneration.[1]–[4] Silicon phthalocyanines (SiPcs) are a promising class of ternary additive due to their low manufacturing cost, industrial abundance and ability to efficiently transport electrons.[5]–[7] Bis(tri-hexylsilyl) SiPcs ($(3HS)_2$-SiPc) and bis(tri-butylsilyl) SiPcs ($(3BS)_2$-SiPc) were previously employed as a ternary additive in poly(3-hexylthiophene):phenyl-C61-butyric acid methyl ester (P3HT:$PC_{61}BM$) bulk heterojunction (BHJ) OPV devices and provided a 20% increase in power conversion

efficiency due to the additional absorption at 685 nm[8], [9] Following these initial studies, researchers have explored engineering new SiPcs through increasing the conjugation of the axial groups with pyrenes to improve absorption in the UV region[10], [11] as well as increasing the conjugation of the macrocycle to increase absorption in the NIR region.[12]–[14] SiPcs have even been modified to impart both additional photogeneration and increased device stability through active layer crosslinking.[15] Our group[16] and others[17][14] have also found that the length of the axial groups and the resulting change in solubility play a critical role in the effectiveness of the ternary additive in a P3HT:$PC_{61}BM$ system. Poly[N-9′-heptadecanyl-2,7-carbazole-alt-5,5-(4′,7′-di-2-thienyl-2′,1′,3′-benzothiadiazole)] (PCDTBT, **Figure 4.1**), is another conjugated polymer of interest due to its high potential for indoor lighting applications, it's chemical scale-up potential and its ability to be easily printed on large areas.[18], [19] Recently, our groups reported $(3HS)_2$-SiPc to also be an effective ternary additive in PCDTBT: $PC_{71}BM$ BHJ devices, leading to an increased photogeneration efficiency compared to the baseline devices without additive. In this study we reported that the choice of processing technique such as blade coating versus spin coating led to different optimal $(3HS)_2$-SiPc loadings; further suggesting the molecular structure of the ternary additive and the film formation process are critical for improving the performance of the device.[20]

However, increased miscibility between donor polymer and ternary additive could lead to improved phase separation between domains leading to improved exciton dissociation, charge transport and potentially enhancement of overall device performance.[21]–[24] $(3HS)_2$-SiPc has been characterized to be preferentially located at the interface of P3HT/$PC_{61}BM$ rather than the bulk phases, leading to favourable device performance due to enhanced charge and energy transfer between $(3HS)_2$-SiPc and P3HT/$PC_{61}BM$ interfaces[17]. However, when using PCDTBT: $PC_{71}BM$ the locations of SiPc based ternary additives yet to be explored in the corresponding ternary thin films.

We believed that improving miscibility between the SiPc ternary additive and the PCDTBT domain would potentially improve the device performance. Therefore, in this study we designed and synthesized a N-9'-heptadecanyl-2,7-carbazole functional SiPc (**Figure 4.1**), which contains the same functional group found in PCDTBT as a repeat unit. By matching the donor polymer with the axial groups of the additive, we surmise improved miscibility will improve the device performance. While the miscibility increased through surface energy calculations, the device

performance did not. Cyclic voltammetry measurement showed that the HOMO energy level of the new additive is around -5.1 eV, which is located above PCDTBT (-5.4 eV). As a result, the new additive could function as hole traps in the devices.

4.3. Experimental section

Materials

PCDTBT (Mn = 36 kDa and Mw=110 kDa) and $PC_{71}BM$ (>99%) were purchased from PCAS Canada Inc. and Nano-C, respectively, and used without any further purification. ZnO nanoparticles were prepared according to previous reports.[25] Molybdenum oxide (MoO_3) (>99.5%) was purchased from Sigma-Aldrich and used with no further purification. The carbazole SiPc based derivative was synthesized according to **Figure 4.1**.

Synthesis of bromo-N-9'-heptadecanyl-2,7-carbazole (1).

The following procedure was adapted from previously reported synthesis.[26] p-Toluenesulfonyl chloride (1.49 g; 7.80 mmol), heptadecan-9-ol (2.00 g, 7.80 mmol) and 4-dimethylaminopyridine (DMAP, 1.43 g ; 11.70 mmol) were placed in a flame-dried 100 ml flask under N_2 to which 40 ml of anhydrous CH_2Cl_2 was added. After stirring the reaction mixture overnight at room temperature, it was poured onto water and washed three times. The organic phase was separated, dried over $MgSO_4$, then concentrated *in vacuo*. The resulting residue was purified by silica-gel column chromatography (90 % hexanes/10 % ethyl acetate as eluent) to give 2.4 g (75 %) of a colorless oil. The oil was redissolved in 15 ml DMSO and added dropwise to a flame-dried round bottom flask under N_2 containing bromocarbazole (500 mg; 2.03 mmol) and KOH (570 mg ; 10.16 mmol) in 10 ml DMSO. After stirring overnight at room temperature, water (≈ 100 ml) was added and the reaction mixture was extracted with hexanes three times. The organic phase was separated, then washed with water before being dried over $MgSO_4$ and concentrated by rotary evaporation. The resulting residue was purified by silica gel column chromatography using hexanes as eluent providing 667 mg (66 %) of a colorless oil. ^1H NMR (δ, $CDCl_3$, RT, 300 MHz): 8.10 (m, 1H), 7.98 (m, 1H), 7.73 (m, 1H), 7.58 (m, 1H), 7.45 (m, 1H), 7.36 (m, 1H), 7.29 (m, 1H), 4.51 (m, 1H), 2.27 (m, 2H), 1.95(m, 2H), 1.17(m, 24H), 0.86 (t, 6H).

Synthesis of phenoxy-N-9'-heptadecanyl-2,7-carbazole (2).

Boronic acid (250 mg ; 1.82 mmol), $Pd(PPh_3)_4$ (19 mg ; 16.51 mmol) and K_2CO_3 (342 mg ; 2.48 mmol) were placed into a 250 ml Schlenk flask and degassed under vacuum. (1) (100 mg; 0.204 mmol) and solvents (NMP:H_2O ; 9:1 v:v ; 100 ml) were placed into a separate flask and degassed by nitrogen bubbling. After 30 min, the liquid phase was transferred to the Schlenk flask *via* cannula. The reaction mixture was then immersed into an oil bath and stirred at 90°C overnight under a nitrogen atmosphere. After cooling to room temperature, the reaction mixture was poured into water (≈ 400 ml) and stirred at room temperature for 30 min. The aqueous phase was extracted three times with hexanes. The organic phase was then washed with water, dried over $MgSO_4$ and the solvent was removed by rotary evaporation. The obtained residue was purified by silica gel column chromatography using DCM as eluent leading to 290 mg (35 %) of a colorless oil. ^{1}H NMR (δ, $CDCl_3$, RT, 300 MHz): 8.11 (dd, 2H), 7.68 (m, 1H), 7.61 (m, 1H), 7.58 (m, 1H), 7.51 (m, 1H), 7.38−7.41 (m, 2H), 7.22 (m, 1H), 6.96 (dt, 2H), 4.60 (m, 1H), 2.31 (m, 2H), 1.94 (m, 2H), 1.12−1.26 (m, 24H), 0.83−0.79 (t, 6H).

Synthesis of bis(N-9'-heptadecanyl-2,7-carbazole-phenoxy) silicon phthalocyanine ($(CBzPhO)_2$-SiPc).

Dichloro silicon phthalocyanine (Cl_2-SiPc) was prepared according to previous reports.[27] Cl_2-SiPc (120 mg; 196 mmol) and (2) (290 mg ; 588 mmol) were added to a 100 ml RBF with 30 ml chlorobenzene and the reaction mixture was stirred at 130 °C for 2 days under a nitrogen atmosphere. After cooling to room temperature, the solvent was removed by rotary evaporation. The crude material was purified by silica gel column chromatography using DCM as eluent affording 150 mg (40%) of a dark blue powder. ^{1}H NMR (δ, $CDCl_3$, RT, 400 MHz): 9.65−9.67 (m, 8H), 8.35−8.37 (m, 8H), 7.73−7.94 (ddd, 4H), 7.28−7.45 (m, 4H), 7.09−7.12 (m, 2H), 6.66−6.83 (m, 2H), 6.56−6.58 (m, 2H), 5.91−5.94 (m, 4H), 4.23−4.37 (m, 2H), 2.55 (dt, 4H), 1.70−2.11 (m, 8H), 1.03−1.14 (m, 48H), 0.75−0.84 (m, 12H).

Materials Characterization.

UV-Vis absorption spectra of $(CBzPho)_2$-SiPc in solution and ternary films and the total absorption spectra of OPV devices were measured using a PerkinElmer LAMBDA 950 UV/Vis/NIR spectrophotometer. The PCDTBT: $PC_{71}BM$ binary solution was prepared in 1, 2-

dichlorobenzene (o-DCB, HPLC grade) with weight ratio of 1:3 and a total concentration of 16 mg/ml. The solution was stirred at 100 °C for 24 h. Ternary solutions were prepared by adding $(CBzPho)_2$-SiPc into the binary solution with various weight contents ranging from 3 to 20 wt.% and stirred for an additional 24 h at 70 °C.

Cyclic voltammograms (CV) were obtained using a VersaSTAT 3 potentiostat, a polished platinum disk as the working electrode, a coiled platinum wire as the counter electrode, and a Ag/AgCl electrode as the reference.[16]these experiments were carried out in dichloromethane (DCM) solutions with tetrabutylammonium perchlorate as the supporting electrolyte. Highest occupied molecular orbital (HOMO) energy levels were estimated according to the empirical correlation E_{HOMO} (eV) = −(Eox, onset − EoxFc/Fc+ ,onset) − 4.80 eV, where Eox,onset and EoxFc/Fc+ ,onset are the onset oxidation potentials of the sample and the ferrocene standard, respectively.[16] Lowest occupied molecular orbital (LUMO) levels were estimated from combining HOMO from CV with onset of the UV/Vis absorption spectra (either solution or solid phase). Tapping-mode atomic force microscopy (AFM) images were acquired with a Veeco scanning probe microscope using a Nanodrive controller with MikroMasch NSC-15 AFM tips and resonant frequencies of ~300 kHz. Water contact angle was measured on a spin-coated film of corresponding material by Folio instruments using pure water. The surface energy of all the pristine and ternary films were estimated from the contact angle.

Device fabrication

The blade-coated devices were fabricated on flexible ITO-coated polyethyleneterapthalate (PET) sheets with dimension of 12 x 15 cm^2, purchased from Sigma Aldrich. The PET sheet thickness, sheet resistance and thickness of the ITO are 125 μm, 60 Ω sq^{-1} and 130 nm, respectively. The ITO sheets were patterned using a screen printable etching paste (SolarEtch AXS Type 20). The etching paste was printed using an EKRA X1-SL flatbed screen printer with a 350-mesh stainless steel screen. After curing the paste at 120 °C for 10 min, the underlying ITO was etched, and then the paste was removed with deionized water. The patterned ITO sheets were afterward scrubbed with a detergent solution and then rinsed with DI water, followed by an additional 5 min sonication in acetone (purity 99.5%), and isopropyl alcohol (IPA, purity 99.999%) sequentially. The ITO sheets were then blown dry with a nitrogen air gun. The cleaned ITO/PET sheets were treated with an oxygen plasma for 30 s. A thin layer of ZnO (~15 nm) was blade coated

at a speed of 2.5 mm/s with a blade gap of 0.3 mm by dropping 250 µl of ZnO nanoparticle solution at the beginning of substrate area. The resulting films were then dried on a hot plate at 110 °C for 10 min in air. The binary baseline and ternary additive films were blade coated at a speed of 15 mm/s with a blade gap of 0.3 mm by dropping 150 µl of blended solutions. The temperature of the blade stage was set at 40 °C during the deposition process, resulting in a film thickness of 75-80 nm. The blade coating of ZnO and active layers was carried out in air under laminar flow hood. The OPV device structure was completed by vacuum deposition (base pressure ~ 2 $x10^{-7}$ Torr) of 10 nm of MoO_x and 100 nm of silver (Ag). All the OPV devices have an active area of 1 cm^2. The thickness of films was measured by a Dektak profilometer and a ZYGO 45 NewView 7300 optical profiler.

Electrical Characterization:

All the OPV device characterizations were performed in ambient air. The photovoltaic parameters were extracted from the current density–voltage (J–V) characteristics measured using a Keithley 2400 digital source meter under AM 1.5G irradiation of 100 $mWcm^{-2}$ (Science Tech SS 500W solar simulator). A calibrated Si photodiode with a KG-5 filter, purchased from PV measurements Inc, was used to adjust the light intensity of solar simulator. The external quantum efficiency (EQE) spectrum was measured using a Jobin-Yvon Triax spectrometer, a Jobin-Yvon xenon light source, a Merlin lock-in amplifier, a calibrated Si UV detector, and an SR570 low noise current amplifier. The short-circuit current density (J_{SC}) of all the blade-coated devices reported in this study were verified from the wavelength integration of the product of the EQE curve and the standard AM 1.5G solar spectrum.

4.4. Results and Discussion

Synthesis and characterization of $(CBzPhO)_2$-SiPc.

$(CBzPhO)_2$-SiPc was synthesized by phenoxylation of Cl_2-SiPc through standard conditions (**Figure 1**).[28] The custom phonoxy derivative was designed to mimic the solubilizing carbazole repeat unit of PCDTBT with the intention to increase miscibility with the donor phase in the resulting BHJ OPVs. A yield of 40% was obtained for the phenoxylation, which is typical for coupling reactions of Cl_2-SiPc.[28], [29] the chemical structure was verified by ^1H NMR and Electrospray ionization (ESI) Mass spectra (supporting information). The $(CBzPhO)_2$-SiPc was

characterized by UV-Vis absorption spectroscopy revealing a characteristic peak at 714 nm in chloroform solution and 720 nm in a neat thin film (**Figure 4.2a**). These values correspond to the Q-band of the silicon phthalocyanine core, which is slightly red shifted by 42-45 nm compared to typical silyl functional SiPcs with a λ_{max} = 669 to 672 nm.[30]The UV-Vis spectra of $(CBzPhO)_2$-SiPc also present an additional broad peak between 300 and 400 nm (**Figure 4.2a**), which is typically not present in silyl functional SiPcs and is likely due to the carbazole axial groups. A similar hump was observed in pyrene functional SiPc derivatives.[10] The HOMO-LUMO or energy band gap (E_{GAP}) for $(CBzPhO)_2$-SiPc was estimated from the onset of the UV-Vis spectra and found to be equal to 1.73 eV and 1.85 eV from solution and thin film, respectively, which is similar to previous reports of silyl functional SiPcs with E_{GAP} = 1.80-1.82 eV (solution) and E_{GAP} = 1.85 (film).[30]

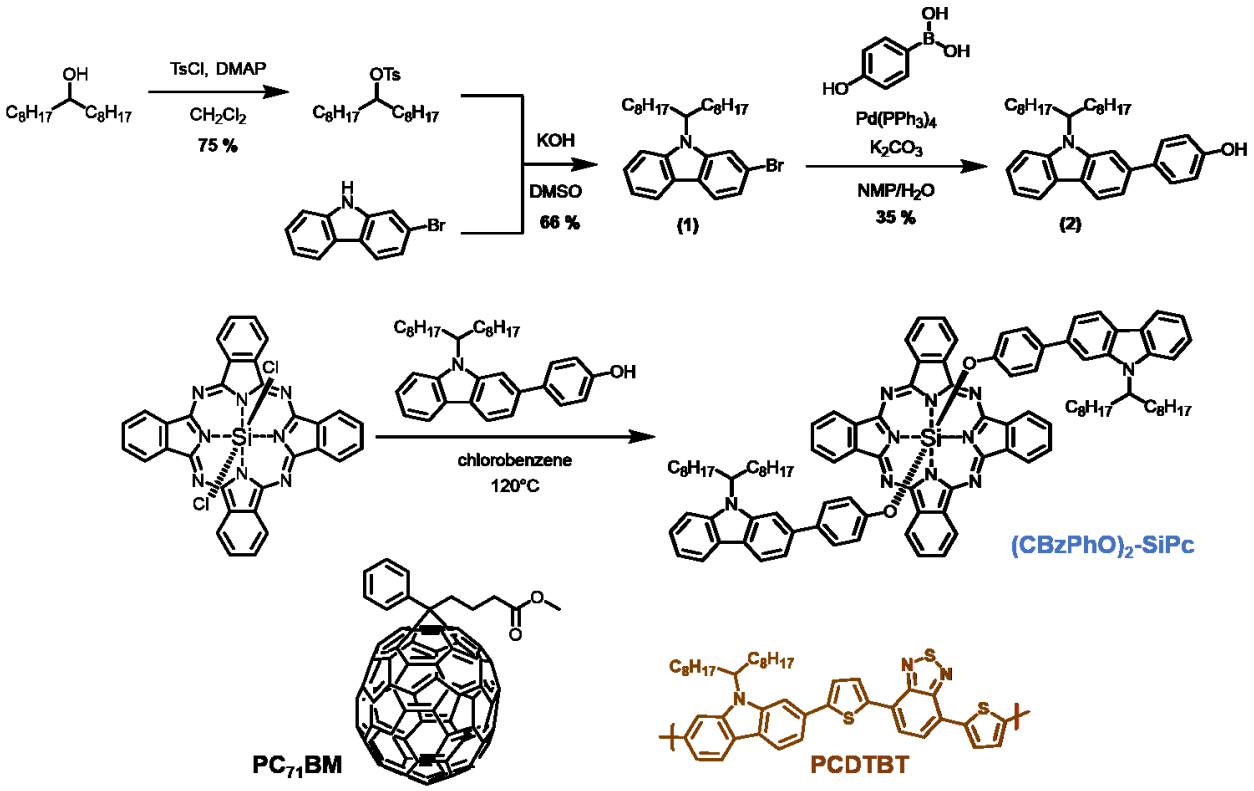

Figure 4-1. Synthesis of bis(N-9'-heptadecanyl-2,7-carbazole-phenoxy) silicon phthalocyanine ($(CBzPhO)_2$-SiPc) in addition to the chemical structure of PCDTBT and $PC_{71}BM$.

Cyclic voltammetry was performed on $(CBzPhO)_2$-SiPc in DCM solvent. The oxidation of the derivative was measured relative to Ag/AgCl reference electrode using a platinum working electrode.[16] An oxidation of potential of *Eox* = 0.36 V and a reduction potential of *Ered* = -0.96 V were obtained **(Figure 4.2b)**. The highest occupied molecular orbital energy level, $E_{HOMO,}$ = -5.1 eV was obtained for $(CBzPhO)_2$-SiPc which is relatively shallow compared to typical silyl functionalized SiPcs with E_{HOMO} = -5.3 eV.[30] The lowest unoccupied molecular orbital energy level, E_{LUMO}, was calculated through the addition of E_{HOMO} and solid state E_{GAP} and found to be equal to -3.3 eV which is also relatively shallow compared to typical silyl functional SiPcs with E_{LUMO} = -3.5 eV.[30]

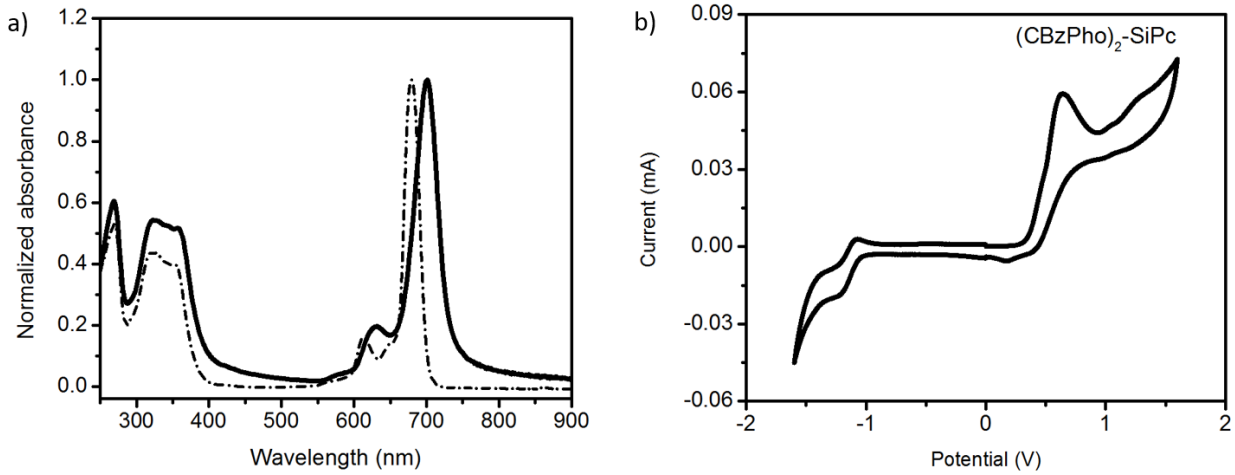

Figure 4-2. a) UV-Vis spectra of $(CBzPho)_2$-SiPc in a chloroform solution (dashed line) and thin film (solid line), b) Redox scans of cyclic voltammograms for $(CBzPho)_2$-SiPc

Miscibility and film morphology

We performed water contact angle measurements on neat films of PCDTBT, $PC_{71}BM$, and $(CBzPho)_2$-SiPc as well as blended ternary films with various weight contents of $(CBzPho)_2$-SiPc to explore their relative hydrophobicity and draw insight on respective miscibility. The surface energy was estimated using the Neumanss's method.[31] **Table 4.1** tabulates water contact angles and surface energy values of pristine thin films prepared on quartz substrates. It has been reported that additives with a surface energy value intermediate between that of the donor and acceptor materials will migrate to the interface[17], [32], [33] As designed, the surface energy of

$(CBzPho)_2$-SiPc is almost identical to that of PCDTBT (~24 N mm^{-1}) where the contact angles of $(CBzPho)_2$-SiPc and PCDTBT are 97º and 96º, respectively. As a comparison, the previously reported $(3HS)_2$-SiPc has a contact angle of ~101º.[32] We performed the same measurements on ternary blends of PCDTBT, $PC_{71}BM$, and $(CBzPho)_2$-SiPc and found that the addition of $(CBzPho)_2$-SiPc led to a slight increase in the contact angle from 93.2° for 3wt.% to 95.3° for 20 wt.% and a slight drop in the corresponding surface energy from 26.5 N mm^{-1} to 25.4 N mm^{-1} (**Table 4.1, Figure S4.7**). The surface energy of $(CBzPho)_2$-SiPc is decreased and almost matching with PCDTBT. This suggests an enhanced miscibility and a decreased likelihood of phase separation between $(CBzPho)_2$-SiPc and PCDTBT. The atomic force microscopy (AFM) images (**Figure 4.3**) show an increase in the feature size and root-mean square roughness (RMS) of ternary films as the $(CBzPho)_2$-SiPc concentration increased from 0 to 10%. While an increased RMS of 2.5 nm was measured when 10 wt.% of $(CBzPho)_2$-SiPc is added, no large islands are present in the phase images, suggesting the SiPc additive is not phase separating into a distinct third phase.

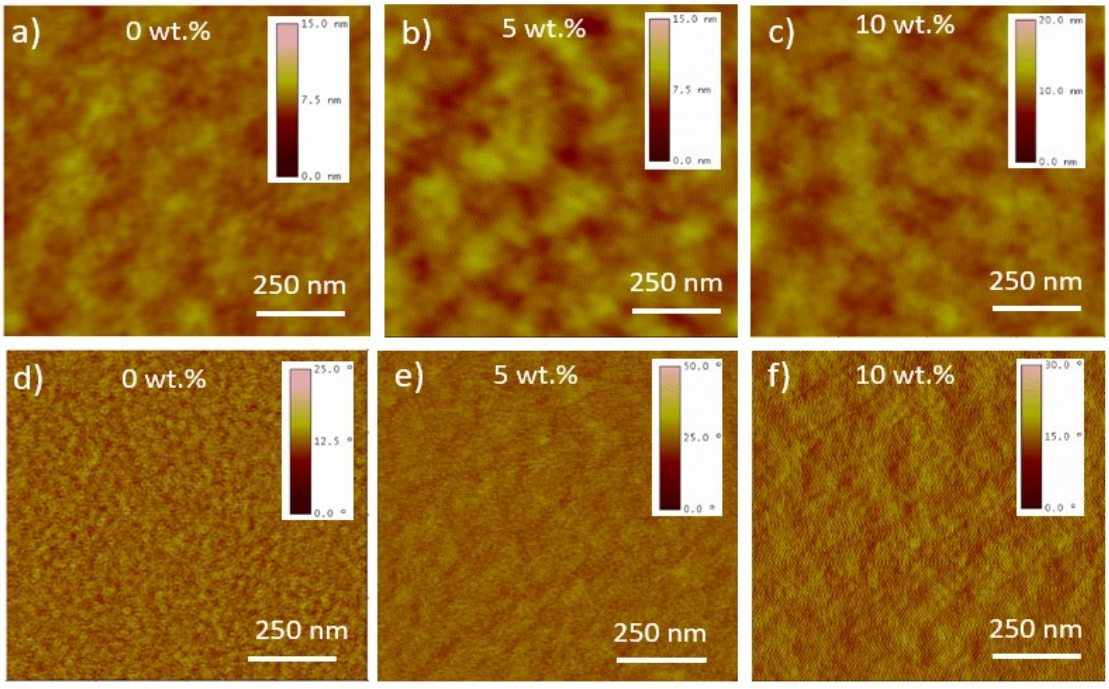

Figure 4-3. Tapping mode AFM height (above) and corresponding phase (below) images of PCDTBT: $PC_{71}BM$:$(CBzPho)_2$-SiPc ternary blends with various $(CBzPho)_2$-SiPc contents deposited by blade-coating a) 0wt% (rms roughness= 0.71 nm); b) 5wt% (rms roughness = 0.91 nm); c) 10 wt. % (rms roughness = 2.5 nm).

Organic photovoltaic device characterization:

$(CBzPho)_2$-SiPc was used as a ternary additive in BHJ PCDTBT:$PC_{71}BM$ inverted devices with the following structure: ITO-PET/ZnO/PCDTBT:$PC_{71}BM$:(CBzPho)2-SiPc/MoOx/Ag. $(CBzPho)_2$-SiPc was added at four different concentrations 3, 5, 10 and 20 wt.% relative to PCDTBT:$PC_{71}BM$ binary blend. **Figure 4.4a** shows the J−V characteristics of the OPV devices as a function of $(CBzPho)_2$-SiPc concentrations, and the corresponding device parameters are summarized in **Table S4.2**. The PCDTBT: $PC_{71}BM$ baseline device (0% of $(CBzPho)_2$-SiPc) exhibited an average PCE of 4.5% with an open circuit voltage (V_{OC}) of 0.84 V, a short-circuit current density (J_{SC}) of 9.4 mA cm^{-2}, a fill factor (FF) of 56.6%, which is consistent with previous reports.[20][34]–[36] The addition of $(CBzPho)_2$-SiPc compound as a ternary additive, resulted in a consistent decrease in overall device performance compared to the baseline devices. The addition of as little as 3 wt.% of $(CBzPho)_2$-SiPc led to a drop in J_{SC} and *FF* values. This reduction is likely due to energy offset between PCDTBT and $(CBzPho)_2$-SiPc (**Figure S4.5**). Although $(CBzPho)_2$-SiPc has shown better miscibility with PCDTBT, the cascade energy transfer at the interface of PCDTBT and $(CBzPho)_2$-SiPc is no longer favorable.

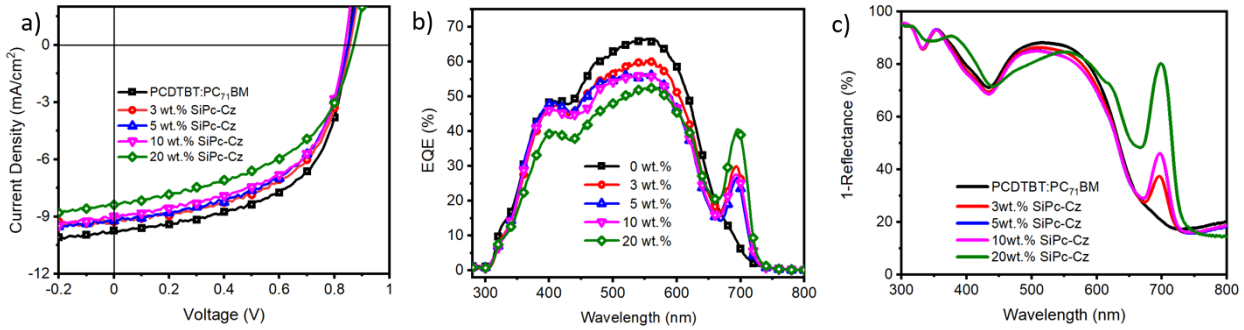

Figure 4-4. (a) J-V characteristics of PCDTBT: $PC_{71}BM$:$(CBzPho)_2$-SiPc ternary BHJ OPV devices fabricated by blade coating on ITO/PET substrates, (b) corresponding EQE curves and (c) UV-Vis total absorption spectra of OPV devices

Charge generation and dissociation probability are measured for binary PCDTBT: $PC_{71}BM$ and ternary devices with different weight content of (CBzPho)2-SiPc (**Figure S4.8, Table S4.3**, Supporting information). The dynamics of charge recombination of PCDTBT: $PC_{71}BM$:$(CBzPho)_2$-SiPc ternary films are investigated through analysis of J_{SC} and V_{OC} under various light intensities (**Figure S4.9**, supporting information). Indicates the significant bimolecular

recombination and trap-assisted recombination associated in the ternary films with different weight content of $(CBzPho)_2$-SiPc. which is in correlation with the coarse texture observed in the AFM images. This charge recombination loss has been previously associated to the SiPc additives not being present at the interface which is consistent with our contact angle measurements[17].

Table 4-1. Surface characterization of thin films.

Sample[a)]	Contact angle (°)	Surface Energy ($N\ mm^{-1}$) [c)]	Reference
PCDTBT	96.7 (±0.4)	24.3 (±0.3)	This work
$PC_{71}BM$	85.5 (±0.5)	31.3 (±0.3)	This work
(CBzPho)2-SiPc	97.3 (±0.4)	23.6 (±0.4)	This work
(3HS)2-SiPc	100.8(±0.5)	21.8 (±0.4)	ref[32]
3 wt.% (CBzPho)2-SiPc [b)]	93.2 (±0.3)	26.5 (±0.3)	This work
20 wt.% CBzPho)2-SiPc [b)]	95.3 (±0.4)	25.4 (±0.3)	This work

a) Pristine thin films spin casted on quartz substrates
b) Ternary thin films spin casted on quartz substrates
c) Surface energy was estimated using the Neumann's method

External quantum efficiency (EQE) spectra show that the addition of the $(CBzPho)_2$-SiPc compound significantly enhanced the photon conversion in the wavelength region of 680−730 nm, corresponding to the $(CBzPho)_2$-SiPc peak absorption (**Figure 4.2a)**. However, the addition of $(CBzPho)_2$-SiPc decreased the PCDTBT:$PC_{71}BM$ contribution in the region of 400−650 nm, which is consistent with the drop in J_{SC} likely due to the disruption of desired BHJ morphology from the segregation at donor phase.[37][8] The total absorption spectra of the devices (**Figure 4.4c**) show about the same pattern as the EQE spectra. At loadings of 3-10 wt% of $(CBzPho)_2$-SiPc, we observe a small drop in absorbance between 450 nm and 600 nm, probably due to the thickness optimization (~75 nm), but its drop is much smaller than the drop in the EQE spectra, which indicates that more excited excitons failed to contribute to the photocurrent with increasing $(CBzPho)_2$-SiPc content, probably due to a hole trapping effect in the BHJ by $(CBzPho)_2$-SiPc. When loading 20 wt% of $(CBzPho)_2$-SiPc, we notice a shoulder peak appearing in the total absorption spectra at 650 nm, suggesting that $(CBzPho)_2$-SiPc is disrupting the PCDTBT domain but remains blended in the PCDTBT domain unlike in previously reported P3HT systems using

$(3HS)_2$-SiPc,[38][8] which led to a tendency to aggregate into a third unique SiPc domain at high loadings.

4.5. Conclusion

We designed and synthesized an N-9'-heptadecanyl-2,7-carbazole functional SiPc ($(CBzPho)_2$-SiPc) with matching functionality to PCDTBT to improve their miscibility. UV-Vis absorption spectroscopy and electrochemical characterization of $(CBzPho)_2$-SiPc revealed slightly shallower HOMO and LUMO energy levels compared to typical silyl functionalized SiPcs. The thin film contact angle and the resulting surface energy calculations suggest very similar characteristics between $(CBzPho)_2$-SiPc and PCDTBT suggesting a good miscibility. As a ternary additive in PCDTBT:$PC_{71}BM$ OPV devices, $CBzPho_2$-SiPc showed a significant EQE contribution from 680 to 730 nm; however, decreased PCDTBT: $PC_{71}BM$ contribution, resulting in a net loss in the short-circuit current density suggested the additive was not at the interface between donor and acceptor and that the $(CBzPho)_2$-SiPc is likely dispersed in the PCDTBT domain and acted as hole traps leading to a drop in the device performance or this drop in performance could simply be a result of poor ternary film morphology. This study further suggests the importance of the solubility and miscibility of the ternary additive when designing organic photovoltaic devices.

4.6. References

[1] L. Lu, M. A. Kelly, W. You, and L. Yu, "Status and prospects for ternary organic photovoltaics," *Nat. Photonics*, vol. 9, no. 8, pp. 491–500, 2015, doi: 10.1038/nphoton.2015.128.

[2] T. Ameri, P. Khoram, J. Min, and C. J. Brabec, "Organic ternary solar cells: A review," *Adv. Mater.*, vol. 25, no. 31, pp. 4245–4266, 2013, doi: 10.1002/adma.201300623.

[3] F. Goubard and G. Wantz, "Ternary blends for polymer bulk heterojunction solar cells," *Polym. Int.*, vol. 63, no. 8, pp. 1362–1367, 2014, doi: 10.1002/pi.4636.

[4] P. Bi and X. Hao, "Versatile Ternary Approach for Novel Organic Solar Cells: A Review," *Sol. RRL*, vol. 3, no. 1, pp. 1–34, 2019, doi: 10.1002/solr.201800263.

[5] B. H. Lessard, "The Rise of Silicon Phthalocyanine: From Organic Photovoltaics to Organic Thin Film Transistors," *ACS Appl. Mater. Interfaces*, vol. 13, no. 27, pp. 31321–31330, 2021, doi: 10.1021/acsami.1c06060.

[6] T. M. Grant, D. S. Josey, K. L. Sampson, T. Mudigonda, T. P. Bender, and B. H. Lessard, "Boron Subphthalocyanines and Silicon Phthalocyanines for Use as Active Materials in Organic Photovoltaics," *Chem. Rec.*, vol. 19, no. 6, pp. 1093–1112, 2019, doi: 10.1002/tcr.201800178.

[7] K. Mitra and M. C. T. Hartman, "Silicon phthalocyanines: synthesis and resurgent applications," *Org. Biomol. Chem.*, pp. 1168–1190, 2021, doi: 10.1039/d0ob02299c.

[8] M. T. Dang, T. M. Grant, H. Yan, D. S. Seferos, B. H. Lessard, and T. P. Bender, "Bis(tri-n-alkylsilyl oxide) silicon phthalocyanines: A start to establishing a structure property relationship as both ternary additives and non-fullerene electron acceptors in bulk heterojunction organic photovoltaic devices," *J. Mater. Chem. A*, vol. 5, no. 24, pp. 12168–12182, 2017, doi: 10.1039/c6ta10739g.

[9] T. M. Grant, N. A. Rice, L. Muccioli, F. Castet, and B. H. Lessard, "Solution-Processable n-Type Tin Phthalocyanines in Organic Thin Film Transistors and as Ternary Additives in Organic Photovoltaics," *ACS Appl. Electron. Mater.*, vol. 1, no. 4, pp. 494–504, 2019, doi: 10.1021/acsaelm.8b00113.

[10] L. Ke *et al.*, "A Series of Pyrene-Substituted Silicon Phthalocyanines as Near-IR Sensitizers in Organic Ternary Solar Cells," *Adv. Energy Mater.*, vol. 6, no. 7, pp. 1–13, 2016, doi: 10.1002/aenm.201502355.

[11] L. Ke *et al.*, "Panchromatic ternary/quaternary polymer/fullerene BHJ solar cells based on novel silicon naphthalocyanine and silicon phthalocyanine dye sensitizers," *J. Mater. Chem. A*, vol. 5, no. 6, pp. 2550–2562, 2017, doi: 10.1039/c6ta08729a.

[12] S. Ito, T. Hirata, D. Mori, H. Benten, H. Ohkita, and S. Honda, "Near-infrared dye sensitization of polymer/polymer thin-film solar cells," *Mol. Cryst. Liq. Cryst.*, vol. 578, no. 1, pp. 19–25, 2013, doi: 10.1080/15421406.2013.802971.

[13] S. Honda, H. Ohkita, H. Benten, and S. Ito, "Multi-colored dye sensitization of polymer/fullerene bulk heterojunction solar cells," *Chem. Commun.*, vol. 46, no. 35, pp. 6596–6598, 2010, doi: 10.1039/c0cc01787f.

[14] B. Lim, J. T. Bloking, A. Ponec, M. D. McGehee, and A. Sellinger, "Ternary bulk heterojunction solar cells: Addition of soluble NIR dyes for photocurrent generation beyond 800 nm," *ACS Appl. Mater. Interfaces*, vol. 6, no. 9, pp. 6905–6913, 2014, doi: 10.1021/am5007172.

[15] T. M. Grant, T. Gorisse, O. Dautel, G. Wantz, and B. H. Lessard, "Multifunctional ternary additive in bulk heterojunction OPV: Increased device performance and stability," *J. Mater. Chem. A*, vol. 5, no. 4, pp. 1581–1587, 2017, doi: 10.1039/c6ta08593h.

[16] M. C. Vebber, T. M. Grant, J. L. Brusso, and B. H. Lessard, "Bis(trialkylsilyl oxide) Silicon Phthalocyanines: Understanding the Role of Solubility in Device Performance as Ternary Additives in Organic Photovoltaics," *Langmuir*, vol. 36, no. 10, pp. 2612–2621, 2020, doi: 10.1021/acs.langmuir.9b03772.

[17] S. Honda, H. Ohkita, H. Benten, and S. Ito, "Selective dye loading at the heterojunction in polymer/fullerene solar cells," *Adv. Energy Mater.*, vol. 1, no. 4, pp. 588–598, 2011, doi: 10.1002/aenm.201100094.

[18] S. Beaupré and M. Leclerc, "PCDTBT: En route for low cost plastic solar cells," *J. Mater. Chem. A*, vol. 1, no. 37, pp. 11097–11105, 2013, doi: 10.1039/c3ta12420g.

[19] Z. Zhang *et al.*, "Printed Sensors for Building Management," *2018 Int. Flex. Electron. Technol. Conf. IFETC 2018*, pp. 10–12, 2018, doi: 10.1109/IFETC.2018.8583970.

[20] C. Sundaresan *et al.*, "Changes in Optimal Ternary Additive Loading when Processing Large Area Organic Photovoltaics by Spin- versus Blade-Coating Methods," vol. 2100432, pp. 1–8, 2021, doi: 10.1002/solr.202100432.

[21] B. Fan *et al.*, "Improved Performance of Ternary Polymer Solar Cells Based on A

Nonfullerene Electron Cascade Acceptor," *Adv. Energy Mater.*, vol. 7, no. 11, 2017, doi: 10.1002/aenm.201602127.

[22] L. Ye, B. A. Collins, X. Jiao, J. Zhao, H. Yan, and H. Ade, "Miscibility–Function Relations in Organic Solar Cells: Significance of Optimal Miscibility in Relation to Percolation," *Adv. Energy Mater.*, vol. 8, no. 28, pp. 1–15, 2018, doi: 10.1002/aenm.201703058.

[23] J. W. Jung *et al.*, "Fluoro-substituted n-type conjugated polymers for additive-free all-polymer bulk heterojunction solar cells with high power conversion efficiency of 6.71%," *Adv. Mater.*, vol. 27, no. 21, pp. 3310–3317, 2015, doi: 10.1002/adma.201501214.

[24] Q. Fan *et al.*, "Synergistic effect of fluorination on both donor and acceptor materials for high performance non-fullerene polymer solar cells with 13.5% efficiency," *Sci. China Chem.*, vol. 61, no. 5, pp. 531–537, 2018, doi: 10.1007/s11426-017-9199-1.

[25] S. Alem, J. Lu, R. Movileanu, T. Kololuoma, A. Dadvand, and Y. Tao, "Solution-processed annealing-free ZnO nanoparticles for stable inverted organic solar cells," *Org. Electron.*, vol. 15, no. 5, pp. 1035–1042, 2014, doi: 10.1016/j.orgel.2014.02.024.

[26] N. Blouin, A. Michaud, and M. Leclerc, "A low-bandgap poly(2,7-carbazole) derivative for use in high-performance solar cells," *Adv. Mater.*, vol. 19, no. 17, pp. 2295–2300, 2007, doi: 10.1002/adma.200602496.

[27] N. J. Yutronkie, T. M. Grant, O. A. Melville, B. H. Lessard, and J. L. Brusso, "Old molecule, new chemistry: Exploring silicon phthalocyanines as emerging N-type materials in organic electronics," *Materials (Basel).*, vol. 12, no. 8, pp. 5–10, 2019, doi: 10.3390/ma12081334.

[28] B. H. Lessard *et al.*, "Assessing the potential roles of silicon and germanium phthalocyanines in planar heterojunction organic photovoltaic devices and how pentafluoro phenoxylation can enhance π-π Interactions and device performance," *ACS Appl. Mater. Interfaces*, vol. 7, no. 9, pp. 5076–5088, 2015, doi: 10.1021/am508491v.

[29] B. H. Lessard, T. M. Grant, R. White, E. Thibau, Z. H. Lu, and T. P. Bender, "The position and frequency of fluorine atoms changes the electron donor/acceptor properties of fluorophenoxy silicon phthalocyanines within organic photovoltaic devices," *J. Mater. Chem. A*, vol. 3, no. 48, pp. 24512–24524, 2015, doi: 10.1039/c5ta07173a.

[30] M. C. Vebber, T. M. Grant, J. L. Brusso, and B. H. Lessard, "Bis (tri-alkylsilyl oxide) silicon phthalocyanines : understanding the role of solubility on device performance as ternary additives in organic," 2020, doi: 10.1021/acs.langmuir.9b03772.

[31] D. Li and A. W. Neumann, "A reformulation of the equation of state for interfacial tensions," *J. Colloid Interface Sci.*, vol. 137, no. 1, pp. 304–307, 1990, doi: 10.1016/0021-9797(90)90067-X.

[32] H. Xu, T. Wada, H. Ohkita, H. Benten, and S. Ito, "Molecular Design of Near-IR Dyes with Different Surface Energy for Selective Loading to the Heterojunction in Blend Films," *Sci. Rep.*, vol. 5, pp. 1–5, 2015, doi: 10.1038/srep09321.

[33] N. Yi *et al.*, "Miscibility Matching and Bimolecular Crystallization Affording High-Performance Ternary Nonfullerene Solar Cells," *Chem. Mater.*, vol. 31, no. 24, pp. 10211–10224, 2019, doi: 10.1021/acs.chemmater.9b03935.

[34] M. Thambidurai *et al.*, "High performance inverted organic solar cells with solution processed Ga-doped ZnO as an interfacial electron transport layer," *J. Mater. Chem. C*, vol. 1, no. 48, pp. 8161–8166, 2013, doi: 10.1039/c3tc31650e.

[35] I. Lee, J. Noh, J. Y. Lee, and T. S. Kim, "Cooptimization of Adhesion and Power Conversion Efficiency of Organic Solar Cells by Controlling Surface Energy of Buffer Layers," *ACS Appl. Mater. Interfaces*, vol. 9, no. 42, pp. 37395–37401, 2017, doi: 10.1021/acsami.7b10398.

[36] Z. Li *et al.*, "Toward Improved Lifetimes of Organic Solar Cells under Thermal Stress: Substrate-Dependent Morphological Stability of PCDTBT:PCBM Films and Devices," *Sci. Rep.*, vol. 5, no. October, pp. 1–9, 2015, doi: 10.1038/srep15149.

[37] S. Honda, T. Nogami, H. Ohkita, H. Benten, and S. Ito, "Improvement of the light-harvesting efficiency in polymer/fullerene bulk heterojunction solar cells by interfacial dye modification," *ACS Appl. Mater. Interfaces*, vol. 1, no. 4, pp. 804–810, 2009, doi: 10.1021/am800229p.

[38] B. H. Lessard, J. D. Dang, T. M. Grant, D. Gao, D. S. Seferos, and T. P. Bender, "Bis(tri- n -hexylsilyl oxide) silicon phthalocyanine: A unique additive in ternary bulk heterojunction organic photovoltaic devices," *ACS Appl. Mater. Interfaces*, vol. 6, no. 17, pp. 15040–15051, 2014, doi: 10.1021/am503038t.

Chapter 5 : Low-Cost Silicon Phthalocyanine as a Non-Fullerene Acceptor for Flexible large area Organic Photovoltaics

This chapter work was accepted in the journal ACS Omega. *Chithiravel Sundaresan, Mario C. Vebber, Jaclyn Brusso, Ye Tao, Salima Alem, and Benoît H. Lessard, ACS Omega 2023, 8, 1, 1588–1596. doi.org/10.1021/acsomega.2c07131.*

Context

In Chapters 3 &4, I demonstrated SiPc as a ternary additive in blade coated OPV devices. In this chapter, I demonstrated large-area photovoltaic devices based on low synthetic complexity of (3BS)2-SiPc as a non-fullerene acceptor (NFA) pairing with (P3HT) as donor polymer. I utilized environmentally-friendly non–halogenated solvents to process the devices via the blade coating method. I explored different active layer deposition configurations: bulk heterojunction (BHJ), Sequential layer-by-layer (Sq), and Alternate sequential layer-by-layer (Alt-Sq). I optimized the optimal morphology and thickness of active layers with different donor/acceptor ratios, blade speeds, and substrate temperatures. I also investigated the vertical distribution of donor (P3HT)-acceptor (3BS)2-SiPc through the BHJ and bilayer active layers, and charge transport properties correlated with OPV device performance.

Contributions

I performed all the device fabrication, blade-coated active layer optimization, electrical characterization, and data analysis. Mario Vebber and Prof. Jaclyn Brusso performed chemical synthesis of $(3BS)_2$-SiPc which was previously reported. Dr. Ye Tao provided the lab facility at the National research council Canada. Prof. Benoit Lessard and Dr. Salima Alem supervised the project. I wrote the first draft of the manuscript. All of the authors were involved in the process of editing, correcting, and finalizing the manuscript.

5.1. Abstract

We demonstrate large area photovoltaic devices based on the low synthetic complexity of bis(tri-n-butylsilyl oxide) Silicon Phthalocyanines $(3BS)_2$-SiPc as a non-fullerene acceptor (NFA) pairing with poly(3-hexylthiophene) (P3HT) as donor polymer. Environment-friendly non-halogenated solvents were utilized to process large area (1 cm^2) organic photovoltaics (OPVs) on flexible indium tin oxide (ITO) coated polyethylene terephthalate (PET) substrates. An alternate sequentially (Alt-Sq) blade-coated active layer with bulk heterojunction-like morphology is developed by utilizing $(3BS)_2$-SiPc processing with o-Xylene/1,3,5-trimethylbenzene solvents. The Sequential (Sq) active layer is prepared by first blade coating $(3BS)_2$-SiPc solution followed by P3HT coated on top without any post-treatment. A conventional bulk heterojunction (BHJ) active layer film prepared by blade coating from the blend solution of P3HT: $(3BS)_2$-SiPc. The conventional sequentially (Sq) blade-coated active layer presents very low performance due to the $(3BS)_2$-SiPc bottom layer being partially washed off by processing the top layer of P3HT. In contrast, alternate sequentially (Alt-Sq) blade coated layer by layer film shows even better device performance compared to BHJ active layer. Notably, the time-of-flight secondary ion mass spectroscopy (TOF-SIMS) and the atomic force microscopy (AFM) studies reveal that the Alt-Sq active layer shows BHJ-like morphology with a well intermixed donor-acceptor component in the active layer. These results provide a straightforward approach to low-cost OPVs with large-scale production.

5.2. Introduction

Organic photovoltaics (OPVs) have gained significant attention due to their potential use in emerging applications such as solar sails, semitransparent curtains and building integration.[1–4] Over the last five years, the use of non-fullerene acceptors has enabled a significant increase in the power conversion efficiency (PCE) of OPVs reaching over 19%.[5,6] However, the majority of the champion non-fullerene acceptor materials involve multiple complex synthetic steps and result in often low yields, which will limit large-scale manufacturing and impact the cost.[7–9]. The commercialization viability of OPV technology depends on the "golden triangle" rule of high PCE, long-term stability and low cost. PCE and stability of OPVs are generally the primary focus of most research groups, while a critical factor associated with low cost, the synthetic complexity of

photoactive materials, are given less consideration.[10] The synthetic complexity is basically ascribed to five steps. (1) Number of synthetic steps, (2) reciprocal yield, (3) number of unit operations for the isolation, (4) the number of column chromatography purification steps, and (5) the number of hazardous chemicals used in their synthesis.[11]

P3HT is one of the most popular donor polymers used in OPV applications due to its stability and ease of synthesis on a kilogram scale.[12,13] P3HT also has good solubility in many non-halogenated solvents, providing a great opportunity for large-scale commercialization of P3HT-based OPVs.[14–17] Non-fullerene acceptor (NFA) based small molecules have been successfully paired with P3HT to obtain high-performance OPVs. However, the NFAs themselves have a high synthetic complexity, reducing the feasibility of the resulting combination. In order to overcome the issue of cost-effectiveness, alternative NFA must be developed for effective large-scale OPV manufacturing to take place.[8,9]

Phthalocyanines are common dye molecules which have been utilized as a semiconducting material in organic light emitting diodes,[18,19] organic thin film transistors[20–22] and organic photovoltaics.[23–28] Phthalocyanines (Pcs) are already synthesized on the ton scale annually and found in everyday textiles, paints, colorants and inks.[29] Silicon phthalocyanine ($(R)_2$-SiPc) are emerging as an exciting class of phthalocyanines due to their ability to enable n-type operation in electronics and their axial groups provide a handle to tune the physical and thermodynamic properties such as miscibility, solubility, nucleation and solid state arrangement.[30–34] In terms of synthetic complexity (SC), SiPcs have been reported with a SC index of 12, almost five times lower than high-performing NFAs such as Y6 (SC of 59) and ITIC (SC of 67).[35] Traditionally, $(R)_2$-SiPcs have been utilized as ternary additives in donor-acceptor OPVs, providing more than 20% increase in photocurrent due to the extended solar absorption[26,36–39] Recently, $(R)_2$-SiPc derivatives have also been used as NFA with different donor polymers: P3HT, PTB7, and PBDB-T, and achieved high power conversion efficiencies (>4 %).[40,41] These promising results demonstrate a great potential for these low complexity and low cost NFAs.

In this work, we aim to bring $(R)_2$-SiPcs forward as scalable NFAs. We report the large-area (1 cm^2) OPVs based on P3HT and $(3BS)_2$-SiPc NFAs acceptor using green solvents and a favourable layer-by-layer solution deposition technique by blade coating. We optimized the choice of solvent, the processing conditions and the deposition order. Interestingly, we report optimized performance as a result of alternate sequential layer-by-layer deposition. The films and resulting

devices are thoroughly characterised providing morphological properties, charge transport properties, and donor-acceptor vertical stratification.

5.3. Experimental Section

Materials

P3HT was purchased from Rieke metals (4002-E, Molecular weight 50-70 kDa, Regioregularity 91-94% and poly dispersity index 2-2.5). $PC_{61}BM$ was purchased from Nano-C and used without any further purification. Bis(tri-n-butyl silyl oxide) silicon phthalocyanine 3$(BS)_2$-SiPc) was synthesized according to previous reports.[37] Zinc oxide (ZnO) nanoparticle solution was used for electron transport interlayer and prepared according to our previous report.[42] Molybdenum oxide (MoO_3) (>99.5 %) was purchased from Sigma-Aldrich and used as received for hole transport layer. Dichlorobenzene (o-DCB), o-Xylene, 1,3,5-trimethylbenzene (TMB) and Toluene were purchased from Sigma-Aldrich.

OPV Device Fabrication

The OPV devices in this study have an inverted structure of ITO/ZnO/Active layer/MoO_3/Ag. All devices were fabricated on ITO-coated, 125 μm-thick-PET sheets, purchased from Sigma Aldrich. The thickness and sheet resistance of the ITO layer are 130 nm and 60 Ω/sq, respectively. Each 15 cm × 12 cm ITO/PET sheet was patterned into 10 individual cells using a screen-printable etching paste (Solar Etch AXS Type 20). The etching paste was printed with 350-mesh stainless steel screen using a flatbed EKRA X1-SL screen printer. The paste was cured at 120 ºC for 10 min to complete the ITO etching, and then washed with deionized water. The ITO patterned sheets were afterwards cleaned using sequentially ultra-sonication of detergent, DI water, acetone and isopropyl alcohol for 5 min respectively, and dried on a hot plate at 120 ºC. Prior to ZnO deposition, The cleaned ITO/PET sheets were treated for 30 seconds with oxygen plasma to change the surface energy and eliminate chemical residues. The ZnO layer was blade coated at a blade speed of 2.5 mm/s with a blade gap of 0.3 mm, by pouring 0.25 ml volume of solution. The ZnO films (~ 20 nm) were then annealed at 120 ºC for 10 min in ambient air.

For BHJ films, the donor-acceptor blend ink was prepared by dissolving P3HT (17mg/ml) and R_2-SiPc with a 1:0.6 donor: acceptor weight ratio, in non-halogenated solvents: o-Xylene, TMB and toluene. The donor and acceptor inks were prepared separately for the sequential bilayer process. P3HT (15mg/ml) and (3$BS)_2$-SiPc) (15mg/ml) were dissolved in o-Xylene and TMB, respectively,

and the solutions were stirred on a hot plate at 80 °C for overnight. In Sq devices, the $(3BS)_2$-SiPc) acceptor layer was first blade coated on top of the ZnO layer, then sequentially, P3HT was coated at different blade speeds. For alternate sequential (Alt-Sq) devices, the P3HT was first coated on top of the ZnO layer and followed sequentially by blade coating the $(3BS)_2$-SiPc) layer. All the blade-coating depositions were performed in ambient air and the thickness of different layers was optimized by adjusting blade coating parameters, such as: ink concentration, blade speed, and substrate temperature. The OPV devices structure was finished by vacuum deposition (base pressure 2 x 10^{-7} bar) of the bilayer MoOx (10 nm) and Ag (100 nm) electrodes, having an active area of 1 cm^2. Film thicknesses were measured using a Dektak profilometer and a ZYGO NewView 7300 optical profiler.

Electrical Characterization

All characterizations of OPV devices were evaluated in ambient air at room temperature. The photovoltaic performance parameters were analysed from the current density–voltage (J–V) characteristics. The J-V curve of OPV is measured using a Keithley 2400 digital source meter under light intensity of 100 $mWcm^{-2}$ corresponding to the AM 1.5G irradiation (Science Tech SS 500W solar simulator). The solar simulator's light intensity was controlled using a calibrated Si photodiode with a KG-5 filter that was purchased from PV measurements Inc. The external quantum efficiency (EQE) spectrum was measured using a Jobin-Yvon Triax spectrometer, a xenon light source, and a Merlin lock-in amplifier. The monochromatic light intensity at each wavelength was calibrated using standard Si UV detector, and an SR570 low noise current amplifier. The short-circuit current density (J_{SC}) of all devices described in this study was verified using wavelength integration of the EQE curve and the standard AM 1.5G solar spectrum.

Time-of-Flight Secondary Ion Spectroscopy:

All three type of active layer films were analyzed using an ION-TOF (GmbH) TOF-SIMS IV that was fully equipped with a Bi cluster liquid metal ion source. In order to generate secondary ions, a 25 keV Bi3+ cluster primary ion beam pulsed at 10 kHz was utilized to bombard the surface of the samples. Positive or negative secondary ions were collected from the sample surface, mass separated, and detected using a reflection-type time-of-flight analyzer, facilitating parallel monitoring of ion fragments with a mass/charge ratio (m/z) up to ~ 900 within 100 µs. A depth profile was obtained by repeating the cycle of alternatively sputtering the surface in an area of 100 µm × 100 µm with a 3 keV Cs^+ beam for 3 s and collecting, upon a waiting time of 1 s, an

ion mass spectrum using the Bi_3^+ primary ion beam at 47 × 47 pixels over an area of 128 µm × 128 µm within the sputtered area (1 shot per pixel).

5.4. Results and Discussion

The chemical structure of P3HT and $(3BS)_2$-SiPc, which were used as the donor and the acceptor, respectively, in the fabrication of OPVs are shown in **Figure 5.1a**. The highest occupied molecular orbital/lowest unoccupied molecular orbital (HOMO/LUMO) energy levels of P3HT and $(3BS)_2$-SiPc) were taken from the literature and represented in **Figure 5.1b.**[37,43] Three different active layer configurations were optimized for device fabrication: 1.Single bulk heterojunction (BHJ) layer, 2. standard sequential (Sq) bilayer deposition (acceptor then donor) and 3. Alternate sequential (Alt-Sq) bilayer deposition (donor then acceptor), as shown in **Figure 5.1c**.

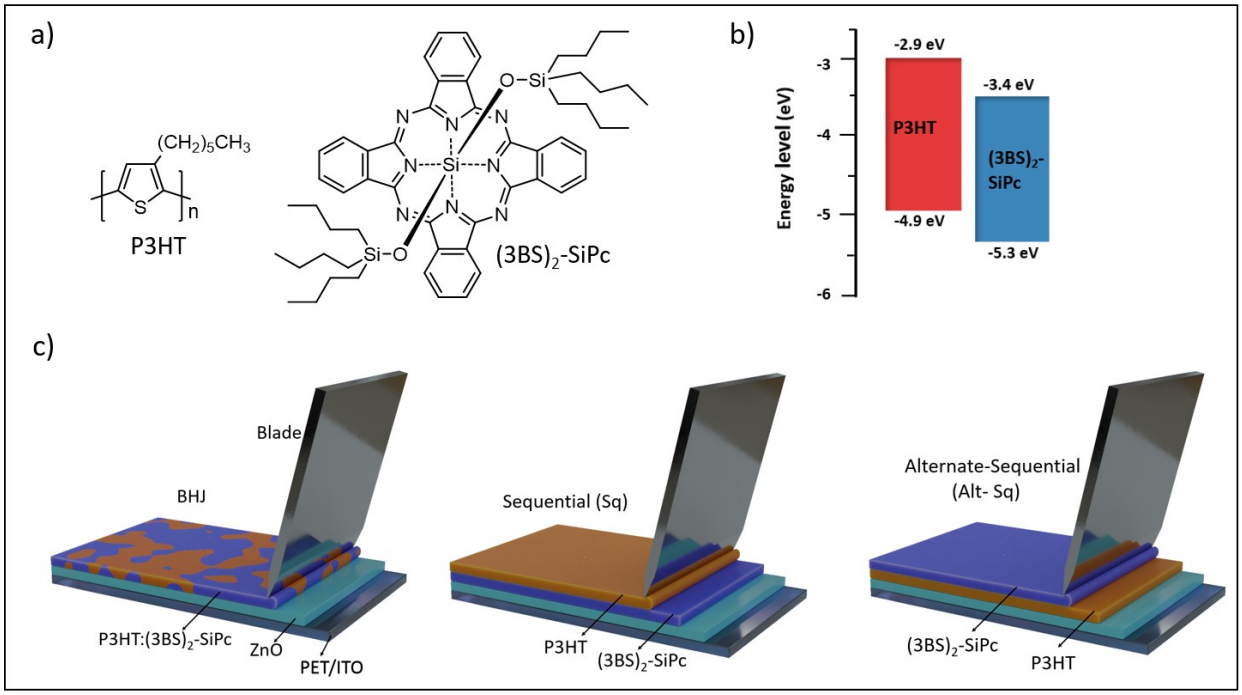

Figure 5-1. (a) Chemical structure of P3HT donor and $(3BS)_2$-SiPc non-fullerene acceptor materials, (b) Energy level diagram of P3HT and $(3BS)_2$-SiPc, and (c) schematic representation of inverted OPV device architecture with three types of active layers deposition of bulk heterojunction (BHJ), sequential (Sq) and alternate sequential (Alt-Sq) by blade coating.

Baseline (P3HT:$PC_{61}BM$) devices fabricated by both spin coating on rigid ITO/glass and blade coating on ITO/PET flexible substrates using o-dichlorobenzene (o-DCB), yielded comparable performances to literature values[44–46] (PCE of 2-3%) which are shown in **Figure S5.1** and **Table S5.1** (Supporting information). BHJ OPVs of $(3BS)_2$-SiPc and P3HT were previously optimized to PCE = 3.6 % with an equal donor-acceptor weight ratio (1:1) using spin coating process, which served as a starting point for optimization of this blade coating process.[40]

In this study, we optimized the performance of blade coated P3HT :$(3BS)_2$-SiPc BHJ OPV devices by controlling blade speed, P3HT:$(3BS)_2$-SiPc weight ratio, and substrate temperature (**Figure S5.2-S5.3 and Table S5.2,** supporting information). o-Xylene was used as a processing solvent. The topography and the thickness of the active layer are mainly impacted by the blade speed. When blade coating the P3HT:$(3BS)_2$-SiPc solution at a speed greater than 25 mm/s, the resulting active layer thickness was larger than 180 nm and the coated films clearly showed larger crystallites of $(3BS)_2$-SiPc, which is not surprising given the tendency of $(3BS)_2$-SiPc to crystalize.[37,47] However, at low blade speeds of 7.5-12.5 mm/s, the active layer films exhibit inhomogeneous thickness with larger domains of likely P3HT, which also led to poor OPV devices.

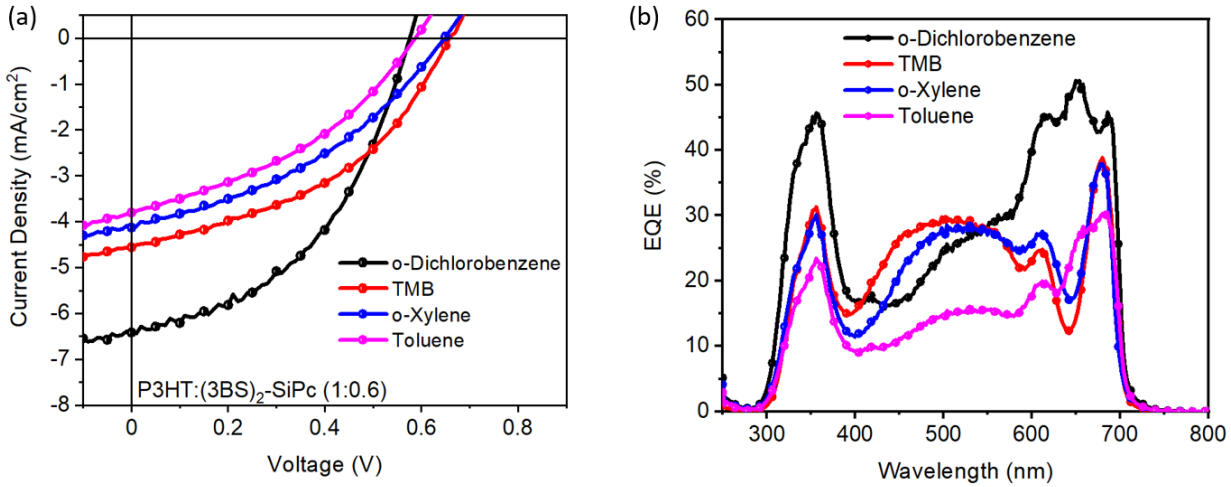

Figure 5-2. a) J-V characteristics of devices with P3HT:$(3BS)_2$-SiPc (1:0.6) active layers, blade coated from different solvents (b) corresponding EQE curves.

When investigating different non-chlorinated solvents, we found that the best device performance (PCE~ 1.3%) was achieved with P3HT :$(3BS)_2$-SiPc layers coated from TMB solvent, with a 1:0.6

weight ratio. **Figure 5.2** and **Table 5.1** show J-V curves, EQE spectra and photovoltaic parameters of P3HT :$(3BS)_2$-SiPc BHJ-based devices blade coated with different solvents. Similar to spin coated devices, post-thermal annealing didn't have a positive effect on the performance (**Figure S5.4**, **Table S5.3**, Supporting information) of BHJ blade coated devices.[48] This suggests that thermal annealing of the blade coated P3HT:$(3BS)_2$-SiPc films leads to further unfavourable crystallisation and phase separation.

Table 5-1. OPV device performance parameters of P3HT: $(3BS)_2$-SiPc (1:0.6) OPVs prepared by blade coating with different solvents

Solvents	**Thickness (~nm)**	**J_{SC} (mA/cm^2) [(a)]**	**V_{OC} (V)**	**FF**	**PCE (%)**
o-DCB	120 (±0.3)	-6.4 (±0.1)	0.58 (±0.03)	0.48 (±0.03)	1.8 (±0.1)
TMB	130 (±0.4)	-4.6 (±0.2)	0.66 (±0.03)	0.42 (±0.02)	1.3 (±0.1)
o-Xylene	140 (±0.5)	-4.1 (±0.2)	0.63 (±0.01)	0.40 (±0.02)	1.0 (±0.1)
Toluene	140 (±0.5)	-3.8 (±0.1)	0.59 (±0.02)	0.38 (±0.03)	0.8 (±0.1)

All values are average with five devices, and the values in parentheses are the standard deviation. [a] Current density *(J_{SC})* calculated from the EQE curve.

The J-V plots and EQE spectra of optimized P3HT :$(3BS)_2$-SiPc-based BHJ, Sq and Alt-Sq blade coated OPVs are shown in **Figure 5.3a** and **Figure 5.3b**, respectively. The extracted values of open-circuit voltage (V_{OC}), short-circuit current density (J_{SC}), and fill factor (FF) are summarized in **Table 5.2**. The optimized BHJ OPVs coated from TMB solvent exhibit an average V_{OC} of 0.66 V, J_{SC} of 4.6 mA/cm^2, and FF of 0.42 and PCE of 1.3% (**Figure S5.5** and **Table S5.4**, supporting information).

The Sq devices, processed from o-xylene, show a maximum PCE of 0.8% (**Figure S5.6** and **Table 5.5,** supporting information). We observed that the P3HT coating washes partially off the bottom $(3BS)_2$-SiPc layer, regardless of the solvent used. As a result, the active layer composition couldn't be finely tuned to get the optimal morphology for efficient exciton dissociation.

The Alt-Sq blade-coated devices processed with o-xylene, show significantly improved photovoltaic performance with an open-circuit voltage V_{OC} of 0.67 V, J_{SC} of 4.3 mA/cm^2, FF of 0.50, and PCE of 1.4% (**Figure S5.7 and Table S5.6**), suggesting a favourable $(3BS)_2$-SiPc and P3HT morphology. Layer by layer deposition enabled further optimization of the P3HT layer through thermal annealing, prior to $(3BS)_2$-SiPc deposition, resulting in a slight improvement in PCE to 1.5%.

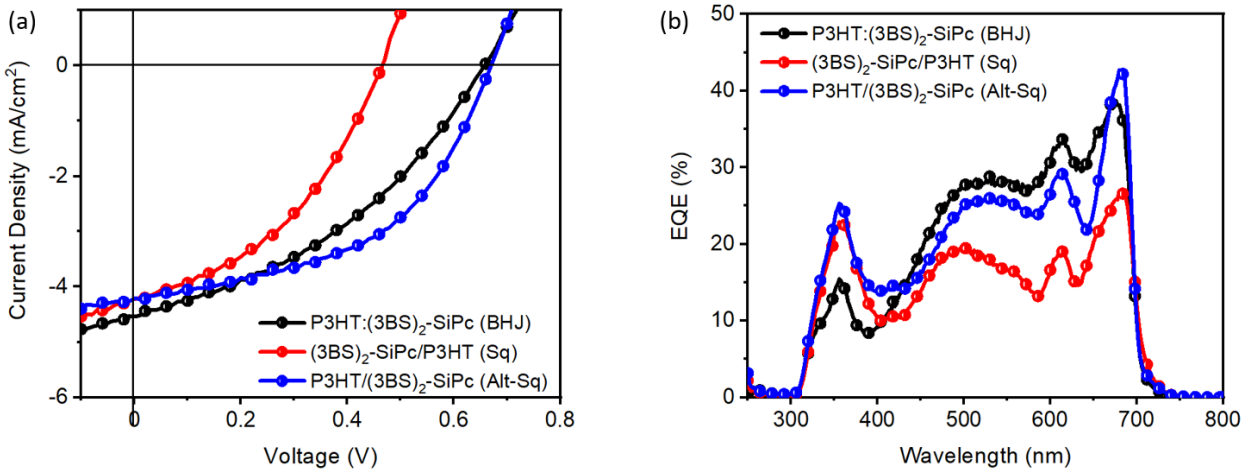

Figure 5-3. (a) J-V characteristics (b) corresponding external quantum efficiency (EQE) spectra of P3HT:$(3BS)_2$-SiPc BHJ, 3$(BS)_2$-SiPc / P3HT sequential (Sq) and P3HT /3$BS)_2$-SiPc alternate sequential (Alt-Sq) devices. Active layers were blade coated with o-Xylene and TMB solvents.

Table 5-2. OPV device performance parameters of optimized (P3HT: $(3BS)_2$-SiPc) BHJ, ($(3BS)_2$-SiPc: P3HT) Sq, (P3HT/ $(3BS)_2$-SiPc) Alt-Sq devices under the illumination of AM 1.5 G, 100 mW cm^{-2}

Active layer	**J_{SC} (mA/cm^2) [(a)]**	**V_{OC} (V)**	**FF**	**PCE (%)**
BHJ	-4.6 (±0.3)	0.66 (±0.01)	0.42 (±0.01)	1.3 (±0.1)
Sq	-4.1 (±0.2)	0.45 (±0.01)	0.41 (±0.02)	0.8 (±0.1)
Alt-Sq	-4.3 (±0.3)	0.67 (±0.02)	0.50 (±0.02)	1.4 (±0.1)

All values are average with five devices, and the values in parentheses are the standard deviation. [a] Current density *(J_{SC})* calculated from the EQE curve.

Charge Carrier Mobility

The charge transport properties of the three types of blade-coated active layers (BHJ, Sq, Alt-Sq) were probed using the space-charge-limited current (SCLC) method. Hole (μ_h) mobilities were measured with a device structure of PET/ITO/PEDOT: PSS/active layers/MoO_3/Ag and electron (μ_e) mobilities with a device structure of PET/ITO/ZnO/active layer/Al. The charge carrier mobility was extracted by fitting the dark current versus voltage to the model of a single-carrier SCLC, which is described by the Mott-Gurney equation.[49,50]

$$J = \frac{9}{8}\,\mu\varepsilon_r\varepsilon_0\,\frac{V^2}{L^3} \qquad (5.1)$$

Where J is the current density, μ is the charge carrier mobility, ε_0 is the permittivity of free space, ε_r is the relative permittivity of the active layer material, L is the thickness of the films, and V is the applied voltage. The log (J-V) plot characteristics of the hole-only and electron-only devices are shown in **Figures S5.4a-b** (supporting information). The calculated mobility values are represented as a bar chart in **Figure S5.4c** (supporting information) and are tabulated in **Table 5.3**.

Table 5.3. SCLC mobilities obtained for P3HT:3$(BS)_2$-SiPc (BHJ, Sq, Alt-Sq active layers) single carrier devices

P3HT: (3BS)2-SiPc	μ_h	μ_e	μ_h/μ_e
	[10^{-5} cm^2 V^{-1} s^{-1}]	[10^{-5} cm^2 V^{-1} s^{-1}]	
BHJ	2.68 (± 0.6)	1.15 (± 0.2)	2.33
Sq	3.14 (± 0.7)	0.47 (± 0.2)	6.68
Alt-Sq	1.62 (± 0.2)	1.25 (± 0.2)	1.30

At least four devices were taken into consideration for the averages. The active layer thickness was obtained by a Dektak profilometry for mobility calculation.

The hole mobility (μ_h) of optimal BHJ, Sq and Alt-Sq devices are 2.68 × 10^{-5} $cm^2V^{-1}s^{-1}$, 3.14 x 10^{-5} $cm^2V^{-1}s^{-1}$, and 1.62 × 10^{-5} $cm^2V^{-1}s^{-1}$; while the electron mobility (μ_e) are 1.15 × 10^{-5} $cm^2V^{-1}s^{-1}$, 0.47 × 10^{-5} $cm^2V^{-1}s^{-1}$, and 1.25 × 10^{-5} $cm^2V^{-1}s^{-1}$, respectively. The molecular packing and the transportation pathways have a significant impact on the charge carrier transport in OPVs.[51] The

reduced μ_h and the improved μ_e in the optimal Alt-Sq devices is likely due to a better vertical phase separation of donor-acceptor in the active layer compared to BHJ and Sq devices; which will be discussed below together with other morphology parameters. As a result, a more balanced μ_h/μ_e of 1.30 was achieved for the Alt-Sq devices compared to that of 2.33 and 6.15 for the BHJ and Sq counterparts, respectively, which is consistent with the relatively larger FF (~ 0.50) of the OPVs.

UV-Vis and Photoluminescence spectra

The UV-vis absorption spectra of pristine P3HT, $(3BS)_2$-SiPc and all OPV active layer films are shown in **Figure 5.5a**. We observe a strong characteristic absorption peak of $(3BS)_2$-SiPc at 650-700 nm (Q-band) with higher intensity in Alt-Sq film than BHJ. This suggests that the content of $(3BS)_2$-SiPc in Alt-Sq layer is higher, allowing a good percolation pathways of $(3BS)_2$-SiPc, which is consistent with the increased electron mobility. Whereas, the absorption spectrum of Sq film reveals less content of $(3BS)_2$-SiPc in the active layer, due to partial dissolution. This has an impact on the generation and dissociation of excitons and the electron mobility in the Sq configuration. Photoluminescence (PL) spectra of BHJ, Sq, Alt-Sq active layers and neat films of P3HT and $(3BS)_2$-SiPc are shown in **Figure 5.5b**. All thin films were excited at the peak absorption of P3HT (530 nm). As expected, P3HT shows a strong emission between 600 and 750 nm and no emission was detected for $(3BS)_2$-SiPc film due to the lack of absorption at 530 nm. Both BHJ and Alt-Sq films exhibit high PL quenching in the range of 600-750 nm, indicating efficient charge transfer between the P3HT and $(3BS)_2$-SiPc.

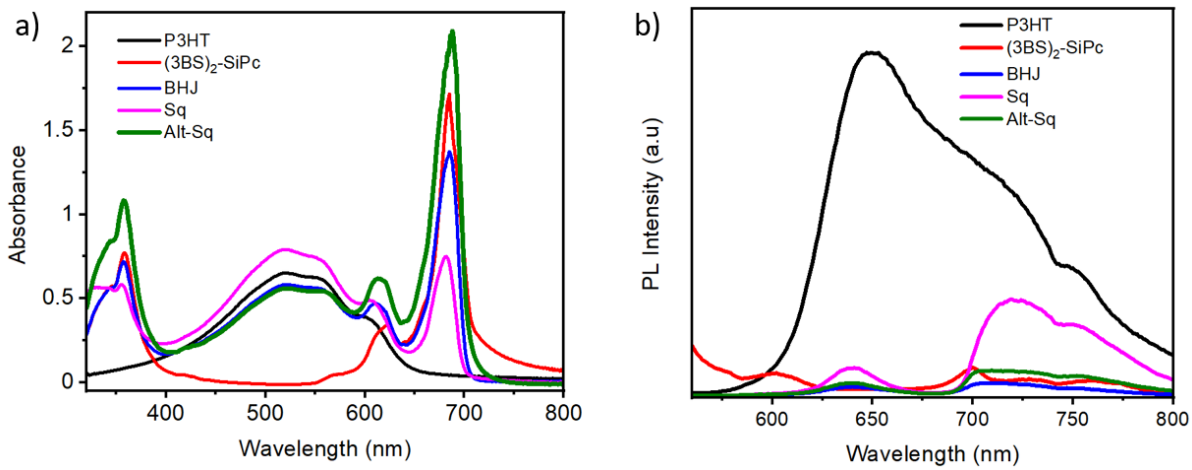

Figure 5-4. a) UV-Vis absorption spectra for pristine thin films of P3HT, $(3BS)_2$-SiPc and Three types of active layers (BHJ, Sq, Alt-Sq) blade coated on PET substrates and b) is the corresponding PL spectra, all films are excited at 530 nm.

Morphology characterization

The surface morphology of BHJ, Sq and Alt-Sq blade-coated active layers was characterized using atomic force microscopy (AFM) (**Figure 5.6a-c)**. Overall, the images reveal smooth surfaces with root-mean-square (RMS) roughness of 3.1, 3.3 and 4.1 nm for BHJ, Sq and Alt-Sq films, respectively. However, the domain features of BHJ and Sq films are larger than those of Alt-Sq blade-coated film, probably due to better reorganization of the P3HT upon sequential deposition of $(3BS)_2$-SiPc. These fine features in the Alt-Sq blade coated films led to a higher FF in the devices due to a better D/A interface and thus improved charge dissociation. This is also in good agreement with obtaining balanced charge carrier mobility by the SCLC method in the case of Alt-Sq blade coated devices.

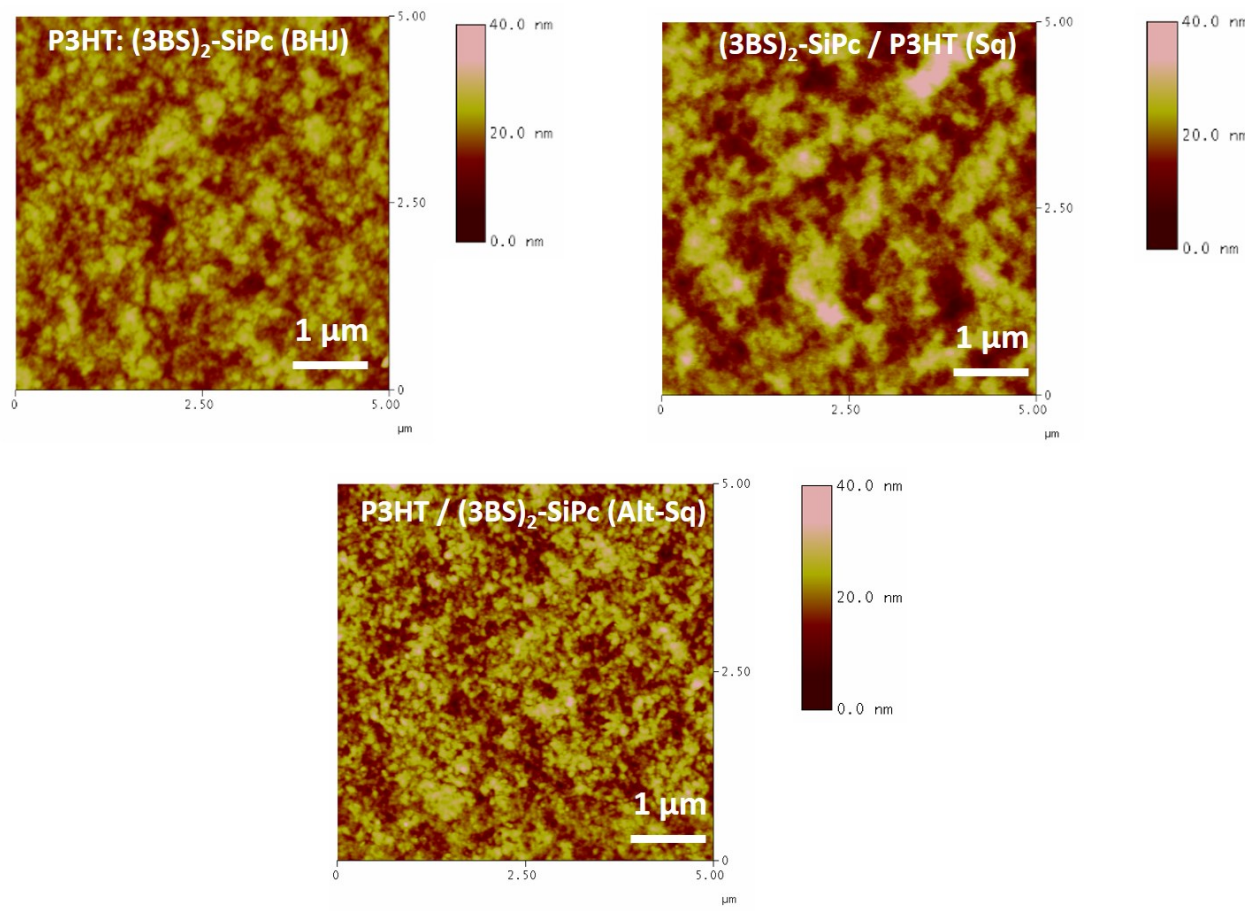

Figure 5-5. Tapping mode AFM height images of P3HT: $(3BS)_2$-SiPc OPVs based on three types of active layers coated on flexible substrates. The roughness of BHJ film (rms roughness = 3.1 nm); for sequential (Sq) layer rms roughness = 3.3 nm; for Alternate sequential (Alt-Sq) layer rms roughness = 4.1 nm.

We also explored the composition of donor-acceptor in the vertical direction throughout the BHJ, Sq and Alt-Sq films, using time-of-flight secondary ion mass spectroscopy (TOF-SIMS) (**Figure 5.7a-c)**. The chemical elements through the active layers were tracked using their respective secondary ions. P3HT was tracked using sulphur ion (S-), silicon ion (SiCN-) for the (3BS)2-SiPc acceptor, ZnO ion (ZnO-) for the electron transport layer (ETL) layer, and indium oxide ion (InO2-) for the ITO layer. There are no significant differences between BHJ and Alt-Sq active layers, suggesting the vertical composition is very similar regardless of process. The intensity depth profiles of S^- and $SiCN^-$ signals are identical across the whole layer, indicating that P3HT and $(3BS)_2$-SiPc are well intermixed in the active layers.

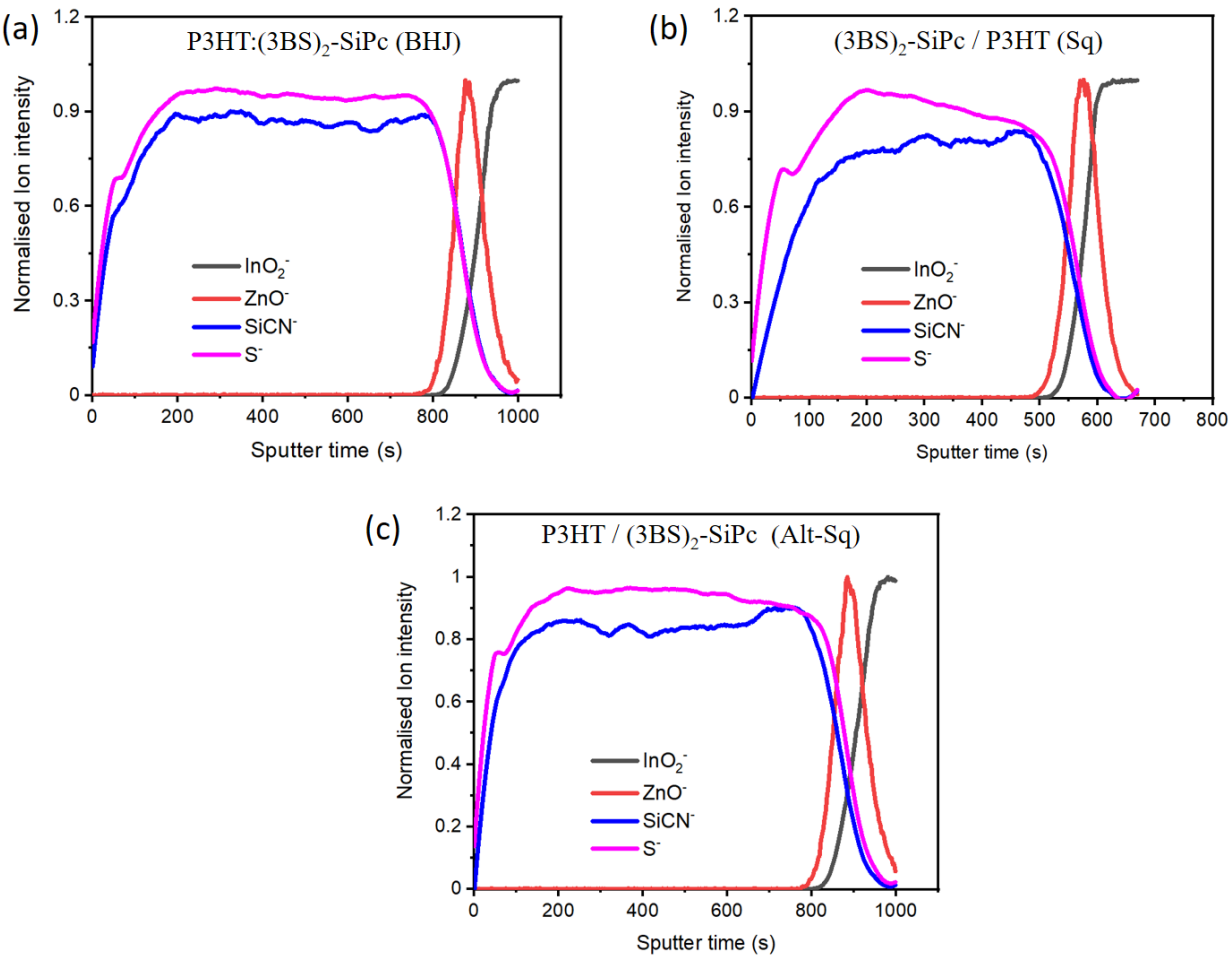

Figure 5-6. TOF-SIMS depth profiles of P3HT: $(3BS)_2$-SiPc OPVs (a) BHJ layer (b) Sequential (Sq) and (c) Alternate sequential (Alt-Sq) photoactive layers coated on ITO substrates.

The sputter time is greater for the BHJ and Alt-Sq structures than for Sq, suggesting the films are thicker and corroborating our initial observation that in the Sq structure, the P3HT solution is dissolving the $(3BS)_2$-SiPc layer and washing it away. Sq blade coated films also show a slight reduction in concentration of Si^- at initial etching times (compared to Alt-Sq and BHJ) suggesting the top of the films are less rich in $(3BS)_2$-SiPc, which is also consistent with P3HT being deposited on top of $(3BS)_2$-SiPc. For Alt-Sq, the TOF-SIMS results suggest that the $(3BS)_2$-SiPc solution does not dissolve the P3HT layer but rather swells and diffuses into the P3HT layer.[52] This results in good agreement with balanced charge carrier transport and OPV device performance.

5.5. Conclusion

In summary, we have optimized the use of simple materials with low-synthetic complexity: P3HT and $(3BS)_2$-SiPc for the development of scalable, large area and flexible OPVs. The devices were fabricated using blade coating and green solvents through different deposition approaches: BHJ, Sq, and Alt-Sq. Alt-Sq deposition, where the acceptor is deposited sequentially on top of the polymer, led to the best device performance, balanced charge carrier mobilities, and favourable morphology. Blade coating BHJ and Alt-Sq active layers with o-xylene solution led to similar vertical distribution of donor-acceptor morphology, suggesting similar performance can be obtained by both techniques. Typically, Alt-Sq deposition is favoured industrially over BHJ as each layer can be independently optimized rather than trying to optimize a more complex blend. These results demonstrate significant steps toward large-scale implementation of silicon phthalocyanines in low-cost, flexible OPVs.

.

5.6. References

1. Lipomi, D. J. & Bao, Z. Stretchable, elastic materials and devices for solar energy conversion. *Energy Environ. Sci.* **4**, 3314–3328 (2011).
2. Li, Y. *et al.* Color-neutral, semitransparent organic photovoltaics for power window applications. *Proc. Natl. Acad. Sci. U. S. A.* **117**, 21147–21154 (2020).
3. Lee, B., Lahann, L., Li, Y. & Forrest, S. R. Cost estimates of production scale semitransparent organic photovoltaic modules for building integrated photovoltaics. *Sustain. Energy Fuels* **4**, 5765–5772 (2020).
4. Hu, Z. *et al.* A critical review on semitransparent organic solar cells. *Nano Energy* **78**, 105376 (2020).
5. Zhu, L. *et al.* Single-junction organic solar cells with over 19% efficiency enabled by a refined double-fibril network morphology. *Nat. Mater.* **21**, 656–663 (2022).
6. Cui, Y. *et al.* Single-Junction Organic Photovoltaic Cells with Approaching 18% Efficiency. *Adv. Mater.* **32**, 1–7 (2020).
7. Wadsworth, A. *et al.* Critical review of the molecular design progress in non-fullerene electron acceptors towards commercially viable organic solar cells. *Chem. Soc. Rev.* **48**, 1596–1625 (2019).
8. Yang, C. *et al.* Molecular design of a non-fullerene acceptor enables a P3HT -based organic solar cell with 9.46% efficiency. *Energy Environ. Sci.* **13**, 2864–2869 (2020).
9. Xu, X., Zhang, G., Yu, L., Li, R. & Peng, Q. P3HT-Based Polymer Solar Cells with 8.25% Efficiency Enabled by a Matched Molecular Acceptor and Smart Green-Solvent Processing Technology. *Adv. Mater.* **31**, 1–7 (2019).
10. Po, R., Bianchi, G., Carbonera, C. & Pellegrino, A. 'all that glisters is not gold': An analysis of the synthetic complexity of efficient polymer donors for polymer solar cells. *Macromolecules* **48**, 453–461 (2015).
11. Moser, M., Wadsworth, A., Gasparini, N. & McCulloch, I. Challenges to the Success of Commercial Organic Photovoltaic Products. *Adv. Energy Mater.* **11**, (2021).
12. Holliday, S. *et al.* High-efficiency and air-stable P3HT-based polymer solar cells with a new non-fullerene acceptor. *Nat. Commun.* **7**, 1–11 (2016).
13. Po, R. *et al.* From lab to fab: How must the polymer solar cell materials design change?-an industrial perspective. *Energy Environ. Sci.* **7**, 925–943 (2014).

14. Xiao, B. *et al.* A2-A1-D-A1-A2 Type Non-Fullerene Acceptors with 2-(1,1-Dicyanomethylene)rhodanine as the Terminal Groups for Poly(3-hexylthiophene)-Based Organic Solar Cells. *ACS Appl. Mater. Interfaces* **10**, 34427–34434 (2018).
15. Baran, D. *et al.* Reducing the efficiency-stability-cost gap of organic photovoltaics with highly efficient and stable small molecule acceptor ternary solar cells. *Nat. Mater.* **16**, 363–369 (2017).
16. Xu, X., Zhang, G., Yu, L., Li, R. & Peng, Q. P3HT-Based Polymer Solar Cells with 8.25% Efficiency Enabled by a Matched Molecular Acceptor and Smart Green-Solvent Processing Technology. *Adv. Mater.* **31**, (2019).
17. Guo, X., Zhang, M., Cui, C., Hou, J. & Li, Y. Efficient polymer solar cells based on poly(3-hexylthiophene) and indene-C60 bisadduct fabricated with non-halogenated solvents. *ACS Appl. Mater. Interfaces* **6**, 8190–8198 (2014).
18. Plint, T., Lessard, B. H. & Bender, T. P. Assessing the potential of group 13 and 14 metal/metalloid phthalocyanines as hole transport layers in organic light emitting diodes. *J. Appl. Phys.* **119**, (2016).
19. Pearson, A. J. *et al.* Silicon phthalocyanines as dopant red emitters for efficient solution processed OLEDs. *J. Mater. Chem. C* **5**, 12688–12698 (2017).
20. Melville, O. A., Grant, T. M. & Lessard, B. H. Silicon phthalocyanines as N-type semiconductors in organic thin film transistors. *J. Mater. Chem. C* **6**, 5482–5488 (2018).
21. Melville, O. A. *et al.* Ambipolarity and Air Stability of Silicon Phthalocyanine Organic Thin-Film Transistors. *Adv. Electron. Mater.* **5**, 1–7 (2019).
22. King, B. *et al.* Silicon phthalocyanines for N-type organic thin-film transistors: Development of structure−property relationships. *ACS Appl. Electron. Mater.* (2021) doi:10.1021/acsaelm.0c00871.
23. Zysman-Colman, E. *et al.* Solution-Processable Silicon Phthalocyanines in Electroluminescent and Photovoltaic Devices. *ACS Appl. Mater. Interfaces* **8**, 9247–9253 (2016).
24. Ke, L. *et al.* Panchromatic ternary/quaternary polymer/fullerene BHJ solar cells based on novel silicon naphthalocyanine and silicon phthalocyanine dye sensitizers. *J. Mater. Chem. A* **5**, 2550–2562 (2017).
25. Lessard, B. H. *et al.* Assessing the potential roles of silicon and germanium phthalocyanines

in planar heterojunction organic photovoltaic devices and how pentafluoro phenoxylation can enhance π-π Interactions and device performance. *ACS Appl. Mater. Interfaces* **7**, 5076–5088 (2015).

26. Sundaresan, C. *et al.* Changes in Optimal Ternary Additive Loading when Processing Large Area Organic Photovoltaics by Spin- versus Blade-Coating Methods. *Sol. RRL* **5**, 1–8 (2021).
27. Faure, M. D. M., Grant, T. M. & Lessard, B. H. Silicon phthalocyanines as acceptor candidates in mixed solution/evaporation processed planar heterojunction organic photovoltaic devices. *Coatings* **9**, (2019).
28. Ke, L. *et al.* A Series of Pyrene-Substituted Silicon Phthalocyanines as Near-IR Sensitizers in Organic Ternary Solar Cells. *Adv. Energy Mater.* **6**, 1–13 (2016).
29. Lomax, S. Q. Phthalocyanine and quinacridone pigments: their history, properties and use. *Stud. Conserv.* **50**, 19–29 (2005).
30. Vebber, M. C., Rice, N. A., Brusso, J. L. & Lessard, B. H. Thermodynamic Property-Performance Relationships in Silicon Phthalocyanine-Based Organic Photovoltaics. *ACS Appl. Energy Mater.* **5**, 3426–3435 (2022).
31. Dindault, C. *et al.* Correlating Morphology, Molecular Orientation, and Transistor Performance of Bis(pentafluorophenoxy)silicon Phthalocyanine Using Scanning Transmission X-ray Microscopy. *Chem. Mater.* (2022) doi:10.1021/acs.chemmater.2c00277.
32. Lessard, B. H. The Rise of Silicon Phthalocyanine: From Organic Photovoltaics to Organic Thin Film Transistors. *ACS Appl. Mater. Interfaces* **13**, 31321–31330 (2021).
33. Cranston, R. R. *et al.* N-Type Solution-Processed Tin versus Silicon Phthalocyanines: A Comparison of Performance in Organic Thin-Film Transistors and in Organic Photovoltaics. *ACS Appl. Electron. Mater.* **3**, 1873–1885 (2021).
34. Cranston, R. R. *et al.* Highlighting the processing versatility of a silicon phthalocyanine derivative for organic thin-film transistors. *J. Mater. Chem. C* **10**, 485–495 (2022).
35. Vebber, M. C., Rice, N. A., Brusso, J. L. & Lessard, B. H. Variance-resistant PTB7 and axially-substituted silicon phthalocyanines as active materials for high-Voc organic photovoltaics. *Sci. Rep.* **11**, 1–8 (2021).
36. Honda, S., Ohkita, H., Benten, H. & Ito, S. Selective dye loading at the heterojunction in

polymer/fullerene solar cells. *Adv. Energy Mater.* **1**, 588–598 (2011).

37. Dang, M. T. *et al.* Bis(tri-n-alkylsilyl oxide) silicon phthalocyanines: A start to establishing a structure property relationship as both ternary additives and non-fullerene electron acceptors in bulk heterojunction organic photovoltaic devices. *J. Mater. Chem. A* **5**, 12168–12182 (2017).
38. Vebber, M. C., Grant, T. M., Brusso, J. L. & Lessard, B. H. Bis(trialkylsilyl oxide) Silicon Phthalocyanines: Understanding the Role of Solubility in Device Performance as Ternary Additives in Organic Photovoltaics. *Langmuir* **36**, 2612–2621 (2020).
39. Sundaresan, C. *et al.* Design of ternary additive for organic photovoltaics: a cautionary tale. *RSC Adv.* **12**, 10029–10036 (2022).
40. Grant, T. M. *et al.* High Voc solution-processed organic solar cells containing silicon phthalocyanine as a non-fullerene electron acceptor. *Org. Electron.* **87**, 105976 (2020).
41. Grant, T. M., Dindault, C., Rice, N. A., Swaraj, S. & Lessard, B. H. Synthetically facile organic solar cells with >4% efficiency using P3HT and a silicon phthalocyanine non-fullerene acceptor. *Mater. Adv.* (2021) doi:10.1039/d1ma00165e.
42. Alem, S. *et al.* Solution-processed annealing-free ZnO nanoparticles for stable inverted organic solar cells. *Org. Electron.* **15**, 1035–1042 (2014).
43. Chen, D. *et al.* Synthesis and photovoltaic properties of two-dimensional D-A copolymers with conjugated side chains. *J. Polym. Sci. Part A Polym. Chem.* **49**, 3852–3862 (2011).
44. Zhou, Y. *et al.* Investigation on polymer anode design for flexible polymer solar cells. *Appl. Phys. Lett.* **92**, 1–4 (2008).
45. Schmidt-Hansberg, B. *et al.* Moving through the phase diagram: Morphology formation in solution cast polymer-fullerene blend films for organic solar cells. *ACS Nano* **5**, 8579–8590 (2011).
46. Kang, H. *et al.* Bulk-Heterojunction Organic Solar Cells: Five Core Technologies for Their Commercialization. *Adv. Mater.* **28**, 7821–7861 (2016).
47. Lessard, B. H. *et al.* Bis(tri- n -hexylsilyl oxide) silicon phthalocyanine: A unique additive in ternary bulk heterojunction organic photovoltaic devices. *ACS Appl. Mater. Interfaces* **6**, 15040–15051 (2014).
48. Grant, T. M., Dindault, C., Rice, N. A., Swaraj, S. & Lessard, B. H. Synthetically facile organic solar cells with >4% efficiency using P3HT and a silicon phthalocyanine non-

fullerene acceptor. *Mater. Adv.* **2**, 2594–2599 (2021).

49. Bozano, L., Carter, S. A., Scott, J. C., Malliaras, G. G. & Brock, P. J. Temperature- and field-dependent electron and hole mobilities in polymer light-emitting diodes. *Appl. Phys. Lett.* **74**, 1132–1134 (1999).
50. Li, X. *et al.* Simplified synthetic routes for low cost and high photovoltaic performance n-type organic semiconductor acceptors. *Nat. Commun.* **10**, 1–11 (2019).
51. Cheng, P. *et al.* Ternary System with Controlled Structure: A New Strategy toward Efficient Organic Photovoltaics. *Adv. Mater.* **30**, 1–8 (2018).
52. Ren, M. *et al.* High-Performance Ternary Organic Solar Cells with Controllable Morphology via Sequential Layer-by-Layer Deposition. *ACS Appl. Mater. Interfaces* **12**, 13077–13086 (2020).

Chapter 6 : Conclusion and Future work

6.1. Conclusion

Despite the significant increase in the power conversion efficiency of OPV devices achieved in the last few years, there are still a few key challenges that need to be addressed for successful commercialization of the technology. These include the overall costs and the scalability of materials and devices. The main cost driver of OPV manufacturing is the material cost. Silicon Phthalocyanines (SiPcs) could be very promising n-type semiconductors for OPV devices, due to their low synthetic complexity cost and also the ease of fine-tuning their optoelectronic properties through axial functionalization. This thesis demonstrates the fabrication of large-area OPV and the utilization of SiPcs as an effective ternary additive and as NFA using a scalable coating technique: blade coating.

In Chapter 3, PCDTBT: $PC_{71}BM$-based OPV devices with a large active area (~1cm^2) were fabricated using spin and blade coating techniques. Blade-coated devices were processed on flexible ITO/PET sheets. The incorporation of $(3HS)_2$-SiPc as a ternary additive in the PCDTBT: $PC_{71}BM$ blend enhances the OPV device performance through increased charge generation and improved charge carrier mobility. The performance of devices fluctuates with the concentration of the ternary additive and the optimal $(3HS)_2$-SiPc loading for blade-coated devices differs from that of spin-coated devices. This study demonstrates that the concentration of the ternary additive in OPV devices needs to be optimized as a function of processing conditions.

In Chapter 4, flexible ternary PCDTBT: $PC_{71}BM$-based OPV devices were demonstrated using a novel design and synthesis of carbazole-functionalized SiPc as a ternary additive. The new functionalized SiPc is hypothesized to increase the miscibility with PCDTBT polymer and improve the device's performance. The contact angle measurements show that PCDTBT polymer and carbazole-functionalized SiPc have similar surface energies, indicating good miscibility. The EQE spectra of ternary devices show a strong photon electron conversion in the SiPc absorption region but a decrease in PCDTBT: $PC_{71}BM$ contribution, suggesting that the additive is likely to be dispersed in the PCDTBT domain and act as hole traps, which led to a decrease in the performance of ternary devices. This study demonstrates the effect of solubility and miscibility properties of additives on the performance of ternary OPV devices.

In Chapter 5, OPV devices were fabricated using green solvents and the blade coating technique. Low synthetic complex acceptor material $(3BS)_2$-SiPc was selected as NFA and paired with P3HT. The active layer was coated from o-Xylene solutions in three different configurations: BHJ, sequential, and alternate sequential (Alt-Sq). The Alt-Sq configuration, where the NFA is deposited sequentially on top of the polymer, led to the best device performance with balanced charge carrier mobilities, and favorable morphology. The vertical distribution of donor-acceptor was well modulated to form an optimal phase separation for efficient charge transport pathways. These results demonstrate significant steps toward large-scale implementation of silicon Phthalocyanines in low-cost, flexible OPVs.

6.2. Recommendation for Future Work

This thesis demonstrated the use of SiPc derivatives in large-area OPV devices. The studies described the methodology for optimizing SiPcs-based active layer in OPV devices, combining the use of industrial-relevant processing solvents and scalable methods. The validity of these findings will ultimately rely on the commercial application of OPVs in which other critical factors than the device PCE are more important.

Improving the ternary film morphology and device performance

The results of Chapter 3 show the potential use of bis (tri-n-alkyl silyl oxide) silicon Phthalocyanines (SiPcs) as a ternary additive in large-area BHJ OPVs. The optimal loading of the ternary additive in spin-coated devices differs from that of blade-coated devices due to different film formation kinetics. I recommend making modifications to the SiPc structure by varying the length of alkyl chains **(Figure 6.1)** which would have an impact on the properties of the ink and the nanostructure of the active layer, processed by blade coating technique. Axial substitution (butyl -hexyl) affects the crystallization properties of SiPc, which could alter the segregation of donor/acceptor in the blend films. Therefore, the use of different alkyl chains-substituted SiPc in a scalable process could lead to a potential way to improve the PCE of PCDTBT: $PC_{71}BM$-based devices.

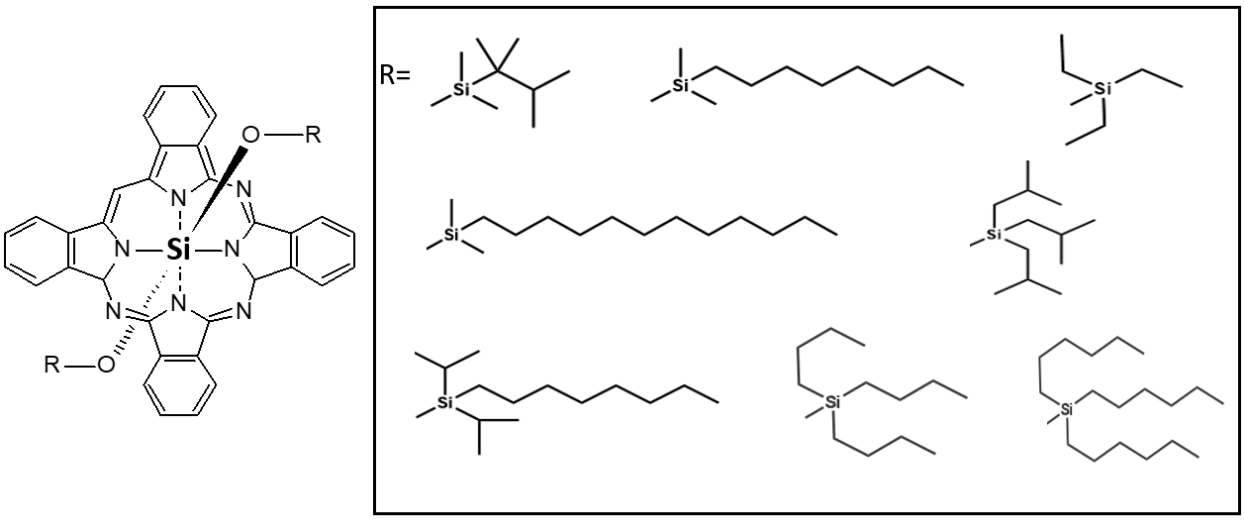

Figure 6-1. Different suggestions of alkyl chains-substituted SiPc for active layer materials in blade coated BHJ OPVs

Interface engineering and charge recombination studies

For the commercial deployment of OPVs, the golden triangle of PCE, stability, and cost should be considered concurrently. Chapter 5 demonstrates the use of industry-relevant parameters in OPV's fabrication, including low synthetic-cost materials, non-halogenated solvents, and large-area processing. The scalability of OPV's fabrication can induce defects in the layers of the device structure or at the interfaces, depending on the film drying kinetics and the physical properties of the coated layers. Understanding the origin of electrical losses in large-scale devices requires in-depth analysis of carrier dynamics. Electrochemical impedance spectroscopy (EIS) is a practical method that can be used to determine the recombination kinetics in SiPcs-based OPV devices. I believe that additional experiments are required to better understand the ternary systems and their operation. A valuable addition to the subject would be to investigate the exciton dissociation, charge transport and recombination dynamics in BHJ and LBL blade coated films. I believe the work I have accomplished can serve as a basis for exploring these approaches in the future through collaborations, which might further demonstrate the practical benefit of these scalable OPVs.

Appendix A: Supplementary Information for Chapter 3: Changes in Optimal Ternary Additive Loading when Processing Large Area Organic Photovoltaics by Spin vs Blade Coating Methods

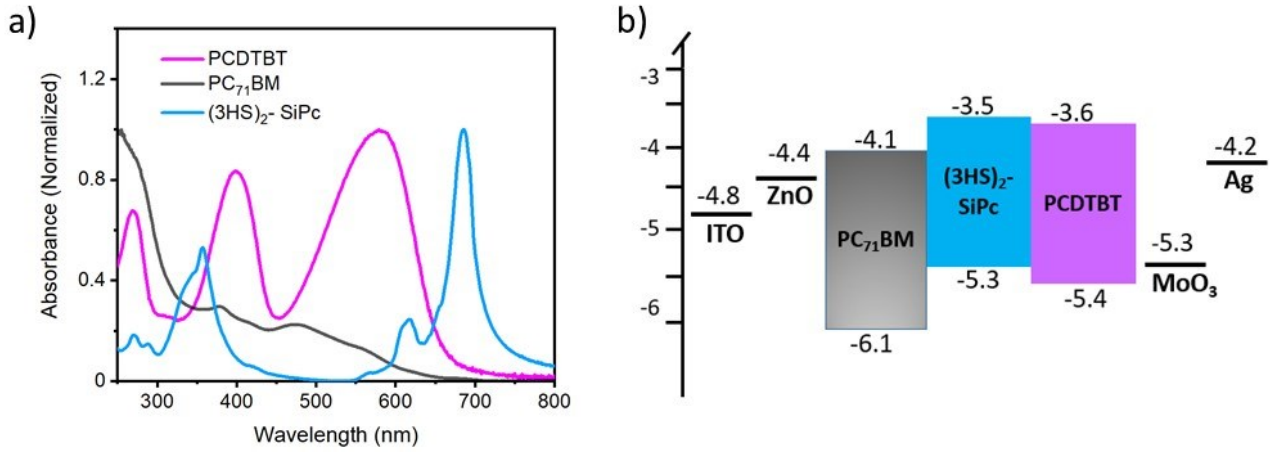

Figure S3.1. (a) Normalized UV-Vis absorption spectra of pure PCDTBT, $PC_{71}BM$, $(3HS)_2$-SiPc thin films. (b) Energy level diagram of all materials

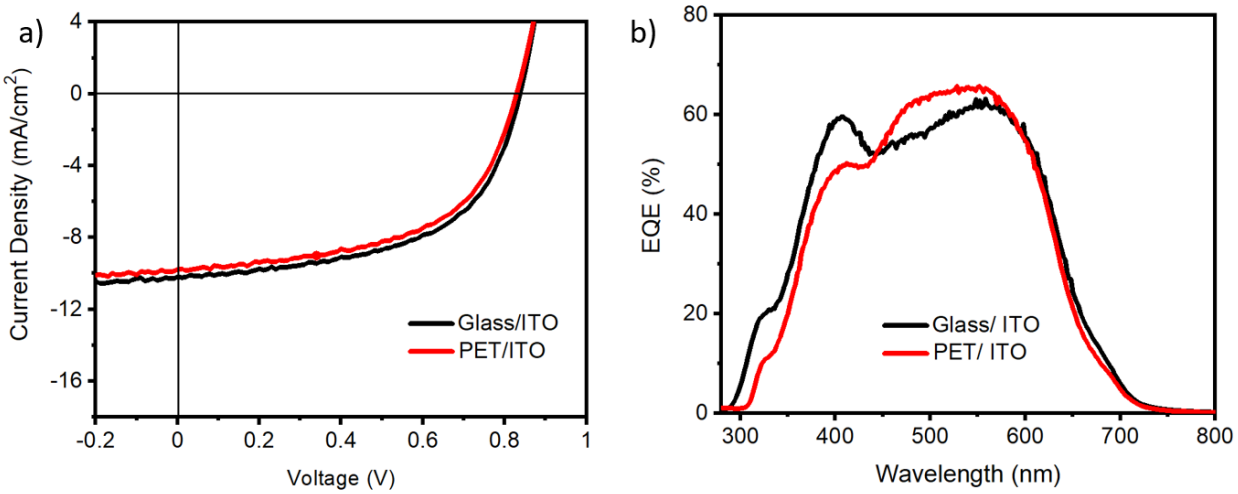

Figure S3.3 (a) J-V characteristics of PCDTBT: $PC_{71}BM$ baseline BHJ OPV devices fabricated by spin coating *on rigid and flexible ITO substrates.* (b) corresponding EQE curve

Table S3.*1*: Photovoltaic performance of baseline PCDTBT: $PC_{71}BM$ OPVs prepared by spin coating on rigid and flexible substrates.

Substrate	Calibrated J_{SC} from EQE (mA/cm^2)	V_{OC} (V)	FF	PCE (%)
Glass/ITO	9.7	0.83	55.8	4.5
PET/ITO	9.5	0.83	55.2	4.4

Table S3.2: Photovoltaic performance of ternary PCDTBT: $PC_{71}BM$ OPVs prepared by spin coating and blade coating with various $(3HS)_2$-SiPc loadings

Process	PCDTBT:PC 71BM: $(3HS)_2$-SiPc	$(3HS)_2$-SiPc Wt. % [(a)]	Calibrated J_{SC} from EQE (mA/cm^2) [b]	V_{OC} (V)	FF (%)	Calibrated PCE (%)
Spin	1:3:0	0	9.9 (±0.1)	0.834 (±0.001)	57.6 (±0.6)	4.7 (±0.1)
	1:3:0.12	3	10.1 (±0.1)	0.845 (±0.001)	58.3 (±0.5)	5.0 (±0.1)
	1:3:0.2	5	10.9 (±0.2)	0.852 (±0.001)	57.8 (±0.4)	5.4 (±0.2)
	1.3:0.4	10	9.8 (±0.1)	0.852 (±0.001)	58.6 (±0.5)	4.9 (±0.2)
	1:3:0.6	15	9.7 (± 0.1)	0.845 (±0.001)	57.4 (±0.5)	4.7 (±0.1)
	1:3:0.8	20	9.5 (± 0.1)	0.844 (±0.001)	57.8 (±0.5)	4.6 (±0.1)
	1:3:1.0	25	9.2 (± 0.1)	0.835 (±0.001)	54.1 (±0.3)	4.1 (±0.1)
Blade	1:3:0	0	9.8 (±0.1)	0.842 (±0.001)	56.5 (±0.3)	4.6 (±0.1)
	1:3:0.12	3	10.2 (±0.1)	0.842 (±0.001)	55.3 (±0.5)	4.7 (±0.2)
	1:3:0.2	5	10.3 (±0.2)	0.844 (±0.001)	54.6 (±0.4)	4.8 (±0.2)
	1.3:0.4	10	11.2 (±0.1)	0.851 (±0.001)	55.8 (±0.5)	5.3 (±0.1)
	1:3:0.6	15	10.4 (± 0.1)	0.844 (±0.001)	55.0 (±0.5)	4.8 (±0.1)
	1:3:0.8	20	9.7 (± 0.1)	0.835 (±0.001)	53.0 (±0.5)	4.3 (±0.2)
	1:3:1.0	25	9.0 (± 0.1)	0.834 (±0.001)	48.2 (±0.3)	3.6 (±0.2)

All OPV devices were characterized under AM 1.5G, 100 $mWcm^{-2}$. Device areas is 1 cm^2. All values are average of more than 4 devices and the values in parentheses is the standard deviation. All spin or blade coating process were performed in air. The base temperature for the blade process is 45 °C. [(a)]$(3HS)_2$-SiPc mass ratio in the blend with respect to total mass of PCDTBT: $PC_{71}BM$. [(b)]Current density (Jsc) calculated from EQE curve.

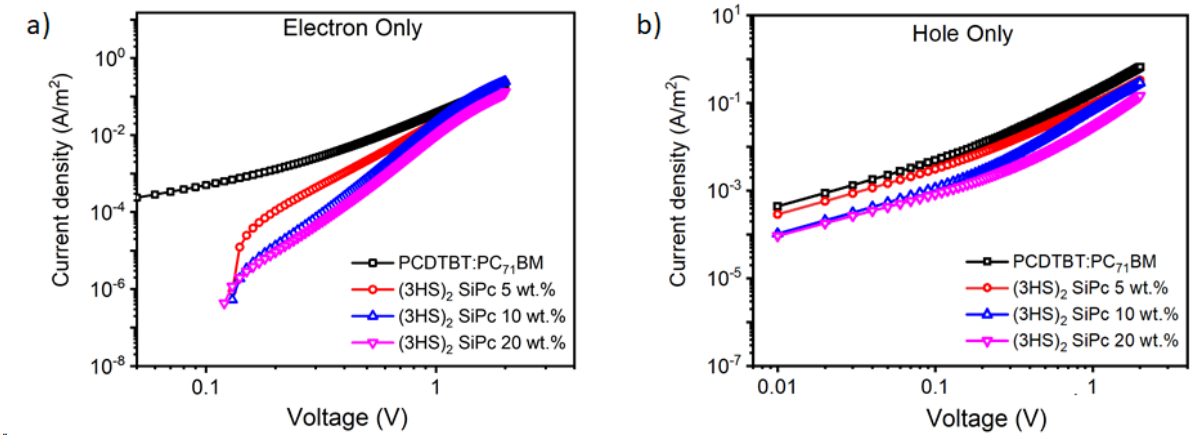

Figure S3.3: Log-log plot of dark J-V characteristics plot of binary and ternary composition of active layer processed by spin coating. a) Electron only devices comprise device structure ITO/ZnO/active layer/LiF/Al. b) Hole only devices comprise device structure ITO/PEDOT: PSS/active layer/MoO_3/Ag.

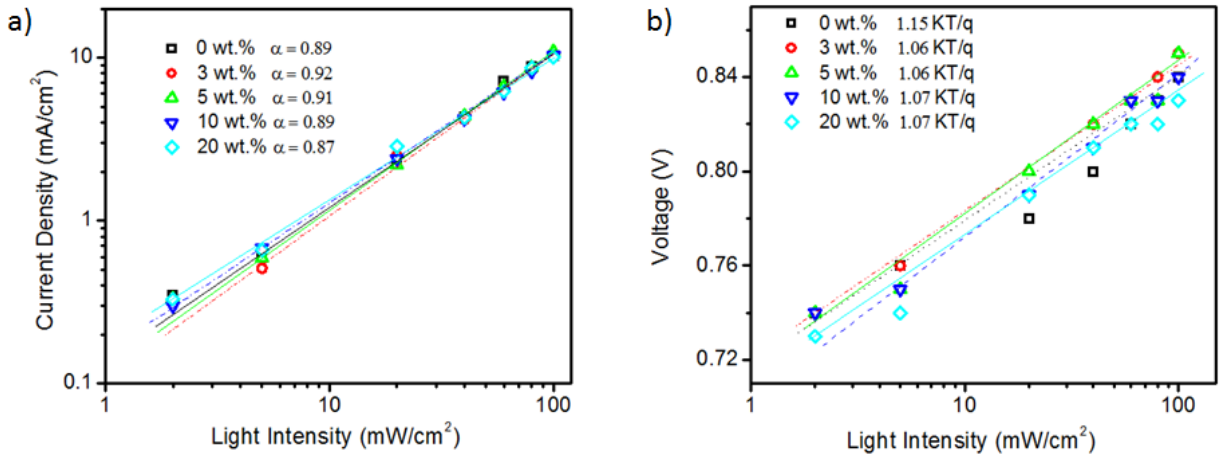

Figure S3.4: Light intensity dependence short circuit density and (a) open circuit voltage (b) of spin-coated PCDTBT:PC_{71}BM:$(3HS)_2$-SiPc devices with various $(3HS)_2$-SiPc loadings.

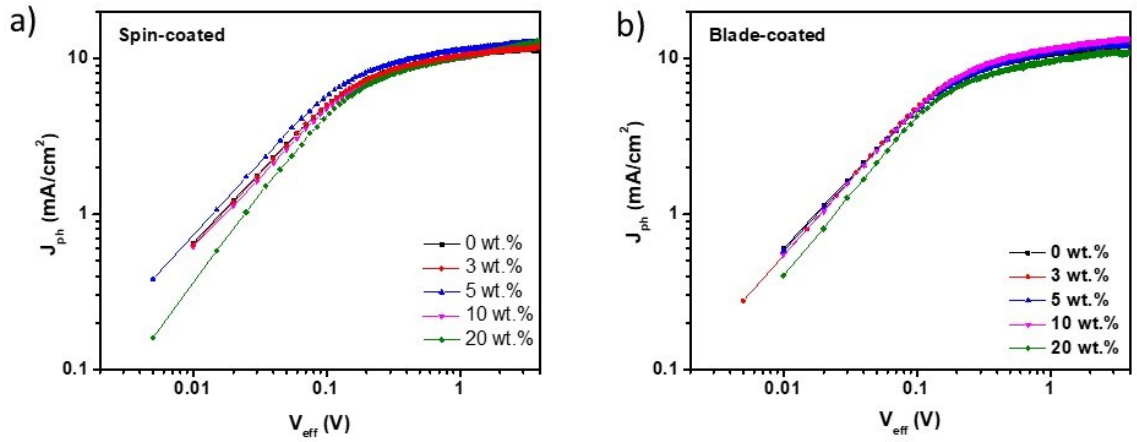

Figure S3.5: Photocurrent density (J_{ph}) as a function of the effective voltage (V_{eff}) for spin-coated (a) and blade-coated (b) PCDTBT:$PC_{71}BM$:$(3HS)_2$-SiPc devices with various $(3HS)_2$-SiPc loadings.

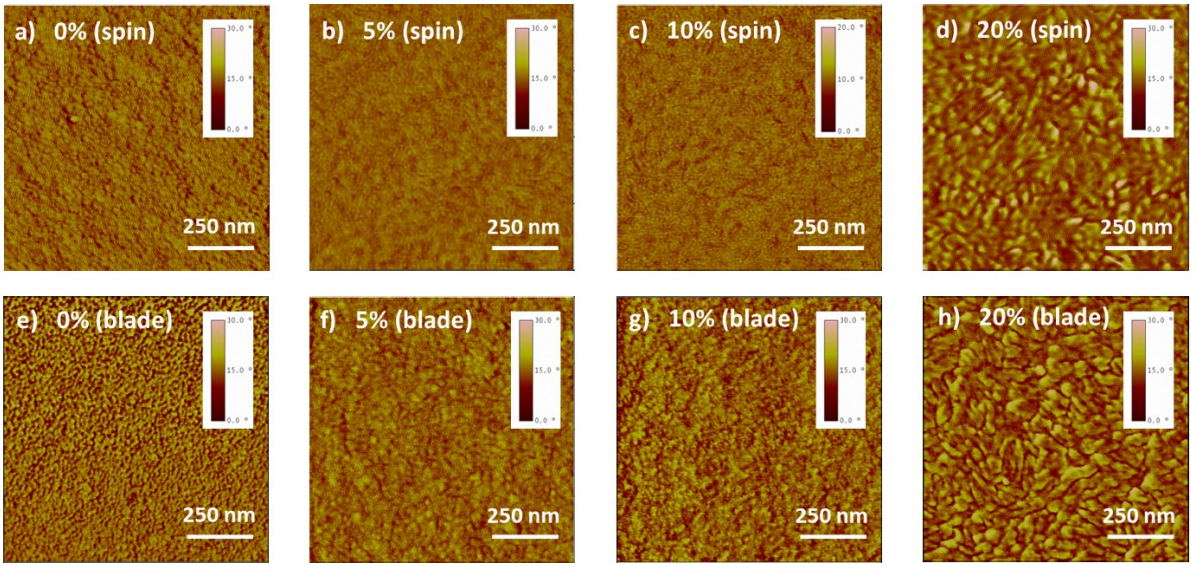

Figure S3.6: Tapping mode AFM phase images of PCDTBT: $PC_{71}BM$:$(3HS)_2$-SiPc ternary blends with various $(3HS)_2$-SiPc contents deposited by spin-coating a) 0wt% (rms roughness= 0.75 nm); b) 5wt% (rms roughness = 0.82 nm); c) 10 wt. % (rms roughness = 0.87 nm); d) 20 wt.% (rms roughness = 1.57 nm) and by blade-coating e) 0wt% (rms roughness = 0.73 nm); f) 5wt% (rms roughness = 0.77 nm); g) 10 wt. % (rms roughness = 0.74 nm); h) 20 wt.% (rms roughness = 1.05 nm).

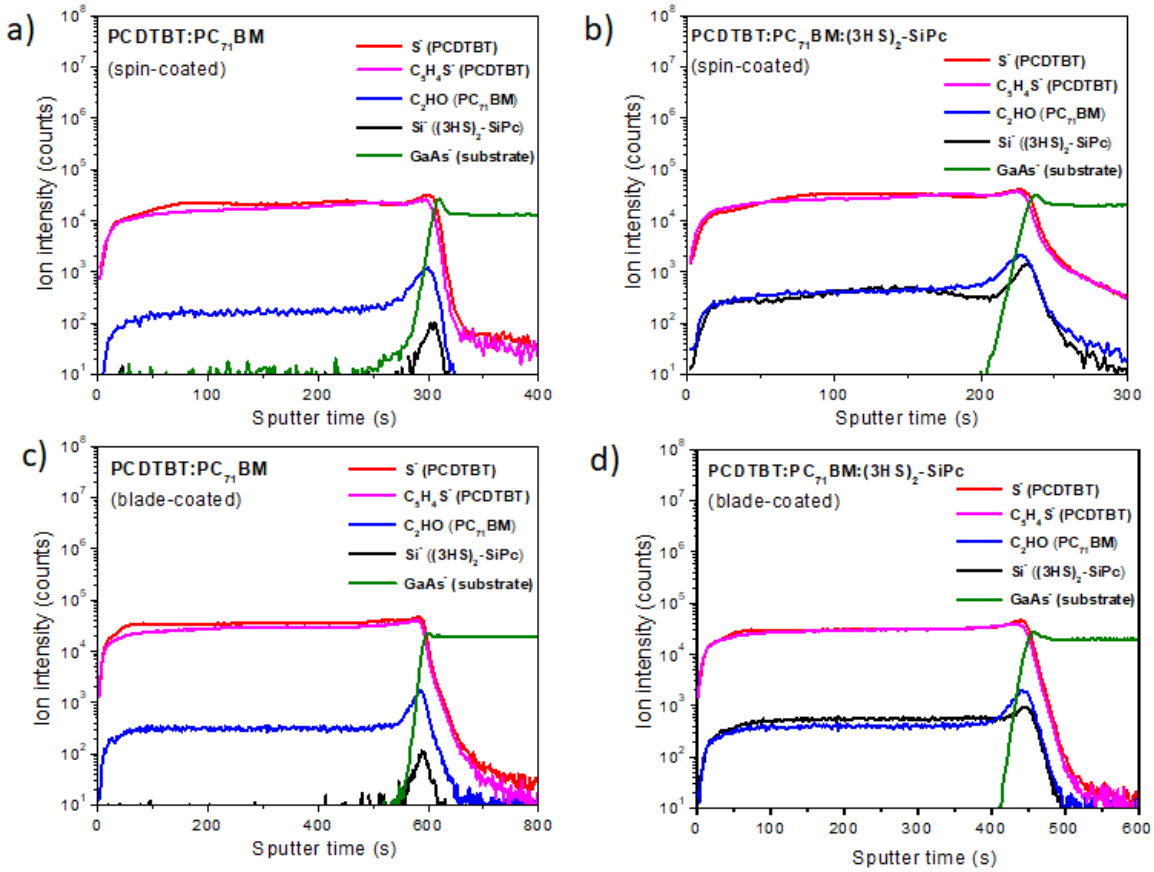

Figure S3.7: TOF-SIMS depth profile of: spin-coated and blade-coated PCDTBT:$PC_{71}BM$ films (a,c) and ternary films with 10wt% of $(3HS)_2$-SiPc additive (b,d). The increase in signals at GaAs interface is due to the sputter yield enhancement caused by the native oxide of the substrate.

Appendix B - Supplementary Information for Chapter 4: Design of Ternary Additive for Organic Photovoltaics: A Cautionary Tail

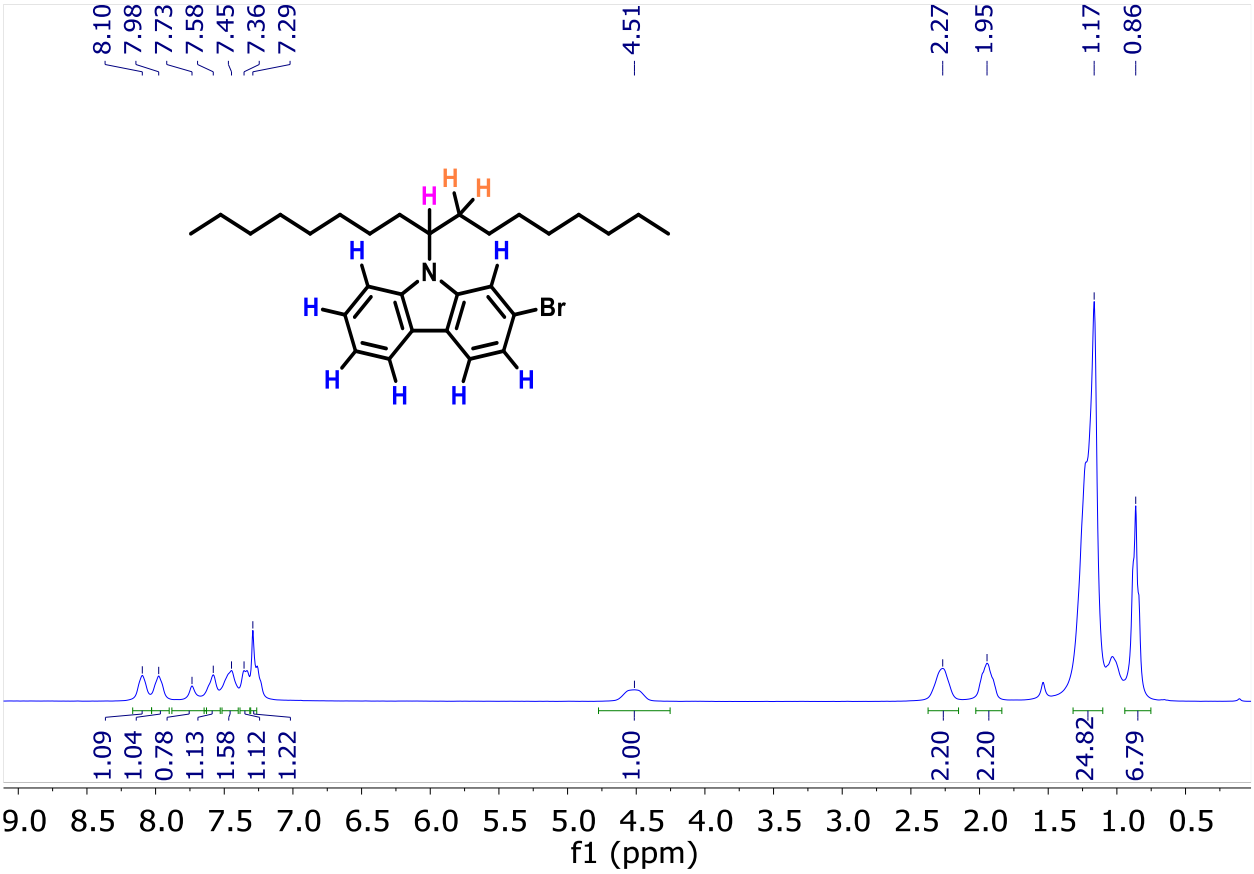

Figure S4.1. 1H NMR spectra recorded at 300K in CDCl3

^{1}H NMR (δ, $CDCl_3$, RT, 300 MHz): 8.10 (m, 1H), 7.98 (m, 1H), 7.73 (m, 1H), 7.58 (m, 1H), 7.45 (m, 1H), 7.36 (m, 1H), 7.29 (m, 1H), 4.51 (m, 1H), 2.27 (m, 2H), 1.95(m, 2H), 1.17(m, 24H), 0.86 (t, 6H).

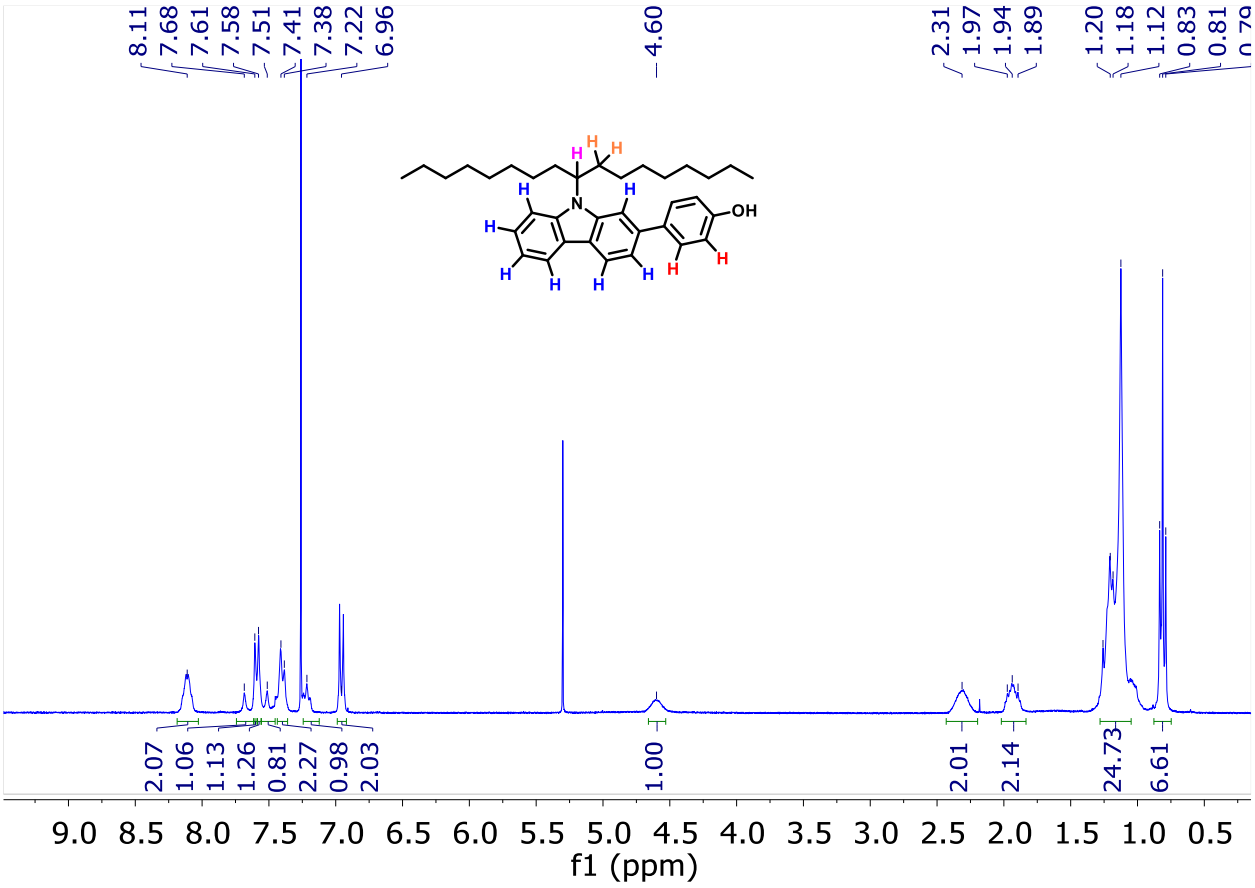

Figure S4.2. 1H NMR spectra recorded at 300K in CDCl3

^{1}H NMR (δ, $CDCl_3$, RT, 300 MHz): 8.11 (dd, 2H), 7.68 (m, 1H), 7.61 (m, 1H), 7.58 (m, 1H), 7.51 (m, 1H), 7.38−7.41 (m, 2H), 7.22 (m, 1H), 6.96 (dt, 2H), 4.60 (m, 1H), 2.31 (m, 2H), 1.94 (m, 2H), 1.12−1.26 (m, 24H), 0.83−0.79 (t, 6H).

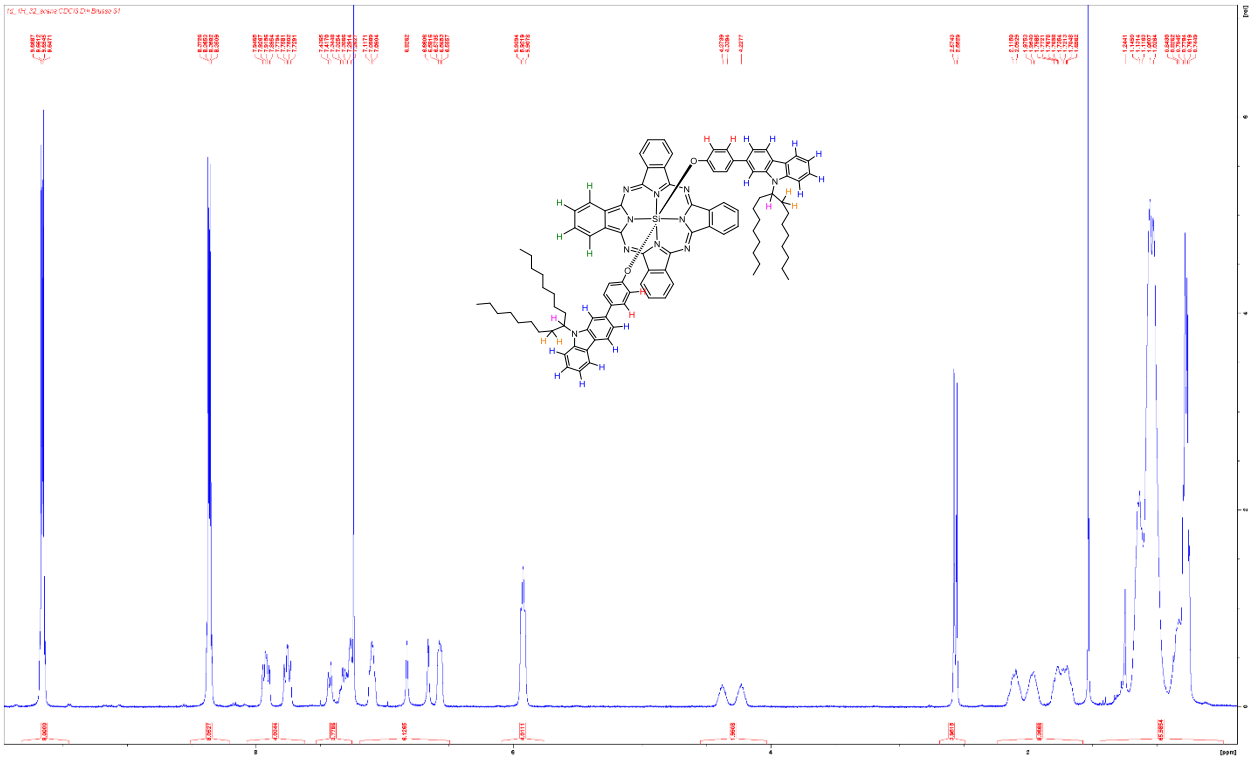

Figure S4.3. 1H NMR spectra recorded at 300K in CDCl3

^{1}H NMR (δ, $CDCl_3$, RT, 400 MHz): 9.65−9.67 (m, 8H), 8.35−8.37 (m, 8H), 7.73−7.94 (ddd, 4H), 7.28−7.45 (m, 4H), 7.09−7.12 (m, 2H), 6.66−6.83 (m, 2H), 6.56−6.58 (m, 2H), 5.91−5.94 (m, 4H), 4.23−4.37 (m, 2H), 2.55 (dt, 4H), 1.70−2.11 (m, 8H), 1.03−1.14 (m, 48H), 0.75−0.84 (m, 12H).

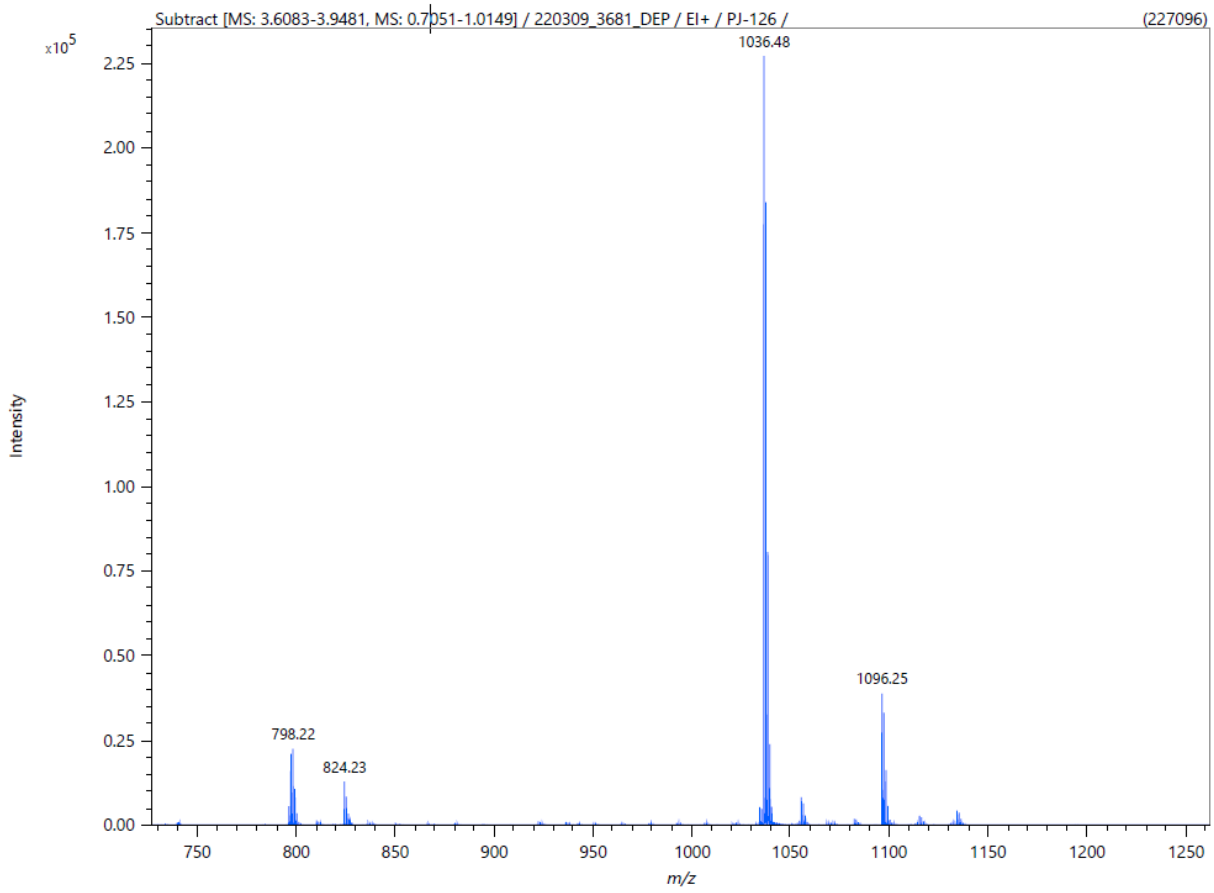

Figure S4.4. Electrospray ionization (ESI) Mass spectra plot of $(CBzPho)_2$-SiPc

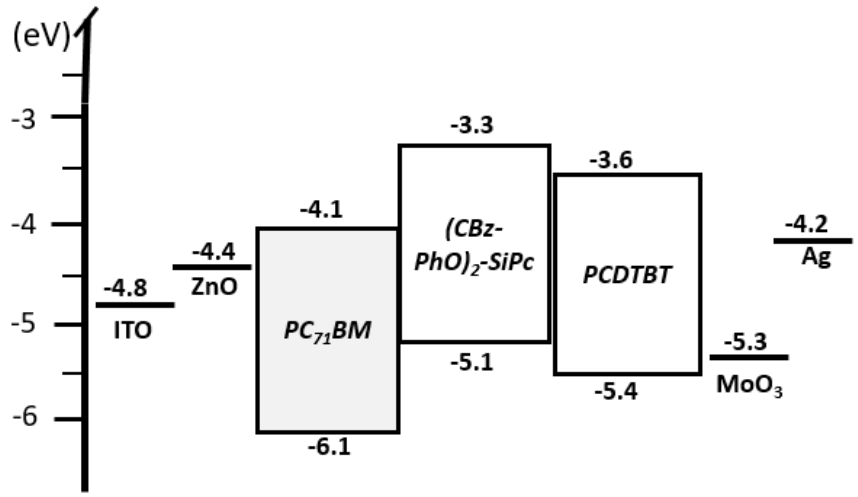

Figure S4.5. Energy level diagram of all materials used in ternary devices.

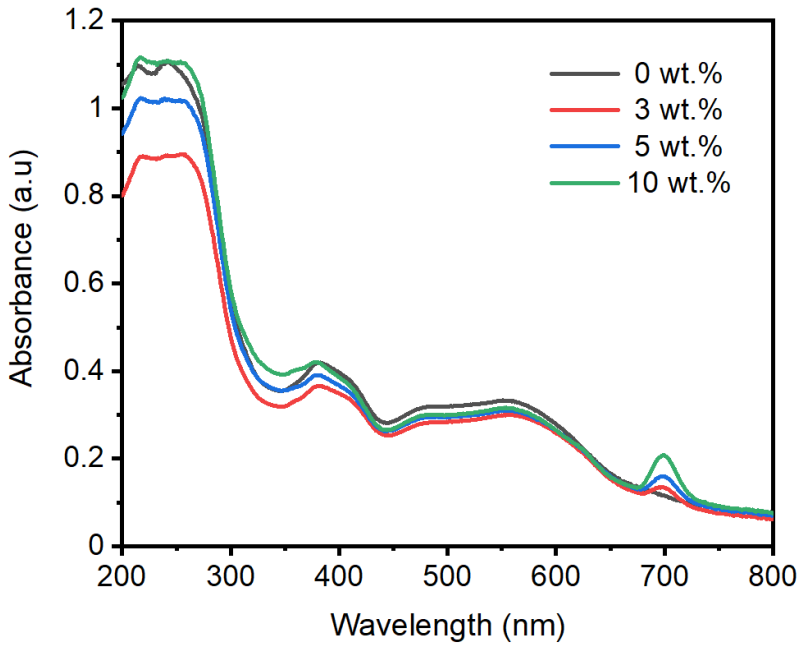

Figure S4.6. UV–vis absorption spectra of PCDTBT: $PC_{71}BM$ binary film and ternary films with different

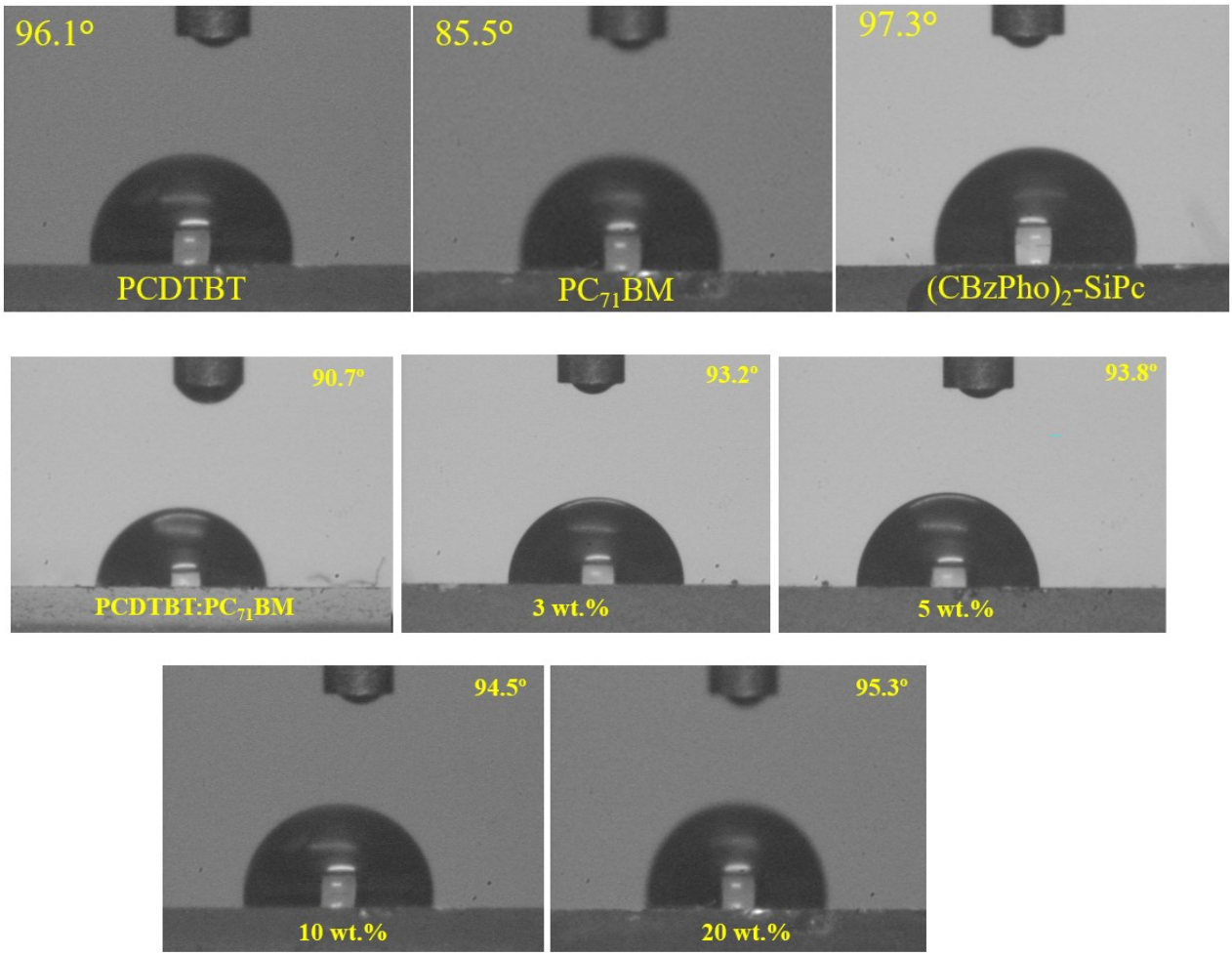

Figure S4.7: Water contact angle images of pristine films, binary and ternary films with different content of (CBzPho)2-SiPc varies from 0 to 20wt.%.

Table S4.1. Summary of H2O Contact Angle Measurements on ternary Films [(a)]

Films [(a)]	**Water Contact Angle (Deg)**	**Surface Energy (N mm^{-1})[(b)]**
PCDTBT:PC71BM	90.7 (± 0.6)	28.1 (± 0.7)
3 wt.% (CBzPho)2-SiPc	93.2 (± 0.4)	26.5 (± 0.7)
5 wt.% (CBzPho)2-SiPc	93.8 (± 0.7)	26.1 (± 0.5)
10 wt.% (CBzPho)2-SiPc	94.5 (± 0.6)	25.7 (± 0.4)
20 wt.% (CBzPho)2-SiPc	95.3 (± 0.5)	25.4 (± 0.3)

Table S4.2: Photovoltaic performance of ternary PCDTBT: $PC_{71}BM$ OPVs prepared by blade coating with various $(CBzPho)_2$-SiPc loadings.

PCDTBT: $PC_{71}BM$: $(CBzPho)_2$-SiPc	$(CBzPho)_2$-SiPc Wt. % [(a)]	Calibrated J_{SC} from EQE (mA/cm^2) [b]	V_{OC} (V)	FF (%)	Calibrated PCE (%)
1:3:0	0	9.4 (±0.1)	0.842 (±0.001)	56.6 (±0.5)	4.5 (±0.1)
1:3:0.12	3	9.2 (±0.1)	0.835 (±0.001)	53.8 (±0.7)	4.1 (±0.1)
1:3:0.2	5	9.1 (±0.1)	0.842 (±0.001)	51.8 (±0.4)	3.9 (±0.1)
1.3:0.4	10	9.0 (±0.1)	0.845 (±0.002)	49.6 (±0.2)	3.8 (±0.1)
1:3:0.6	20	8.4 (± 0.3)	0.862 (±0.002)	48.6 (±0.2)	3.5 (±0.1)

All OPV devices were characterized under AM 1.5G, 100 $mWcm^{-2}$. Device areas is 1 cm^2. All values are average of more than 5 devices and the value in parentheses is the standard deviation. Blade coating process were performed in air. The base temperature for the blade process is 45 °C. [(a)]$(CBzPho)_2$-SiPc mass ratio in the blend with respect to total mass of PCDTBT: $PC_{71}BM$. [(b)]Current density (Jsc) calculated from integration wavelength of EQE curve.

Charge generation and recombination dynamics

In order to further investigate the exciton generation and dissociation process of the binary and ternary devices, the exciton generation rates *(G_{max})* and charge dissociation probabilities (P_{diss}) were analysed by characterization of photocurrent density (J_{ph}) against the effective voltage (V_{eff}), as shown in Figure S8. J_{ph} is defined as J_{ligh}–J_{dark}, where J_{Light} and J_{Dark} are the photocurrent densities under light illumination and in the dark, respectively. And $V_{eff} = V_0 - V_{appl}$, where V_0 is the voltage at which $J_{ph} = 0$, and V_{appl} is the applied bias.[1] The photogenerated excitons were almost dissociated into free charge carriers when V_{eff} reached <2 V, and thus J_{ph} could reach saturation (J_{sat}). We adopted the ratio of J_{ph}/J_{sat} to evaluate the exciton dissociation probability (P_{diss}) in the devices.[2] Assuming that all of the photogenerated excitons are dissociated and contributed to the current in the saturated regime due to sufficiently high electric field, the values of G_{max} can be obtained by $J_{sat} = qLG_{max}$, where q is the elementary charge and L is the thickness of the binary or ternary organic layer and Jsat is saturation current density at elevated V_{eff} (3.8V). Table S3 shows the values obtained for various (CBzPho)2-SiPc weight ratio loading. As expected the value of G_{max} for various addition of (CBzPho)2-SiPc are reduces compare to the baseline devices due to the high density of recombination sites as replicated in the performance of J-V curve. Under the short-circuit conditions, the (P_{diss}) values were 85.4%, 80.2%, 80.5%, and 81.5% for the devices with 0, 3, 5, and 10wt.% **(CBzPho)2-SiPc,** respectively.

The dynamics of recombination in PCDTBT:PC_{71}BM:(CBzPho)2-SiPc devices were investigated through the analysis of J_{SC} and V_{OC} under various light intensities (P_{light}). The J-V characterizations of binary and ternary devices with different content of $(CBzPho)_2$-SiPc. The plot ln (J_{SC}) versus ln (P_{light}) provides information on the degree of bimolecular recombination. The slope (α) implies close to unity means, negligible bimolecular recombination associated with the

OPV devices.[3], [4] all the ternary devices slope (α) values shows higher values than the baseline devices. (Figure S9a). In addition, trap assisted monomolecular recombination extracted for the binary and ternary devices from the (Voc) versus Natural logarithmic (P_{light}) plot. Typically, a slope (S) equal to kT/q suggests the absence of bimolecular recombination, whereas an S ranging between 1 and 2 indicates the presence of monomolecular recombination and trap assisted recombination losses.[5], [6] It can be observed that the higher Slope (S) value of the PCDTBT: $PC_{71}BM$: (CBzPho)2-SiPc indicates (Figure S4.9b) that adding a small concentration of (CBzPho)2-SiPc results in a higher trap-assisted recombination associated, resulting in lower J_{SC} and FF as compared to those of the binary system.

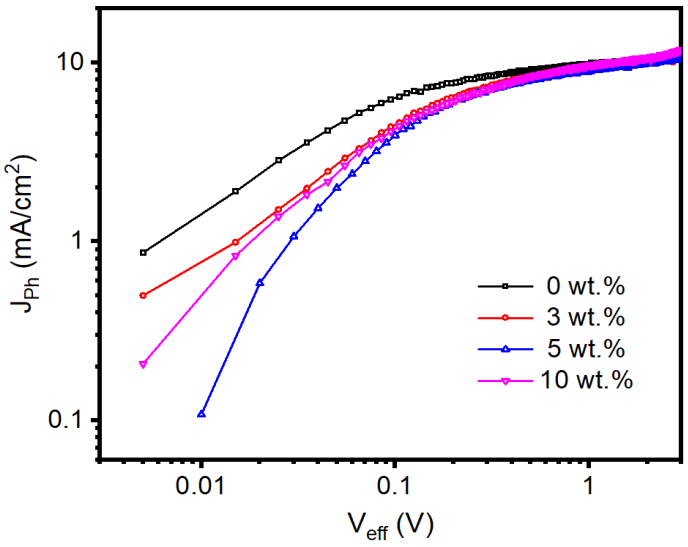

Figure S4.8. Photocurrent density *(J_{ph})* as a function of the effective voltage *(V_{eff})* of blade-coated PCDTBT:PC71BM:(CBzPho)2-SiPc devices with various (CBzPho)2-SiPc loadings.

Table S4.3: Charge generation parameters of blade coated PCDTBT: $PC_{71}BM$:$(CBzPho)_2$-SiPc ternary devices with different $(CBzPho)_2$-SiPc contents

$(CBzPho)_2$-SiPc Wt. %	J_{sat} (mA/cm^2)	G_{max} (cm^{-3}s^{-1})	P_{diss} (%)
0	11.8 (±0.1)	8.87 x 10^{21}	85.4
3	11.6 (±0.1)	8.72 x 10^{21}	80.2
5	12.5 (±0.2)	9.20 x 10^{21}	80.5
10	11.5 (± 0.1)	8.65 x 10^{21}	81.5

J_{sat} *is* the saturation current density, P_{diss} is the charge dissociation probability, G_{max} is the charge carrier generation.

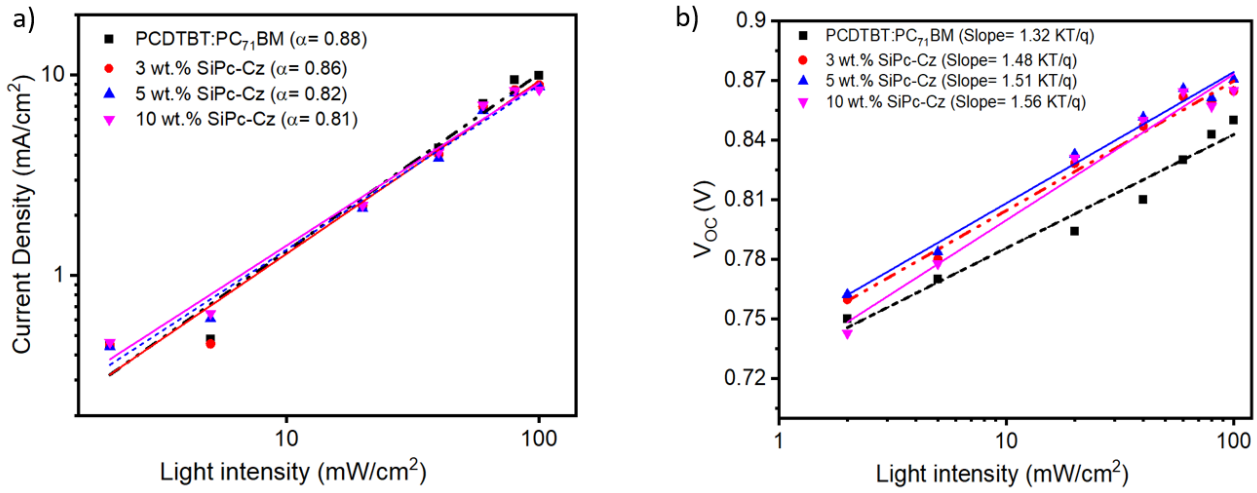

Figure S4.9. Light intensity dependence short circuit density and (a) open circuit voltage (b) of blade-coated PCDTBT: $PC_{71}BM$:$(CBzPho)_2$-SiPc devices with various $(CBzPho)_2$-SiPc loadings.

Table S4.4. Energy levels of silicon phthalocyanine and Silicon Napththalocyanine derivatives incorporated into OPV devices

SiPc derivatives	HOMO (eV)	LUMO (eV)	Ref.
$(CBzPho)_2$-SiPc	-5.1	-3.3	This Work
$(HxN_3)_2$-SiPc	-5.4	-3.6	[7]
$(3XS)_2$-SiPc	-5.3	-3.4	[8][9]
X_2-SiPc	-5.3	-3.5	[10]
$(XF)_2$-SiPc	-5.9	-4.0	[11]
Carboxyl-SiPc	-5.4	-3.6	[12]
(Pys-SiPc)	-5.3	-3.6	[13]
(3XS-SiNc)	-4.8	-3.4	[14]

References:

[1] P. Bi and X. Hao, "Versatile Ternary Approach for Novel Organic Solar Cells: A Review," *Sol. RRL*, vol. 3, no. 1, pp. 1–34, 2019, doi: 10.1002/solr.201800263.

[2] F. Paquin, J. Rivnay, A. Salleo, N. Stingelin, and C. Silva, "Multi-phase semicrystalline microstructures drive exciton dissociation in neat plastic semiconductors," *J. Mater. Chem. C*, vol. 3, no. 207890, pp. 10715–10722, 2015, doi: 10.1039/b000000x.

[3] A. K. K. Kyaw *et al.*, "Intensity dependence of current-voltage characteristics and recombination in high-efficiency solution-processed small-molecule solar cells," *ACS Nano*, vol. 7, no. 5, pp. 4569–4577, 2013, doi: 10.1021/nn401267s.

[4] D. Credgington, F. C. Jamieson, B. Walker, T. Q. Nguyen, and J. R. Durrant, "Quantification of geminate and non-geminate recombination losses within a solution-processed small-molecule bulk heterojunction solar cell," *Adv. Mater.*, vol. 24, no. 16, pp. 2135–2141, 2012, doi: 10.1002/adma.201104738.

[5] L. Xiao *et al.*, "Multiple Roles of a Non-fullerene Acceptor Contribute Synergistically for High-Efficiency Ternary Organic Photovoltaics," *Joule*, vol. 2, no. 10, pp. 2154–2166,

2018, doi: 10.1016/j.joule.2018.08.002.

[6] L. J. A. Koster, M. Kemerink, M. M. Wienk, K. Maturová, and R. A. J. Janssen, "Quantifying bimolecular recombination losses in organic bulk heterojunction solar cells," *Adv. Mater.*, vol. 23, no. 14, pp. 1670–1674, 2011, doi: 10.1002/adma.201004311.

[7] T. M. Grant, T. Gorisse, O. Dautel, G. Wantz, and B. H. Lessard, "Multifunctional ternary additive in bulk heterojunction OPV: Increased device performance and stability," *J. Mater. Chem. A*, vol. 5, no. 4, pp. 1581–1587, 2017, doi: 10.1039/c6ta08593h.

[8] M. T. Dang, T. M. Grant, H. Yan, D. S. Seferos, B. H. Lessard, and T. P. Bender, "Bis(tri-n-alkylsilyl oxide) silicon phthalocyanines: A start to establishing a structure property relationship as both ternary additives and non-fullerene electron acceptors in bulk heterojunction organic photovoltaic devices," *J. Mater. Chem. A*, vol. 5, no. 24, pp. 12168–12182, 2017, doi: 10.1039/c6ta10739g.

[9] S. Honda, S. Yokoya, H. Ohkita, H. Benten, and S. Ito, "Light-harvesting mechanism in polymer/fullerene/dye ternary blends studied by transient absorption spectroscopy," *J. Phys. Chem. C*, vol. 115, no. 22, pp. 11306–11317, 2011, doi: 10.1021/jp201742v.

[10] T. M. Grant and J. L. Brusso, "Bis(trialkylsilyl oxide) Silicon Phthalocyanines: Understanding the Role of Solubility in Device Performance as Ternary Additives in Organic Photovoltaicś," 2020, doi: 10.1021/acs.langmuir.9b03772.

[11] T. M. Grant, R. White, E. Thibau, Z. Lu, and T. P. Bender, "Donor / Acceptor Properties of Fluorophenoxy Silicon Phthalocyanines within Electronic Supporting Information .," 2015.

[12] E. Zysman-Colman *et al.*, "Solution-Processable Silicon Phthalocyanines in Electroluminescent and Photovoltaic Devices," *ACS Appl. Mater. Interfaces*, vol. 8, no. 14, pp. 9247–9253, 2016, doi: 10.1021/acsami.5b12408.

[13] L. Ke *et al.*, "A Series of Pyrene-Substituted Silicon Phthalocyanines as Near-IR Sensitizers in Organic Ternary Solar Cells," *Adv. Energy Mater.*, vol. 6, no. 7, pp. 1–13, 2016, doi: 10.1002/aenm.201502355.

[14] B. Lim, J. T. Bloking, A. Ponec, M. D. McGehee, and A. Sellinger, "Ternary bulk heterojunction solar cells: Addition of soluble NIR dyes for photocurrent generation beyond 800 nm," *ACS Appl. Mater. Interfaces*, vol. 6, no. 9, pp. 6905–6913, 2014, doi: 10.1021/am5007172.

Appendix C: Supporting information for Chapter 5: Low-Cost Silicon Phthalocyanine as a Non-Fullerene Acceptor for Flexible large area Organic Photovoltaics

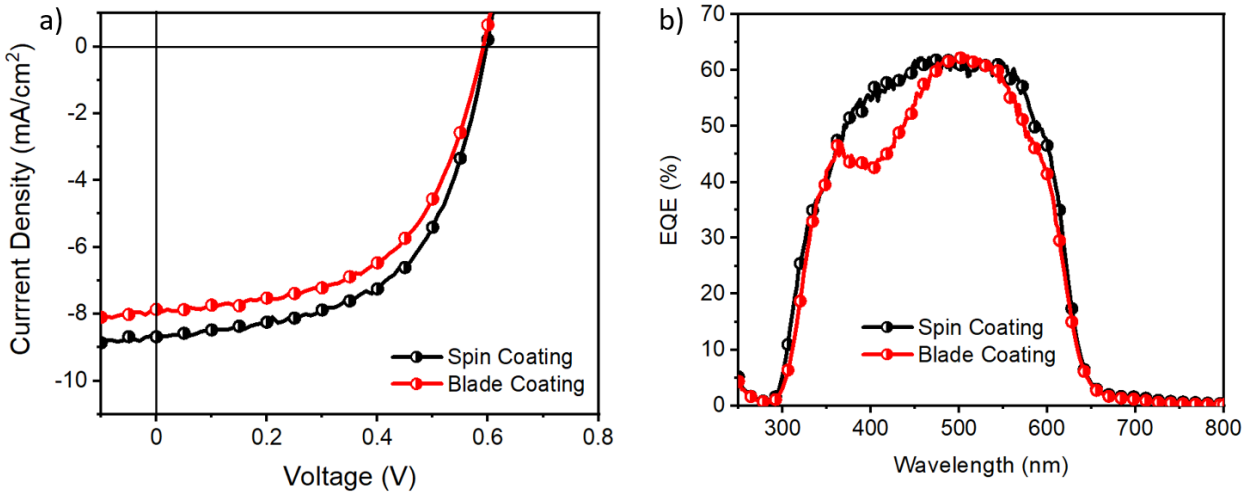

Figure S5.0-1. (a) J-V curves of P3HT: $PC_{61}BM$ BHJ photovoltaics fabricated on glass/ITO and PET/ITO flexible substrates by spin and blade coating respectively, (b) corresponding EQE curves.

Table S5.1: Photovoltaic performance parameters of baseline P3HT: $PC_{61}BM$ OPVs fabricated using o-DCB by spin and blade coating methods.

Device Structure	Process	J_{SC} (mA/cm²) [(a)]	V_{OC} (V)	FF	PCE (%)
Inverted	Spin Coating	8.60 (±0.20)	0.59 (±0.01)	0.55 (±0.01)	2.8 (±0.17)
	Blade Coating	7.3 (±0.16)	0.59 (±0.01)	0.52 (±0.02)	2.2 (±0.24)

All values are average with five devices, and the values in parentheses are the standard deviation. [a] Current density (J_{SC}) calculated from the EQE curve

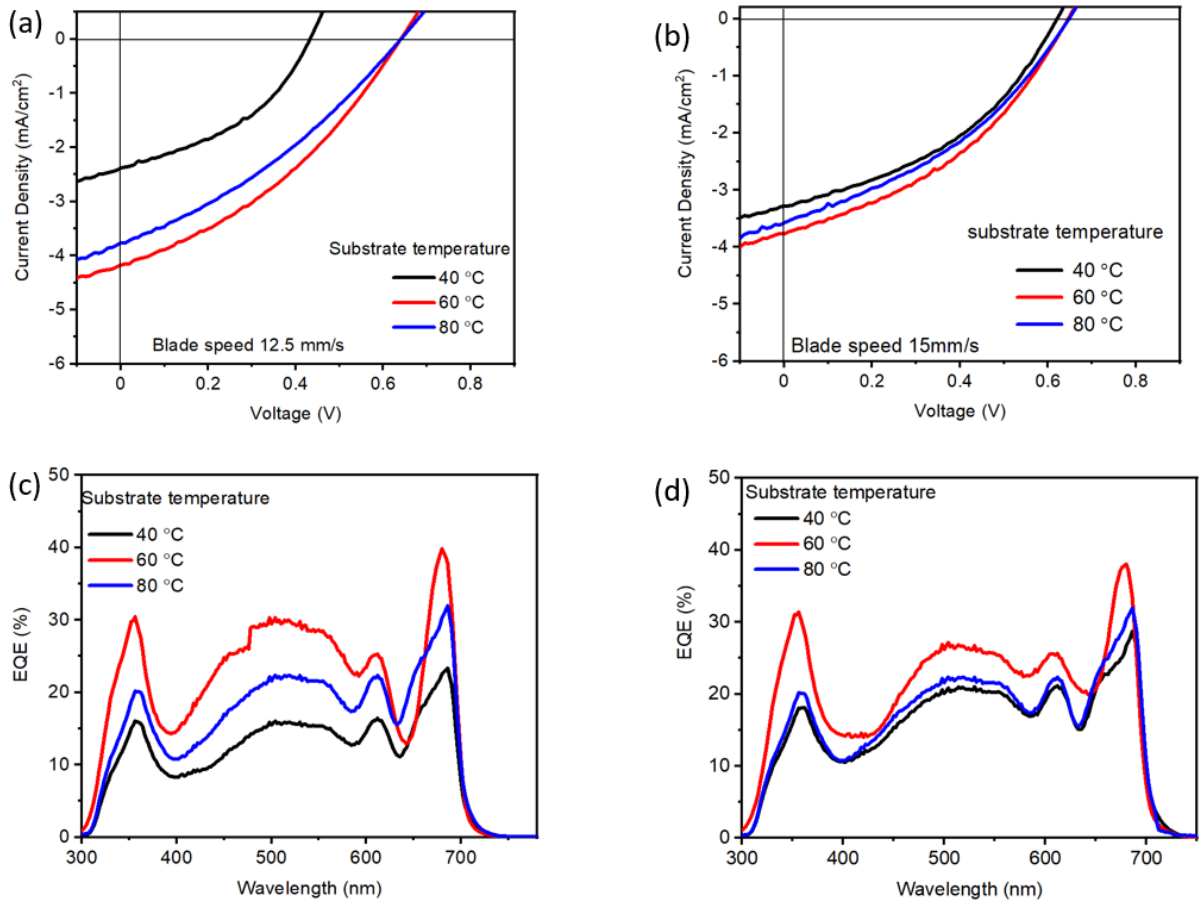

Figure S5.2. J-V and corresponding EQE curves of P3HT: $(3BS)_2$-SiPc BHJ OPVs fabricated using o-Xylene and thickness optimization under different substrate temperatures and blade speeds. (a, c) P3HT: $(3BS)_2$-SiPc (1:1) weight ratio and (b,d) P3HT: $(3BS)_2$-SiPc (1:0.6) weight ratio.

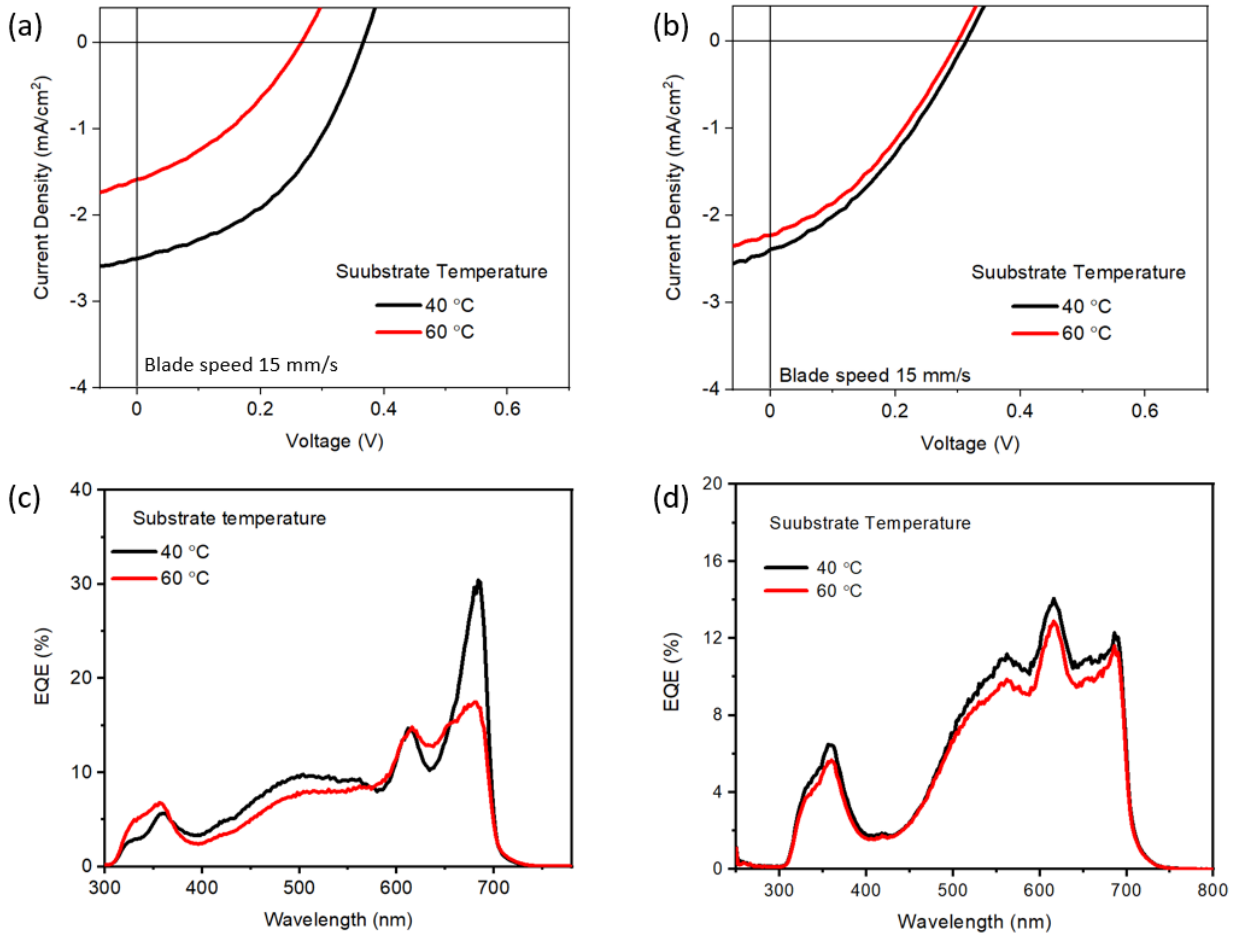

Figure S5.3. J-V and corresponding EQE curves of P3HT: $(3BS)_2$-SiPc BHJ OPVs fabricated using o-Xylene and thickness optimisation under different substrate temperatures. (a, c) P3HT: $(3BS)_2$-SiPc (1:0.4) weight ratio and (b,d) P3HT: $(3BS)_2$-SiPc (0.6:1) weight ratio.

Table S5.2. Photovoltaic performance parameters of P3HT:3(BS)$_2$-SiPc BHJ OPVs processed in o-Xylene. Active layers optimization with donor-acceptor ratios, substrate temperature, and active layer thickness

S.No	D:A blend ratio	Substrate temperature (°C)	Blade Speed (mm/s)	Thickness ~(nm)	J_{SC} (mA/cm^2)[a]	V_{OC} (V)	FF	PCE (%)
1	1:1	40	12.5	190 (±4)	2.60 (±0.2)	0.44 (±0.01)	0.39 (±0.05)	0.45 (±0.1)
2	1:1	60	12.5	120 (±5)	4.20 (±0.2)	0.61 (±0.01)	0.38 (±0.05)	0.92 (±0.1)
3	1:1	80	12.5	110 (±3)	3.82 (±0.2)	0.60 (±0.01)	0.36 (±0.05)	0.79 (±0.1)
4	1:0.6	40	15	180 (±6)	3.32 (±0.2)	0.60 (±0.01)	0.39 (±0.03)	0.77 (±0.2)
5	1:0.6	60	15	120 (±5)	4.11 (±0.2)	0.63 (±0.01)	0.44 (±0.05)	1.13 (±0.1)
6	1:0.6	80	15	90 (±8)	3.70 (±0.2)	0.64 (±0.01)	0.43 (±0.03)	1.02 (±0.1)
7	1:0.4	40	15	155 (±5)	2.68 (±0.4)	0.36 (±0.02)	0.42 (±0.07)	0.39 (±0.1)
8	1:0.4	60	15	110 (±5)	1.88 (±0.4)	0.25 (±0.02)	0.34 (±0.07)	0.28 (±0.1)
9	0.6:1	40	15	110 (±5)	2.69 (±0.3)	0.26 (±0.02)	0.34 (±0.04)	0.23 (±0.1)
10	0.6:1	60	15	104 (±5)	2.32 (±0.3)	0.25 (±0.02)	0.32 (±0.04)	0.18 (±0.1)

[a] current density (J_{SC}) calculated from the EQE curve

At least five devices were taken into consideration for average value calculations

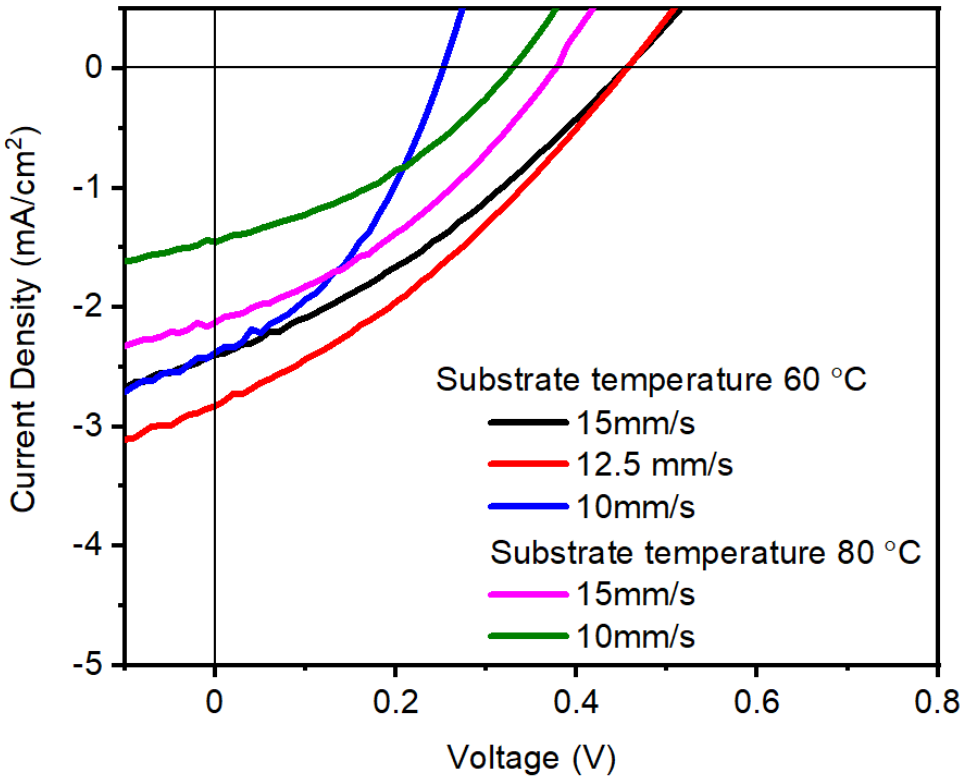

Figure S5.4. J-V curves of P3HT :$(3BS)_2$-SiPc (1:1) BHJ OPVs fabricated using o-Xylene with different thicknesses of active layer annealed at 110 °C for 30 min.

Table S5.3. Photovoltaic performance parameters of P3HT :$(3BS)_2$-SiPc (1:1) BHJ devices processed in o-Xylene and the devices were annealed at 110 °C for 30 min.

S.No	Blade speed (mm/s)	Substrate temperature (°C)	Thickness ~(nm)	J_{SC} (mA/cm^2)[a]	V_{OC} (V)	FF	PCE (%)
1	15	60	180 (±5)	2.41 (±0.3)	0.42 (±0.02)	0.34 (±0.04)	0.34 (±0.2)
2	12.5	60	120 (±5)	2.81 (±0.2)	0.42 (±0.01)	0.32 (±0.03)	0.37 (±0.2)
3	10	60	110 (±4)	2.40 (±0.2)	0.23 (±0.03)	0.39 (±0.05)	0.21 (±0.3)
4	15	80	155 (±5)	2.23 (±0.3)	0.35 (±0.02)	0.34 (±0.03)	0.27(±0.2)
5	12.5	80	110 (±5)	1.60 (±0.2)	0.30 (±0.01)	0.36 (±0.02)	0.17 (±0.2)

[a] current density (J_{SC}) calculated from the EQE curve

At least four devices were taken into consideration for average value calculations

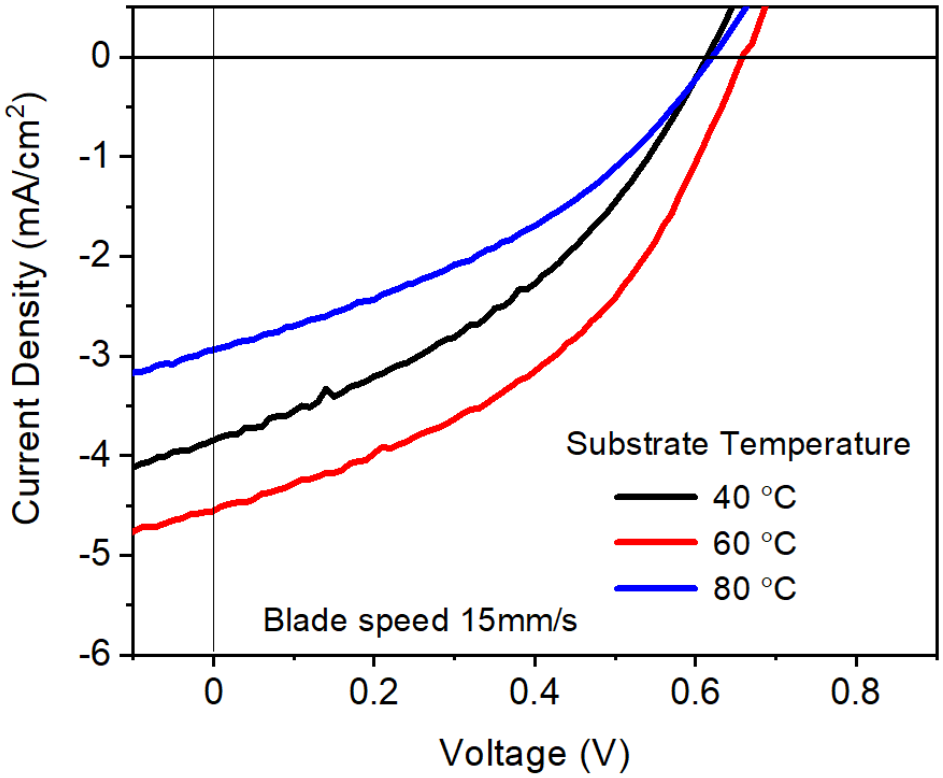

Figure S5.5 J-V curves of P3HT :$(3BS)_2$-SiPc (1:0.6) BHJ OPVs fabricated using TMB solvent with optimized active layer thickness processed under different substrate temperature

Table S5.4 Photovoltaic performance parameters of P3HT :$(3BS)_2$-SiPc (1:0.6) BHJ devices processed in TMB solvent, and the active layer coated with blade speed at 15mm/s.

S.No	Substrate temperature (°C)	Thickness ~(nm)	J_{SC} (mA/cm^2)[a]	V_{OC} (V)	FF	PCE (%)
1	40	170 (±5)	-3.8 (±0.3)	0.61 (±0.02)	0.37 (±0.04)	0.80 (±0.2)
2	60	130 (±5)	-4.6 (±0.3)	0.65 (±0.01)	0.44 (±0.03)	1.31 (±0.1)
3	80	110 (±5)	3.1 (±0.2)	0.62 (±0.03)	0.40 (±0.05)	0.71 (±0.3)

[a] current density (J_{SC}) calculated from the EQE curve

At least four devices were taken into consideration for average value calculations

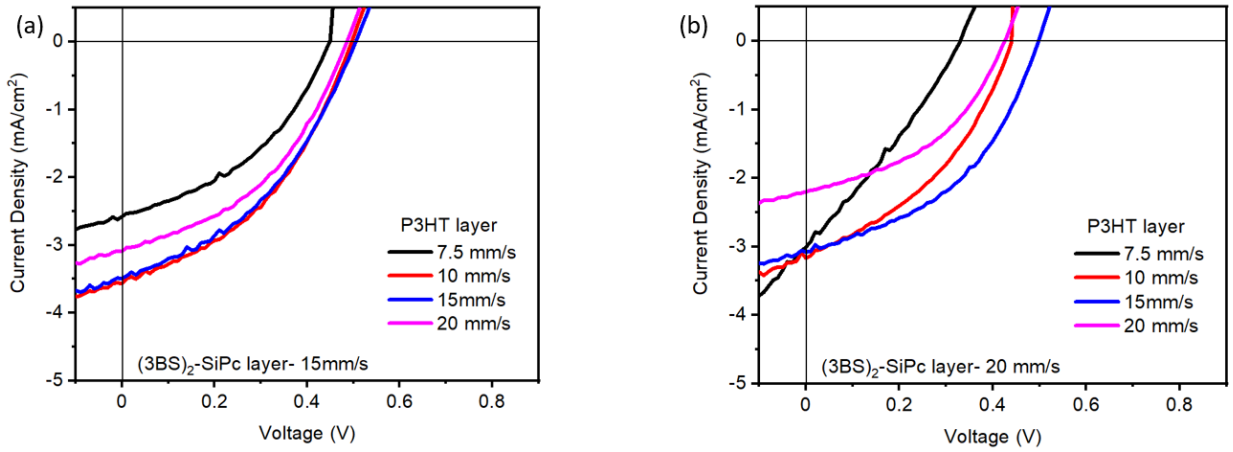

Figure S5.6: J-V curves of $(3BS)_2$-SiPc / P3HT (1:0.6) sequential bilayer (Sq) OPVs fabricated using O-xylene/TMB solvent with optimized active layer thickness processed under different blade speed

Table S5.5. Photovoltaic performance parameters of $(3BS)_2$-SiPc/P3HT (Sq) layer by layer processed with o-Xylene solvent and different blade coating speeds.

S.No	Blade speed (mm/s)		Thickness ~(nm)	J_{SC} (mA/cm^2)[a]	V_{OC} (V)	FF	PCE (%)
	$(3BS)_2$-SiPc	P3HT					
1	15	7.5	120 (±6)	2.57 (±0.2)	0.40 (±0.01)	0.41 (±0.05)	0.42 (±0.1)
2	15	10	130 (±6)	3.71 (±0.2)	0.49 (±0.01)	0.41 (±0.05)	0.73(±0.1)
3	15	15	140 (±4)	3.62 (±0.1)	0.51 (±0.01)	0.44 (±0.04)	0.80 (±0.05)
4	15	20	140 (±5)	3.20 (±0.2)	0.48 (±0.01)	0.40 (±0.03)	0.62 (±0.1)
5	20	7.5	125 (±5)	3.24 (±0.4)	0.33 (±0.02)	0.28 (±0.05)	0.28 (±0.1)
6	20	10	140 (±6)	3.30 (±0.4)	0.45 (±0.02)	0.40 (±0.05)	0.55 (±0.1)
7	20	15	150 (±6)	3.20 (±0.3)	0.51 (±0.02)	0.43 (±0.04)	0.66 (±0.1)
8	20	20	160 (±8)	2.20 (±0.3)	0.42 (±0.02)	0.43 (±0.04)	0.40 (±0.1)

[a] Current density (J_{SC}) calculated from the EQE curve,
At least five devices were taken into consideration for average value calculations

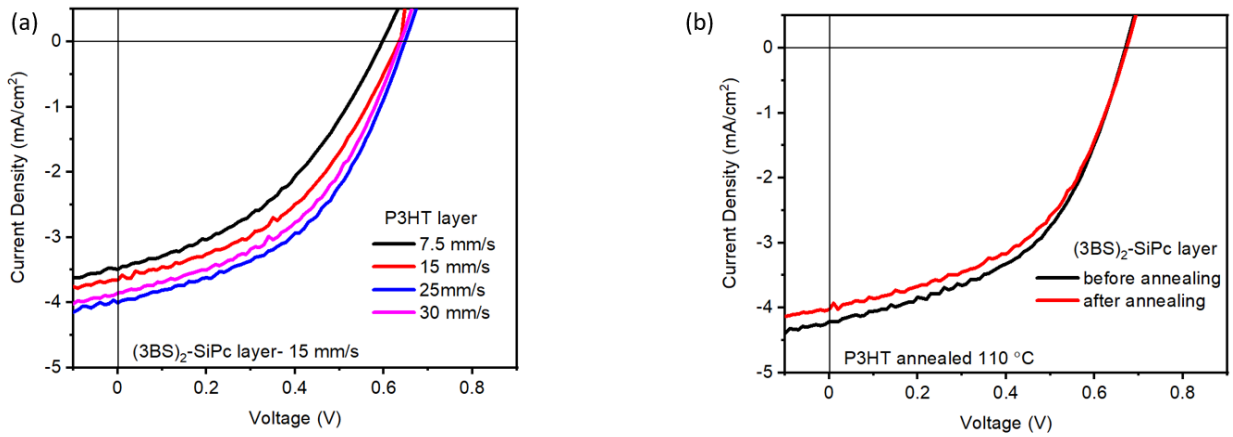

Figure S5.7: J-V curves of P3HT/ 3BS)$_2$-SiPc Alternate sequential bilayer (Alt-Sq) OPVs fabricated using O-xylene/TMB solvent with optimized active layer thickness processed under different blade speed and annealing conditions.

Table S5.6. Photovoltaic performance parameters of P3HT / 3(BS)2-SiPc (Alt-Sq) layer by layer processed with o-Xylene solvent and different blade coating speeds.

S.No	Blade speed (mm/s)		Thickness ~(nm)	J_{SC} (mA/cm^2)[a]	V_{OC} (V)	FF	PCE (%)
	P3HT	(3BS)2-SiPc					
1	7.5	15	80 (±6)	3.42 (±0.2)	0.49 (±0.01)	0.38 (±0.03)	0.63 (±0.1)
2	12.5	15	110 (±6)	3.66 (±0.2)	0.58 (±0.01)	0.42 (±0.02)	0.90 (±0.1)
3	15[b]	15	120 (±5)	4.35 (±0.1)	0.67 (±0.01)	0.50 (±0.02)	1.42 (±0.1)
4	15[b]	15[c]	120 (±4)	4.01 (±0.2)	0.67 (±0.01)	0.43 (±0.03)	1.30 (±0.1)
5	25	15	140 (±5)	4.25 (±0.1)	0.65 (±0.02)	0.43 (±0.02)	1.17 (±0.1)
6	25	15[b]	140 (±4)	3.83 (±0.2)	0.63 (±0.02)	0.45 (±0.03)	1.06 (±0.1)
7	30	15	160 (+4)	3.82 (±0.2)	0.63 (±0.02)	0.43 (±0.02)	1.06 (±0.1)
8	30	15[b]	160 (+4)	3.54 (±0.2)	0.65 (±0.02)	0.47 (±0.03)	1.20 (±0.1)
9	30	30	180 (±6)	2.42 (±0.1)	0.35 (±0.02)	0.32 (±0.03)	0.23 (±0.1)
10	30	30[b]	180 (±6)	2.20 (±0.1)	0.31 (±0.02)	0.38 (±0.02)	0.30 (±0.1)

[a] Current density (J_{SC}) calculated from the EQE curve, [b] P3HT layer annealed at 100 ºC, [c] the active layer was annealed at 110 ºC after (BS)$_2$-SiPc deposition in o-Xylene. At least 6 devices were taken into consideration for average value calculations

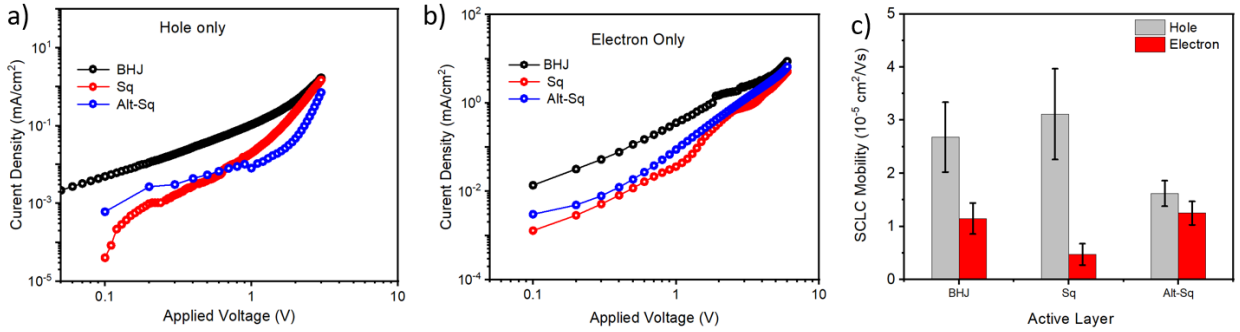

Figure S0-2. Log-log plot of J-V characteristics of (a) Hole-only devices with a structure of ITO/PEDOT:PSS/active layer/MoO_x/Ag. (b) Electron-only devices with a structure of ITO/ZnO/active layer/Al with BHJ, Sq and Alt-Sq blade coated active layers (c) Bar chart representation of charge carrier mobility values, standard deviation calculated for four device measurements.

Copyright permissions

Chapter 3

Reprinted and adopted with permission

Changes in Optimal Ternary Additive Loading when Processing Large Area Organic Photovoltaics by Spin- versus Blade-Coating Methods. *Chithiravel Sundaresan, Salima Alem, Chase L. Radford, Trevor M. Grant, Timothy L. Kelly, Jianping Lu, Ye Tao, Benoît H. Lessard. Sol. RRL2021,5, (2100432), DOI: 10.1002/solr.202100432*.

Copyright 2021 Wiley online library

Chapter 4

Reprinted and adopted with permission

Design of Ternary Additive for Organic Photovoltaics: A Cautionary Tale.
Chithiravel Sundaresan, Pierre Josse, Mario C. Vebber, Jaclyn Brusso, Jianping Lu, Ye Tao, Salima Alem and Benoit H. Lessard. RSC Adv. 2022, 12 (16),10029–10036.
DOI: 10.1039/d2ra00540a.

Copyright 2022 Royal Society of Chemistry

Chapter 5

Reprinted and adopted with permission

Low-Cost Silicon Phthalocyanine as a Non-Fullerene Acceptor for Flexible large area Organic Photovoltaics. *Chithiravel Sundaresan, Mario C. Vebber, Jaclyn Brusso, Ye Tao, Salima Alem, and Benoît H. Lessard. ACS Omega 2023, 8, 1, 1588–1596. doi.org/10.1021/acsomega.2c07131.*

Copyright 2023 American Chemical Society